The Crystal Structure of Olivine Group Minerals and the Effect of Crystal Orientation on X-ray Absorption Spectroscopy

A Dissertation
Presented in Partial Fulfillment of the Requirements for the
Degree of Doctorate of Philosophy
with a
Major in Geological Sciences
in the
College of Graduate Studies
University of Idaho
by
Nichole R. Valdez

Major Professor: Mickey Gunter, Ph.D.
Committee Members: Thomas Bitterwolf, Ph.D.; Thomas Williams, Ph.D.; Mark Roll, Ph.D.
Department Administrator: Leslie Baker, Ph.D.

August 2017

AUTHORIZATION TO SUBMIT DISSERTATION

This dissertation of Nichole R. Valdez, submitted for the degree of Doctorate of Philosophy with a Major in Geological Sciences and titled "The Crystal Structure of Olivine Group Minerals and the Effect of Crystal Orientation on X-ray Absorption Spectroscopy," has been reviewed in final form. Permission, as indicated by the signatures and dates below, is now granted to submit final copies to the College of Graduate Studies for approval.

Major Professor: _____ Date: _____
Mickey Gunter, Ph.D.

Committee Members: _____ Date: _____
Thomas Bitterwolf, Ph.D.

_____ Date: _____
Thomas Williams, Ph.D.

_____ Date: _____
Mark Roll, Ph.D.

Department Administrator: _____ Date: _____
Leslie Baker, Ph.D.

ABSTRACT

X-ray absorption near edge structure (XANES) spectra have been shown to be dependent on crystal orientation. This study characterizes the variation in spectra along the a, b, and c crystallographic axes for olivine group minerals of varying compositions with the formula $Mg_xFe_{1-x}SiO_4$. Single crystal X-ray diffraction was used to collect the unit cell parameters, atomic coordinates, and bond lengths. The same single crystals were then oriented optically using a spindle stage for X-ray absorption spectroscopy, and for some crystals, the composition was determined by electron probe microanalysis (EPMA) afterward. The compositions from refinement were compared to EPMA results from analysis of the bulk mineral samples, or the same single crystal when possible, and are nearly identical. The partitioning of Mg and Fe into the M1 and M2 crystallographic sites was found to be correlated to the total %Mg in each sample. A small site preference was observed at high levels of total iron, where there is a higher percentage of the total magnesium in the M2 site than there is in the M1 site. The pattern is not as strong for iron in the M1 site at high levels of total magnesium. Neither site seems to be influenced by the concentration of Fe^{3+}. The three crystallographic axes are distinct in the XANES spectra, however samples with lower iron are more easily distinguishable, possibly due to self-absorption. There is a correlation at the pre-edge between peak intensity and total iron, particularly along the b axis.

ACKNOWLEDGEMENTS

I would like to thank Dr. Mickey Gunter, Dr. M. Darby Dyar, and Dr. John M. Hughes for helping me reach this point. Mickey provided the funding necessary to compete a Ph.D. in mineralogy at the University of Idaho and encouraged me not to abandon geology as an undergraduate student. Darby welcomed me into her mineral research group and guided me through learning X-ray absorption spectroscopy and also arranged synchrotron beamline time for our samples. John mentored me at the University of Vermont where a large portion of the mineralogical crystallography was completed.

For Mindy

TABLE OF CONTENTS

LIST OF FIGURES

LIST OF TABLES

CHAPTER ONE: CRYSTAL STRUCTURE REFINEMENT OF OLIVINE GROUP MINERALS

1.1 Introduction

The crystal structure of forsterite was first determined by William Lawrence Bragg and G.B. Brown in 1926. William Lawrence Bragg later played a large role in charactering silicates as composed of SiO_4 tetrahedra (Bragg and West, 1927; Bragg, 1929; Bragg, 1930). The space group of the olivine group minerals is Number 62, and the historical space group setting of the olivine group minerals is *Pbnm* $\left(P\frac{2_1}{b}\frac{2_1}{n}\frac{2_1}{m}\right)$, though the standard setting would be *Pnma* $\left(P\frac{2_1}{n}\frac{2_1}{m}\frac{2_1}{a}\right)$ as defined by the International Union of Crystallography (International Tables for Crystallography A). Nevertheless, mineralogists continue to use *Pbnm* to this day for the ease of comparison with older refinements.

The unit cell of olivine group minerals is orthorhombic with a *Z* of 4. The oxygen atoms in the structure assume a close-packed hexagonal arrangement (see **Figure 1.1-1**). One-half of the octahedral voids are occupied by Fe or Mg atoms, and one-eighth of the tetrahedral voids are occupied by Si atoms (Birle et al., 1968). The two metal sites are crystallographically distinct, where M1 lies on an inversion center and M2 is located along a mirror plane.

Figure 1.1-1: Forsterite looking down the a crystallographic axis
a) Hexagonal close packing of atoms.

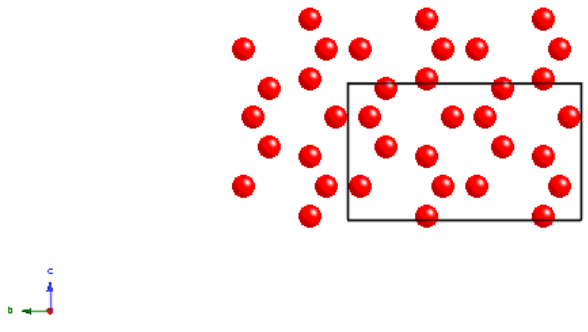

b) Hexagonal close packing rotated slightly to show depth

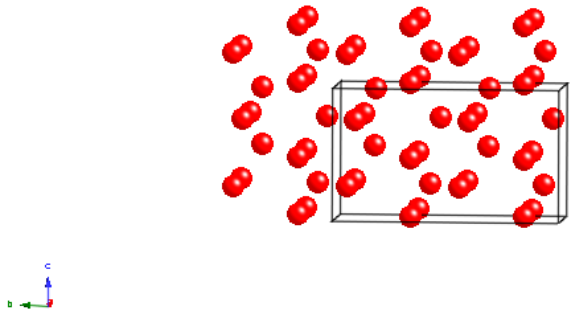

c) polyhedral model of the olivine group minerals looking down a
M1 is shown in orange, M2 is shown in green, and the silicon tetrahedron is in yellow.

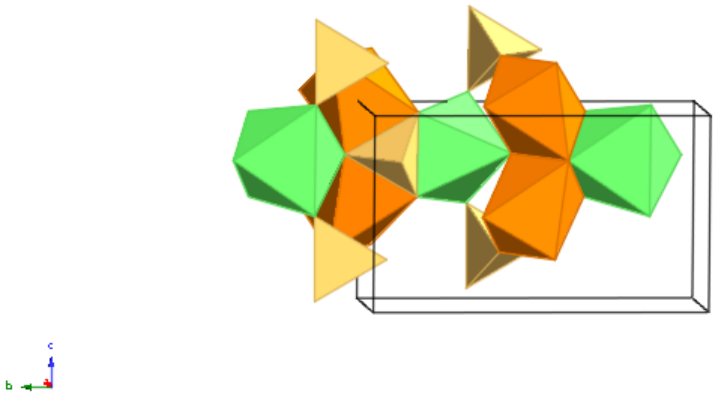

Several olivine group mineral samples were examined as the first step in a larger project that characterizes the effect of crystal orientation on X-ray absorption spectroscopy. The data were processed in both the *Pbnm* and *Pnma* settings to deposit into a crystal structure database so future researchers could use the data in whichever format they choose.

1.2 Experimental Methods

Single crystal X-ray diffraction data were collected at the University of Vermont in Burlington, Vermont in partnership with Dr. John. M. Hughes using a Bruker APEX II CCD detector and Mo*K*α radiation. A single crystal was chosen from each olivine sample for X-ray analysis and mounted for room temperature data collection using Bakelite and a glass fiber. The temperature of the diffractometer room was consistent at 18.3 °C, and a low temperature device was not used. A full sphere of data was collected with Bruker APEX2 (Bruker, 2012)

for each sample, resulting in an average redundancy above 9.0 and completeness above 99.0%. The frame data were integrated with a narrow-frame algorithm using Bruker SAINT in the APEX2 software package. For most samples, the frame queue length had to be increased from the default 7 to 8 or 9 in order to lower the amount of spots exceeding the frame queue size. Unit cells in traditional space group *Pbnm* and standard space group *Pnma* were determined using XPREP in APEX2. The effective maximum resolution (Müller, 2009) of the datasets was determined to be 0.66 Å for most samples. The structures in *Pnma* were solved with SHELXT using a dual-space algorithm (Scheldrick, 2015) and structures in *Pbnm* were solved with SHELXS using direct methods (Sheldrick, 2007), as SHELXT will reassign a non-standard space group to the standard space group during solution and XS will not. Both *Pnma* and *Pbnm* data were refined against F2 for all data with SHELXL (Sheldrick, 2014). The refinement R1 was consistently below 1.5% for the observed data and below 4.0% *w*R2 for all data. Some crystals were lost between the X-ray analysis step and optical orientation for X-ray Absorption Near Edge Structure (XANES), so a new crystal was selected for a repeat analysis. Because of this, some samples are represented with two complete single crystal X-ray diffraction datasets and are labeled with "R2," meaning round two.

The M1 and M2 sites can each contain a magnesium atom or an iron atom. To represent this, the refinement instruction file contains commands to calculate the ratio of Mg:Fe in each site using a free variable. The free variable allows for a partial occupancy of each element that adds up to one total metal atom per site. The ratio is determined from the total electron density in the M1 and M2 sites by calculating what percent of a magnesium atom (12 electrons) and an iron atom (26 electrons) fits the density. A high electron density will have a higher percent of iron, and a low electron density will have a higher percent of magnesium. The free variable was later used to calculate the percent of total magnesium and percent of total iron in each site metal site.

The M1 site occupies a special position in both space groups, and thus has fixed coordinates. The M2 site has one fixed coordinate (*y* for *Pnma* and *z* for *Pbnm*). The elements within each site are constrained so that the partial magnesium and partial iron atoms both have the same *x*,

y, and *z* coordinates. This allows for the M1 and M2 sites to be fit to the center of the electron density, but prevents the partial magnesium atom and partial iron atom from drifting apart from one another during refinement. Similarly, the anisotropic displacement parameters were also constrained to be identical for the partial magnesium and partial iron atoms. The most disagreeable reflections were examined for each refinement, and one or two reflections were omitted, when appropriate, for each sample. Hazen (1976) noted secondary extinction in forsterite when $F_{obs} << F_{calc}$. One reflection consistently fit this definition and appeared at the top of the most disagreeable reflection list, (0 0 2) in *Pnma* and (2 0 0) in *Pbnm*. The unit cell parameters from refinement can be found in **Appendix A**.

1.3 Results and Discussion

1.3.1 Linear increases in the unit cell

There is a linear increase in the volume of the unit cell with respect to the amount of iron in the sample (see **Figure 1.3.1-1**). This pattern holds true for all three axes (a, b, and c), where the length of each axis increases with increasing %Fe in the sample (see **Figure 1.3.1-2**). This most likely due to the increase in bond length with increasing %Fe in the sample (see **Figure 1.3.1-3** and **Figure 1.3.1-4**).

Figure 1.3.1-1: Linear increase in unit cell volume with respect to %Fe in sample

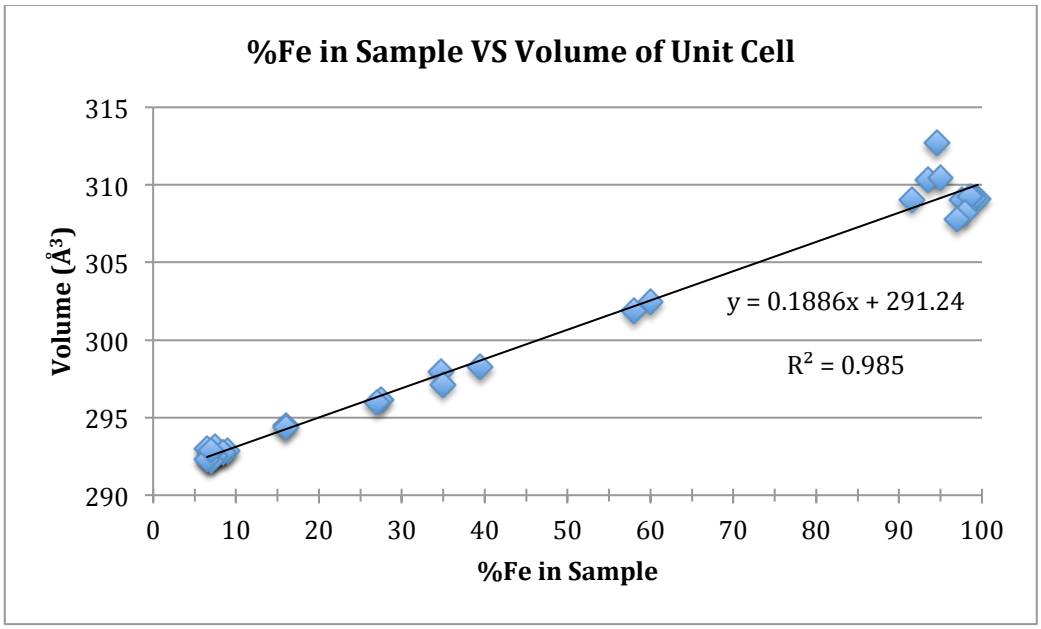

The linear fit of %Fe in Sample VS Volume (Å^3) gives an intercept of 291.24 (±0.25) Å^3 for a pure forsterite sample. A study of synthetic forsterite by Hazen (1976) reports a room temperature unit cell volume of 289.5 Å^3, which is within the uncertainty of the calculated intercept. In an earlier paper, Smyth and Hazen (1973) report a unit cell volume of 209.30 Å^3, but this is far too small for an olivine group mineral, and is possibly a typo that should read 290.30 Å^3. With the assurance of a synthetic forsterite fitting at the intercept, the composition of a Mg-Fe olivine group mineral could be predicted based on the unit cell volume using the equation:

$$\text{Volume} = 0.1886(\pm 0.0043) \times (\%\text{Fe}) + 291.237(\pm 0.249)\text{Å}^3$$

The equation can be improved with the addition of more refinement data.

Figure 1.3.1-2: Linear increase in unit cell length with respect to %Fe in sample

a) Increasing length of a with increasing %Fe in sample

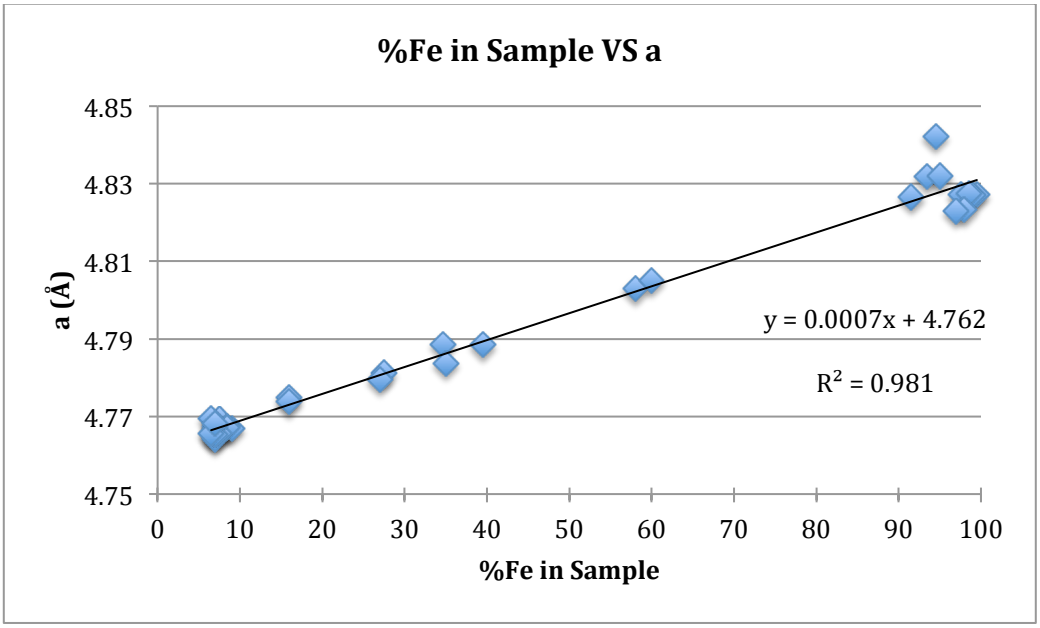

b) Increasing length of b with increasing %Fe in sample

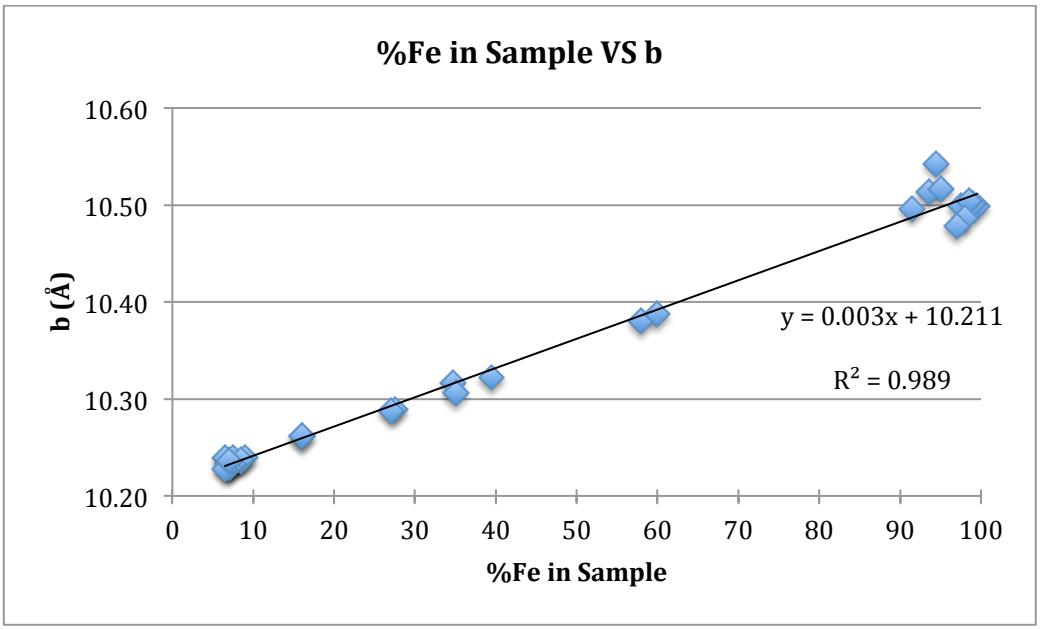

c) Increasing length of c with increasing %Fe in sample

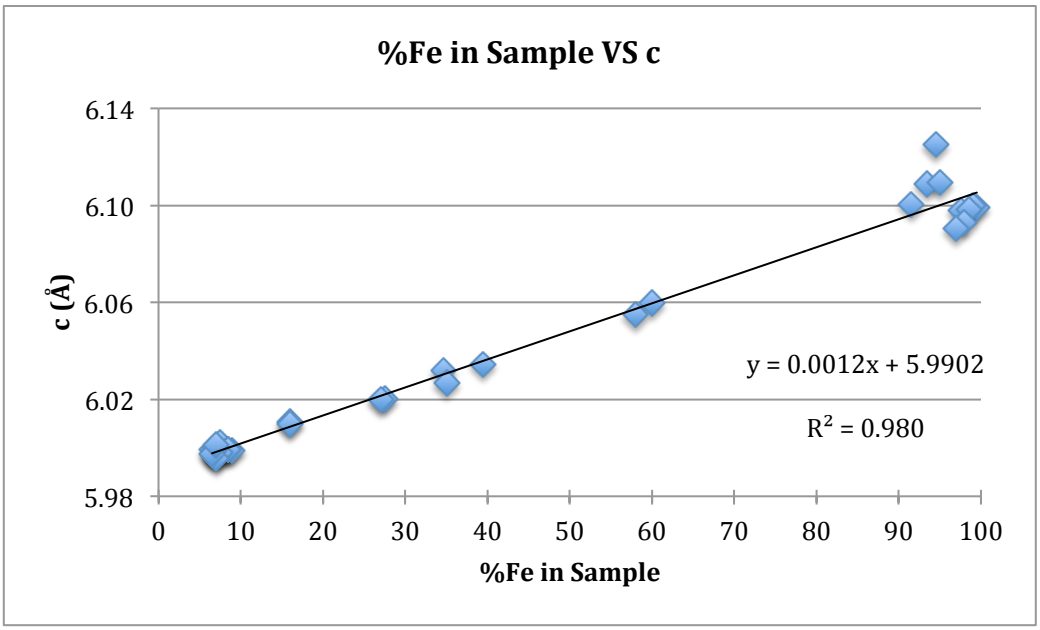

Figure 1.3.1-3: %Fe VS bond lengths in M1

a) Bond length M1-O1

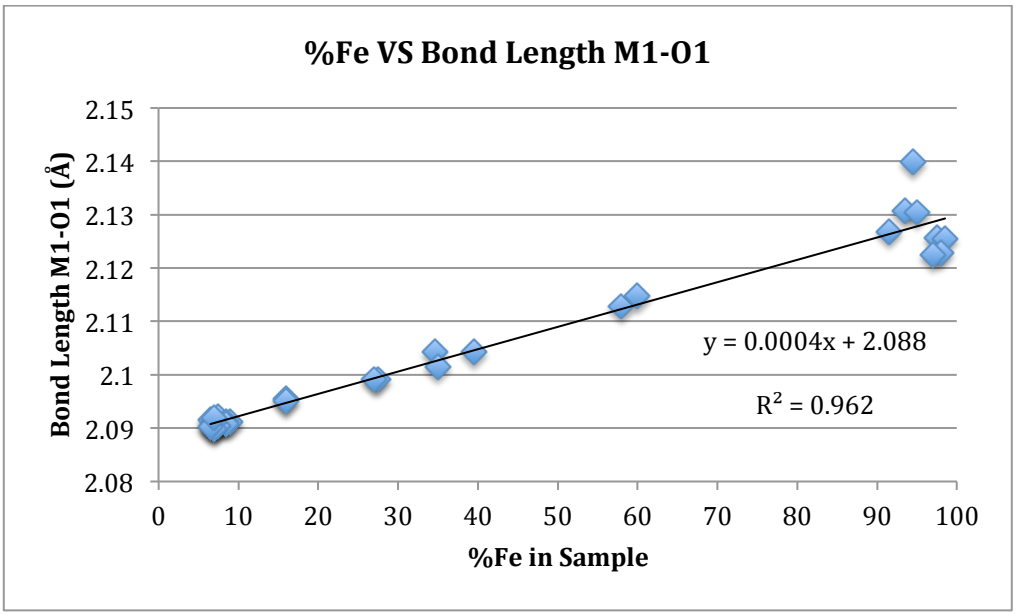

b) Bond Length M1-O2

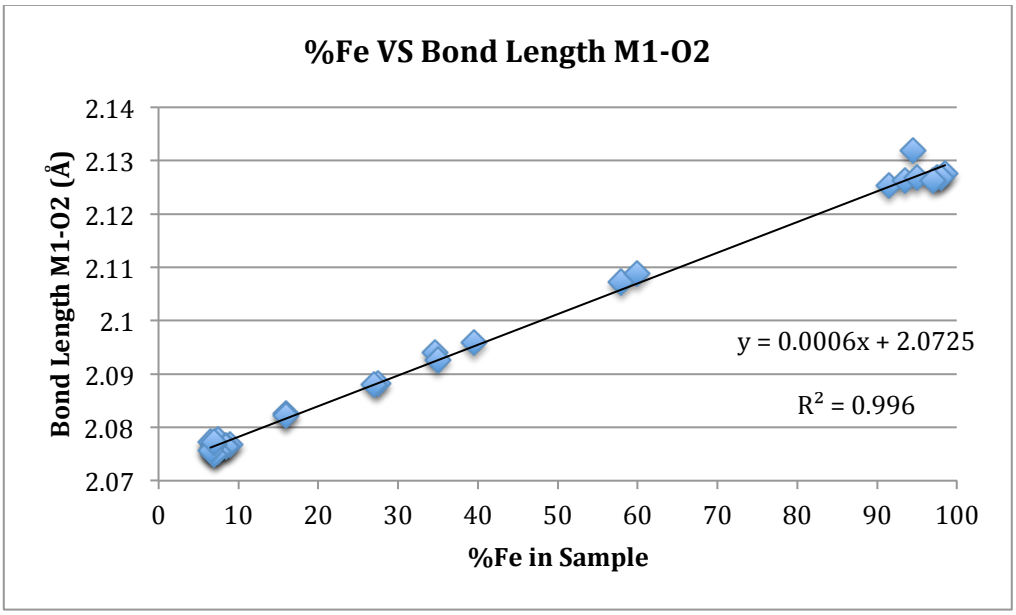

c) Bond Length M1-O3

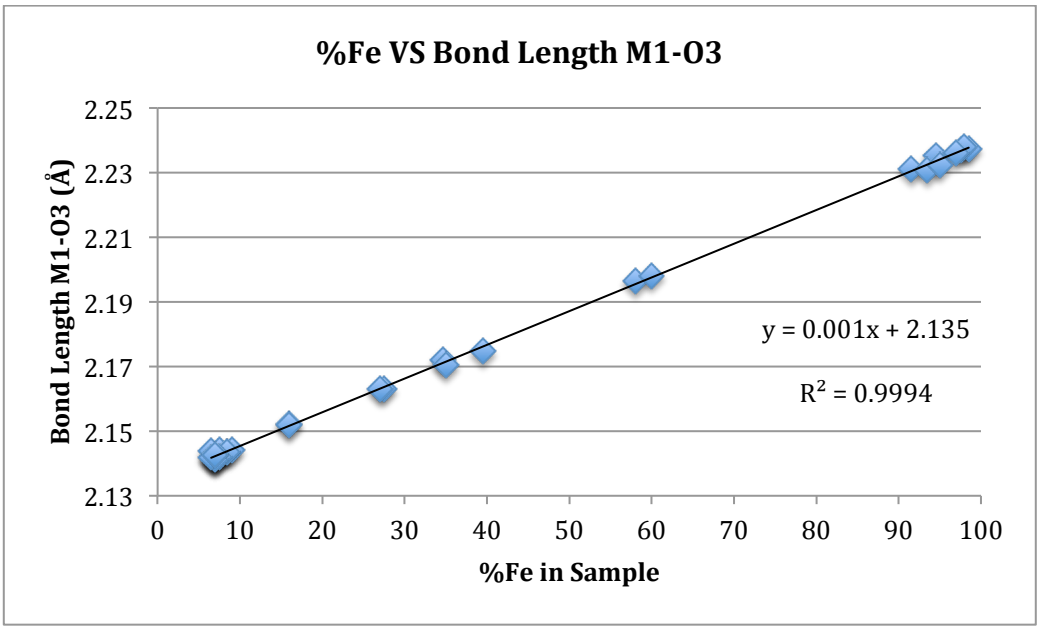

Figure 1.3.1-4: %Fe VS bond lengths in M2

a) Bond length M2-O1

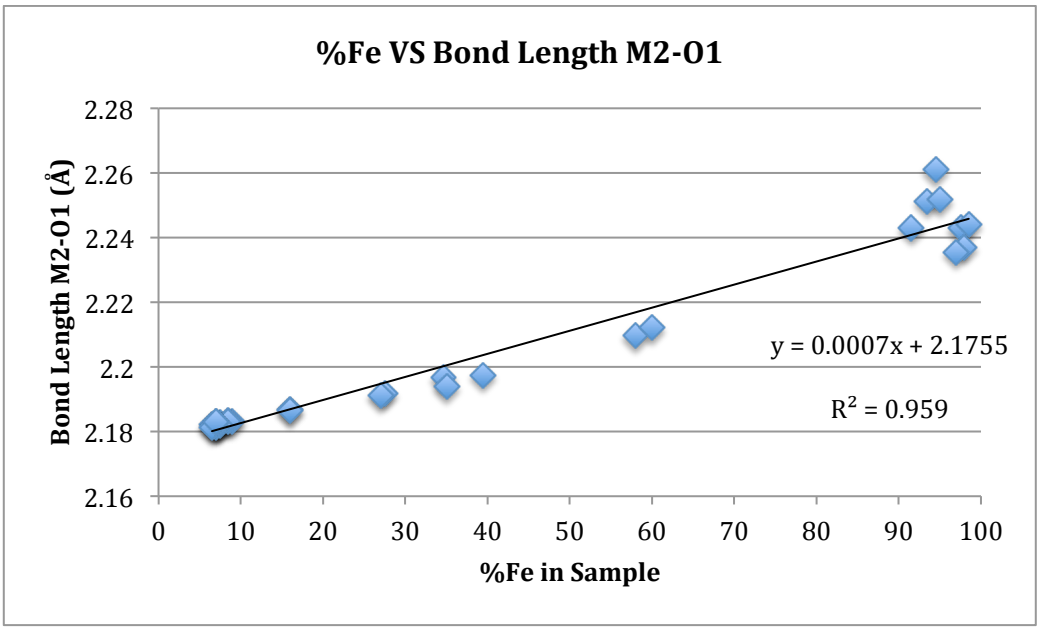

b) Bond length M2-O2

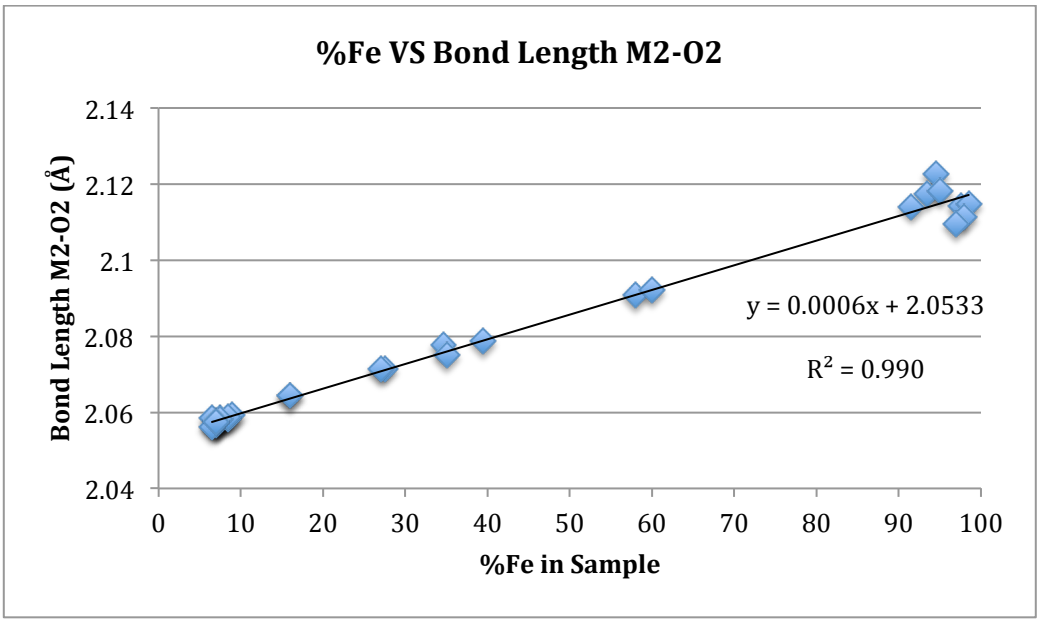

c) Bond length M2-O3

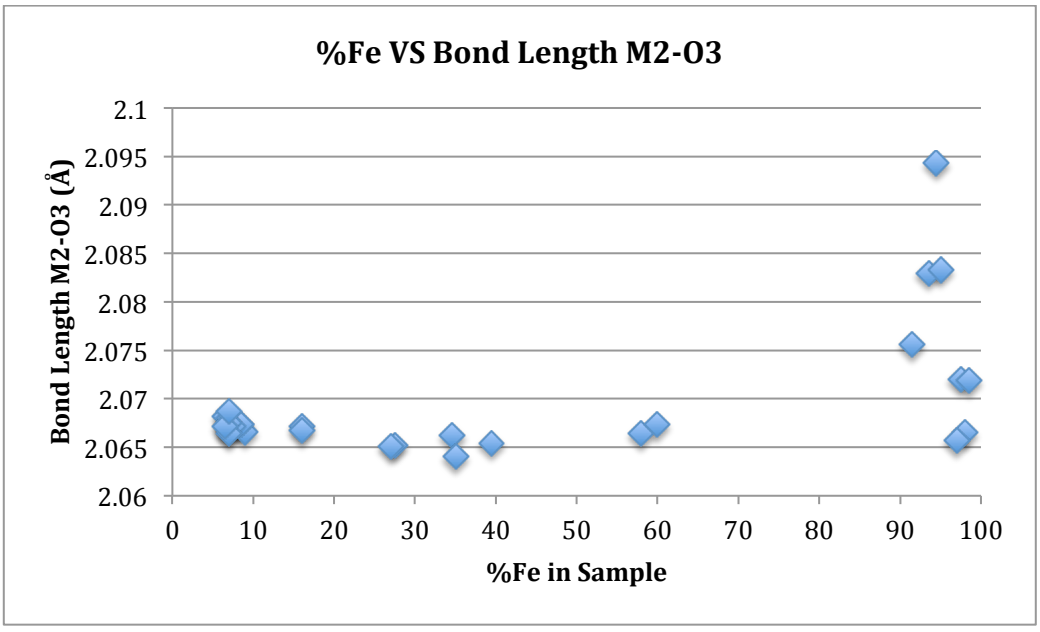

d) Bond length M2-O3'

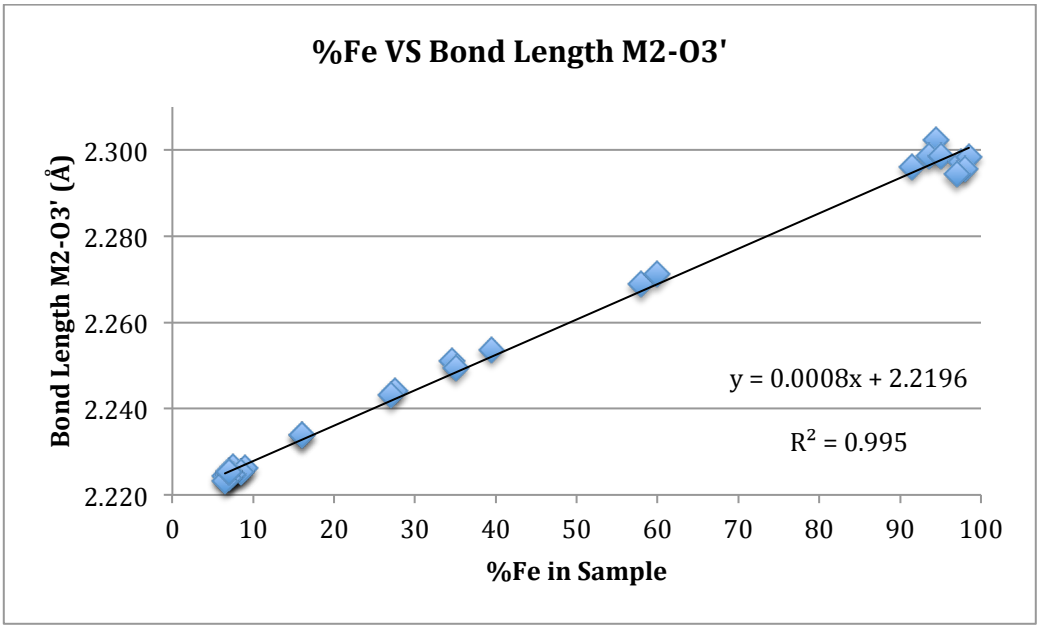

The bond length between M2 and O3 is the only bond that does not follow the linear elongation with increasing iron content of the sample. This could be a function of a more complex distortion of the M2 octahedron position (See **Figure 1.3.1-4c**).

Birle et al. (1968) observed that the longest Si-O bond length is to O2, and that O2 had the shortest M-O bond length. In a larger dataset, the pattern holds for the Si-O2 and M2-O2 bonds, but is less sure for the M1-O2 bond. Furthermore, the longest bonds correspond to the shared edges as observed by Birle et al. (1968). All of the bond lengths are listed in **Appendix B**.

1.3.2 Shifting atomic coordinates

The position of M1 is fixed at (0, 0, 0) in the unit cell, however the effect of increasing %Fe in the sample can be seen in the positions of the other atoms. The result is usually a linear increase in axis value with a couple of notable exceptions (see Figure 1.3.2-1 through Figure 1.3.2-5). The M2 *x* coordinate (see **Figure 1.3.2-1a**) decreases in value with increasing iron content in the sample up until about 60% Fe where it begins to increase again. An attempt was made to model this strange movement, but what the eyes sees as a pattern is best described

with a polynomial line, which leaves much to be desired statistically. The fit line with uncertainties on the last digits in parenthesis is the following:

$$\text{M2 x coordinate} = 8.44(73)\times10^{-7}(\%\text{Fe})^2 - 1.26(8)\times10^{-4}(\%\text{Fe}) + 0.9908(1)$$

A linear fit of the data up to 60% iron accentuated the slight curve of these data. More work can be done in the future to characterize the movement of the M2 position, and would require samples with 70-85% Fe.

O1 does not follow any pattern that can be fit with one line of best fit. The *x* and *y* coordinates increase linearly with %Fe in the sample up until about 65% Fe. At above 90% Fe, there is no longer a pattern (**Figure 1.3.2-3**). This effect could, again, be better characterized by acquiring some samples in the range of 70-85% Fe. Between the M2 *x* coordinate and the O1 *x* and *y* coordinates, there seems to be something in this range that causes a break in the predictable movement of the atoms. The system would perhaps be better modeled in two parts, or modeled only up to a certain %Fe content. The *x* coordinate of O2 is decreasing linearly with increased %Fe in the sample (**Figure 1.3.2-4a**).

Figure 1.3.2-1: Movement of *x* and *y* coordinates of M2 with increasing %Fe in sample

a) Polynomial fit of *x* coordinate movement

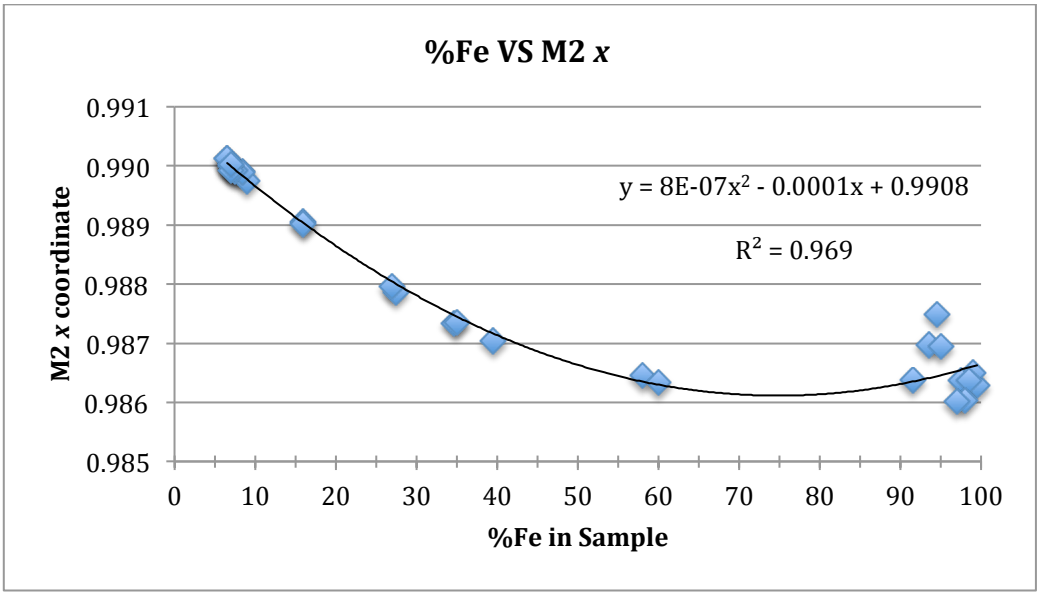

b) Linear fit of *y* coordinate movement

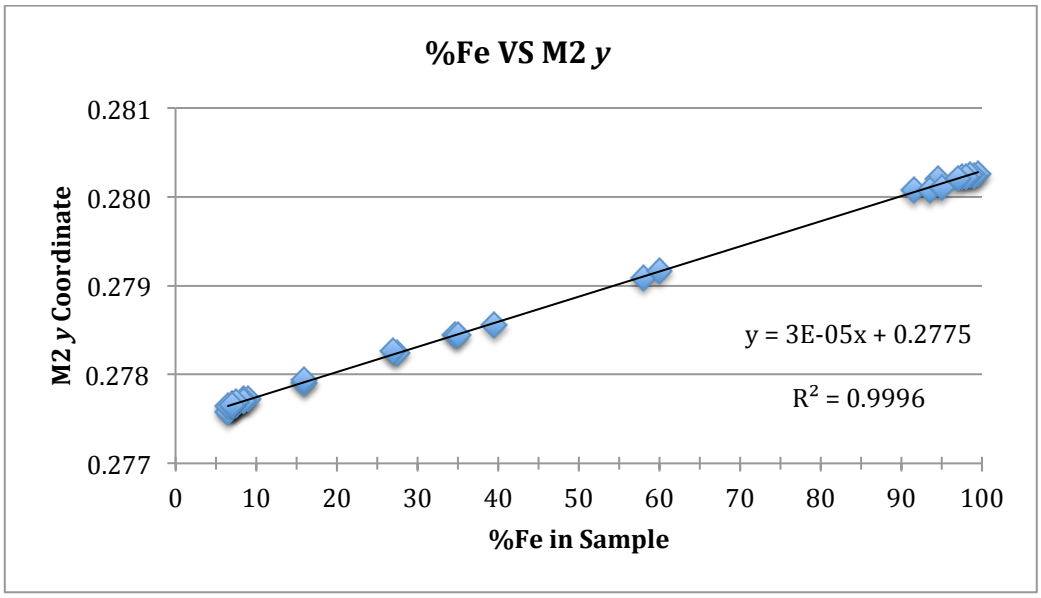

Note the *z* coordinate is fixed at 0.25.

Figure 1.3.2-2: Movement of *x* and y coordinates of Si with increasing %Fe in sample

a) Linear fit of *x* coordinate movement

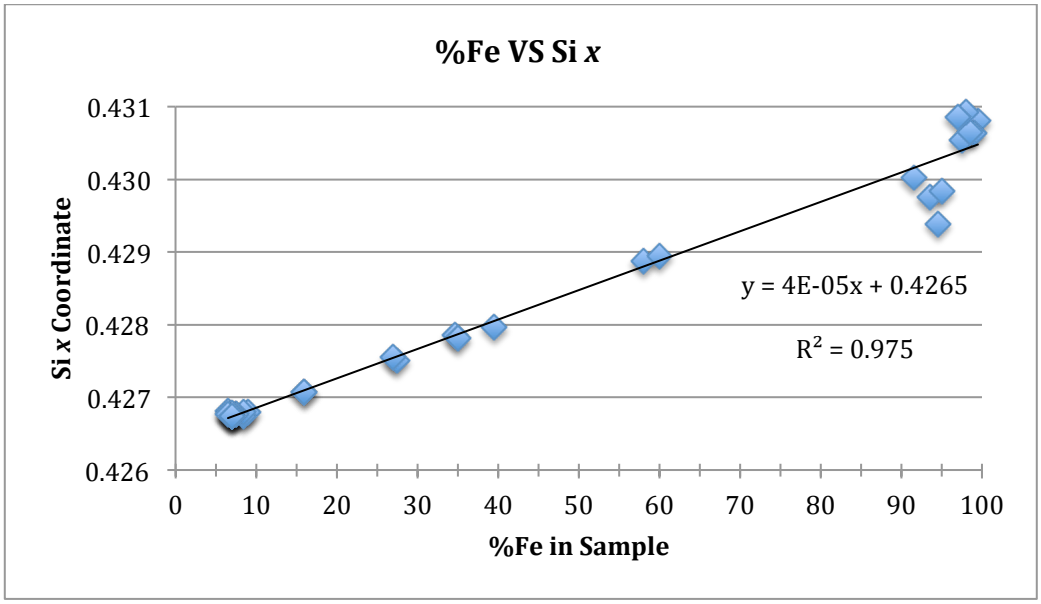

b) Linear fit of Y coordinate movement

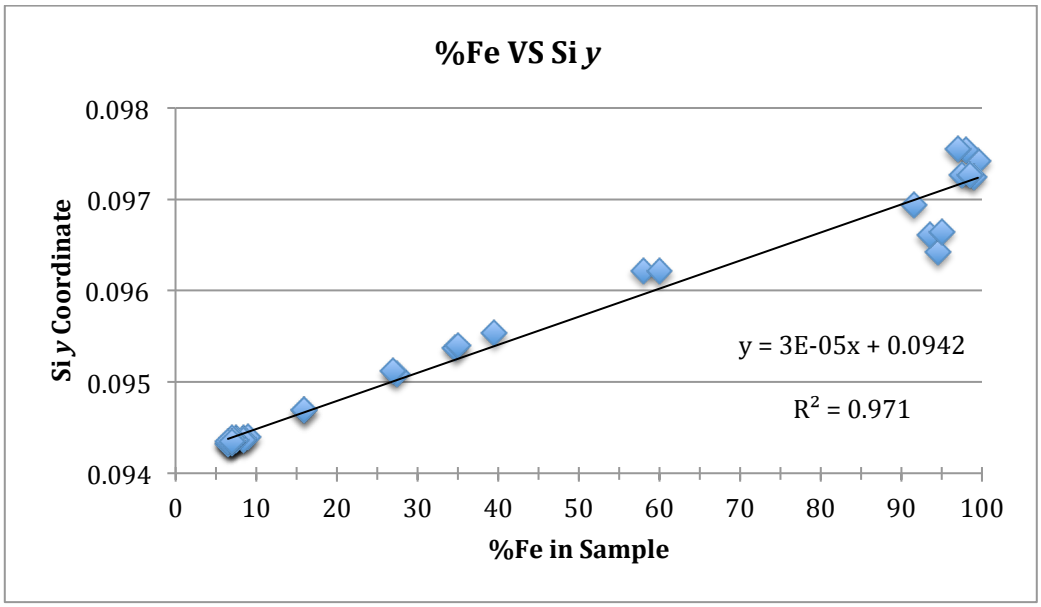

Note the *z* coordinate is fixed at 0.25.

Figure 1.3.2-3: Movement of *x* and *y* coordinates of O1 with increasing %Fe in sample

a) *x* coordinate movement

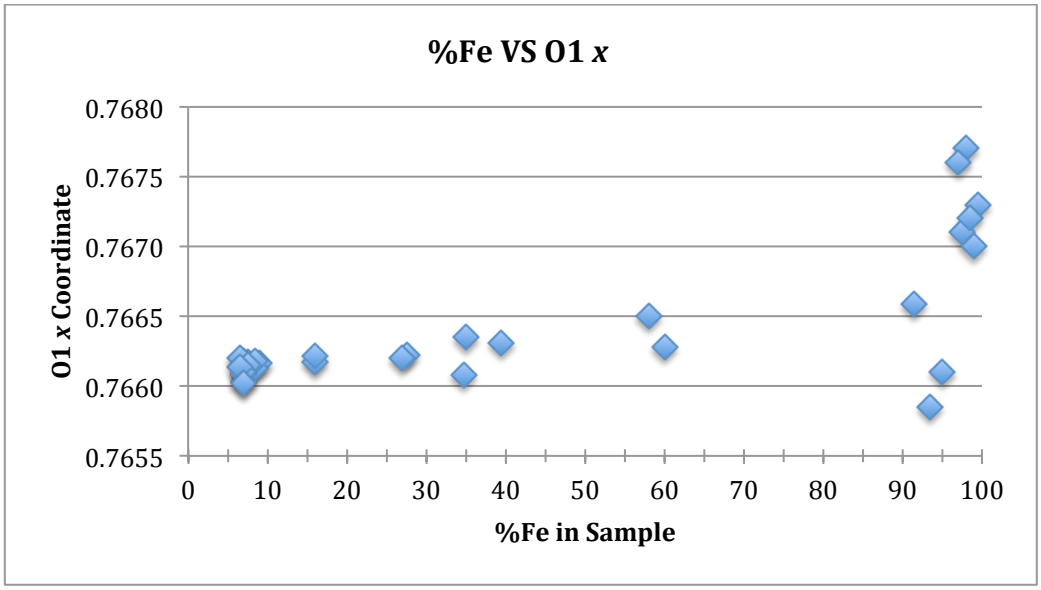

b) *y* coordinate movement

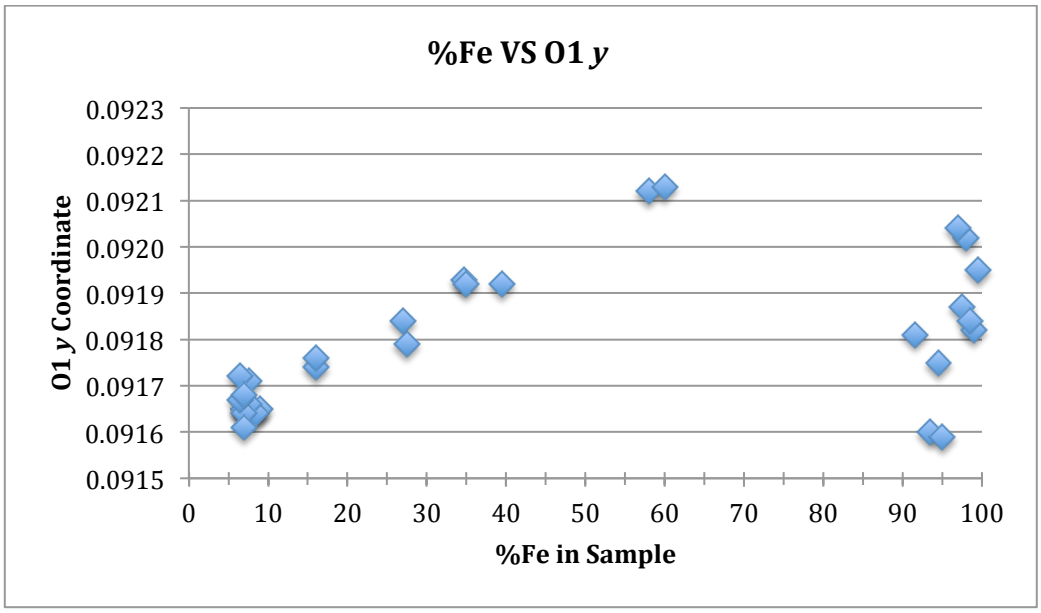

Note the *z* coordinate is fixed at 0.25.

Figure 1.3.2-4: Movement of *x* and *y* coordinates of O2 with increasing %Fe in sample

a) Linear fit of *x* coordinate movement

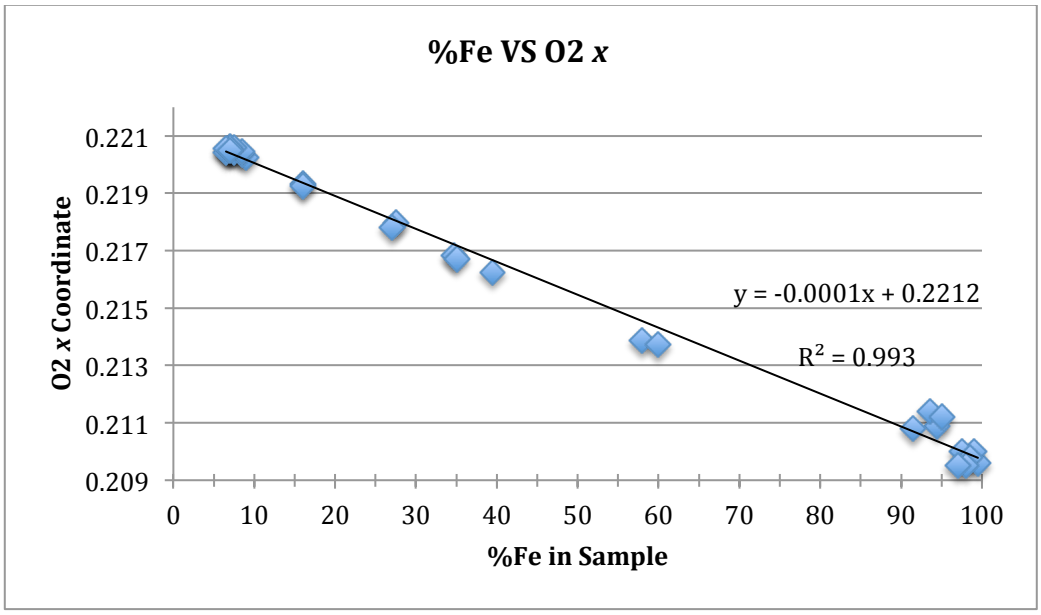

b) Linear fit of *y* coordinate movement

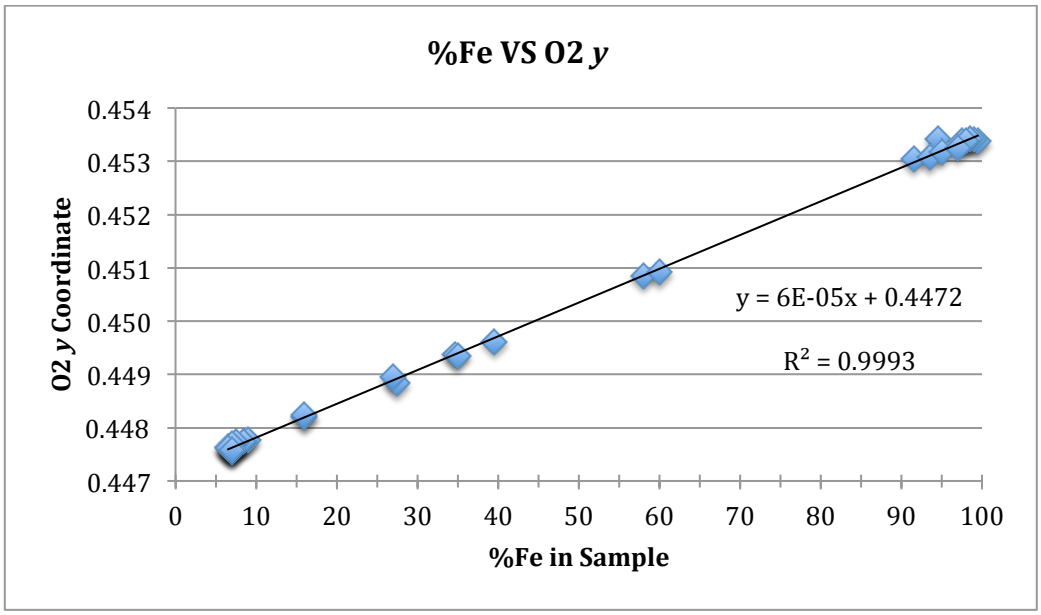

Note the *z* coordinate is fixed at 0.25.

Figure 1.3.2-5: Movement of *x* and *y* coordinates of O3 with increasing %Fe in sample

a) Linear fit of *x* coordinate movement

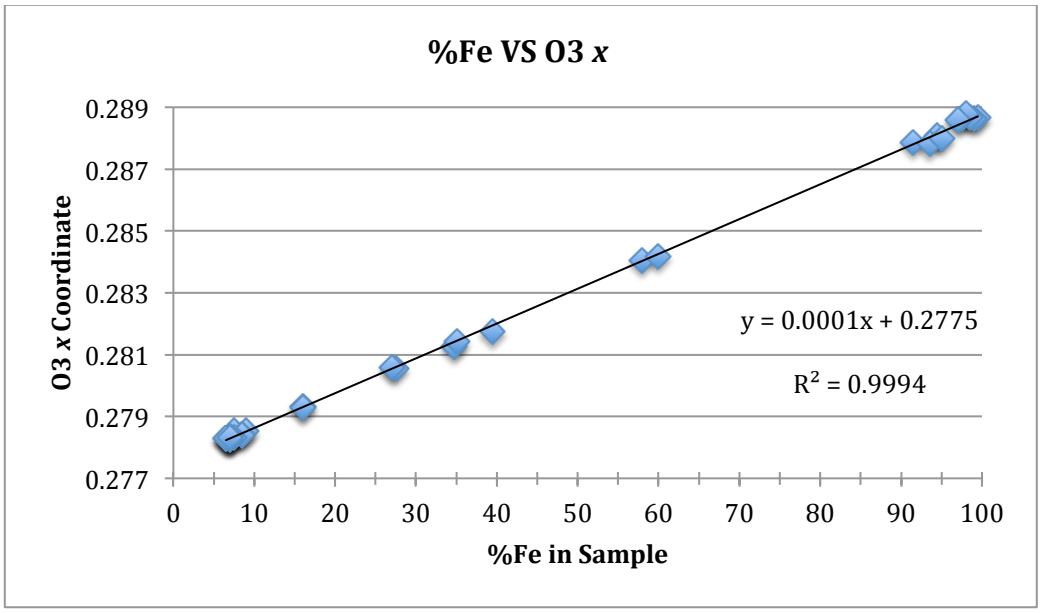

b) Linear fit of *y* coordinate movement

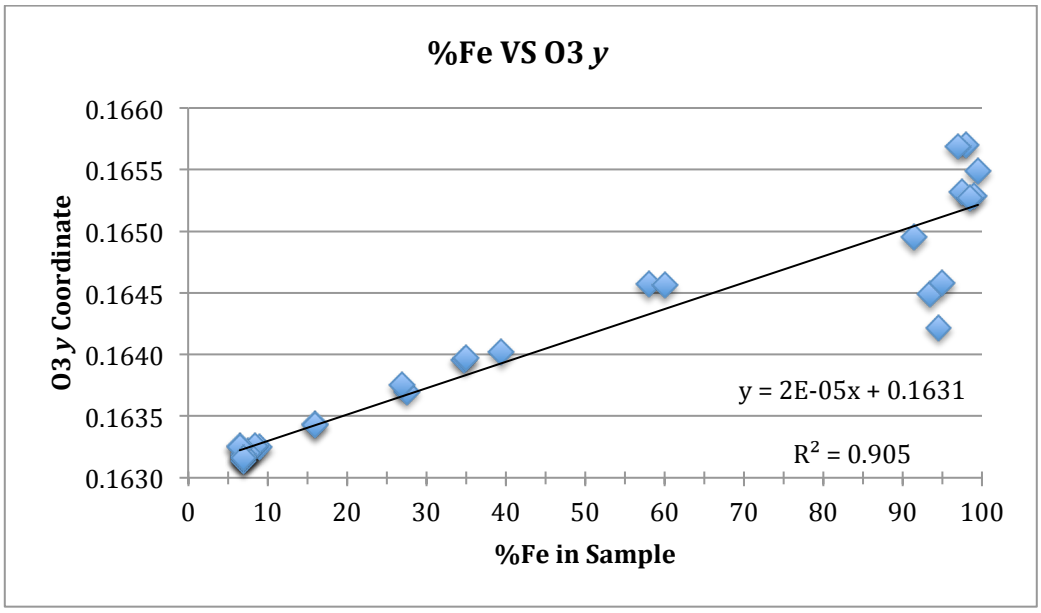

c) Linear fit of *z* coordinate movement

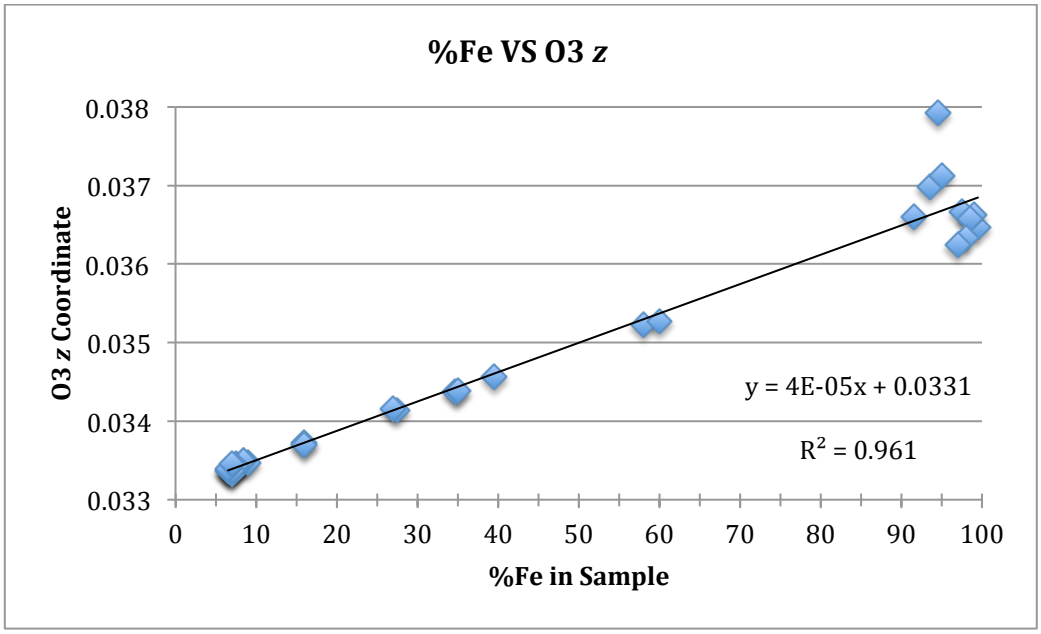

1.3.3 Octahedral distortion

One possible cause of this strange break after 60% Fe could be octahedral distortion of the M2 site as the iron content of the site increases. The distortion of the bond lengths can be quantified by the mean quadratic elongation (Robinson et al., 1971) through the following relationship:

$$\lambda_{oct} = \frac{1}{6}\sum_{i=1}^{6}\left(\frac{l_i}{l_0}\right)^2$$

Where the bond lengths in the M2 octahedron (l_i) deviate from the ideal length of a bond in an octahedron of the same volume (l_0). See **Appendix C** for more information. The samples with the highest iron content have the highest λ_{oct} value; see **Table 1.3.3-1** below. The full table of bond lengths and λ_{oct} values can be found in **Appendix B** and **Appendix D**. It is unclear why sample KI3054 does not follow this pattern. A repeat analysis with more crystals from the KI3054 locality is planned for the future.

Table 1.3.3-1: Mean quadratic elongation (λ_{oct}) values of M2 for all samples

Sample	%Fe	λ_{oct}	Sample	%Fe	λ_{oct}
DH101D	6.50	1.027	KI3648	27.50	1.029
San Carlos	7.00	1.027	NWA2737 R2	27.00	1.029
H30B4	6.50	1.027	KI3054 R2	35.00	1.030
H30B1 R2	7.00	1.027	KI3362	39.50	1.031
DH101E	7.00	1.027	KI4143	58.00	1.033
H30B1	7.00	1.027	KI4143 R2	60.00	1.033
DH101C R2	7.00	1.027	85540	**91.50**	**1.036**
DH101C	7.50	1.027	90613	**93.50**	**1.036**
EP3139D R2	7.50	1.027	LLV	**97.00**	**1.037**
EP3139C	8.46	1.027	112085	**95.00**	**1.037**
EP3139C R2	8.46	1.027	LFC	**98.00**	**1.037**
DH101D R2	7.00	1.027	Mourne	**97.51**	**1.037**
DH101B	9.00	1.027	85539	**94.50**	**1.037**
KBH941	16.00	1.028	Rockport	**98.51**	**1.037**
KBH941 R2	16.00	1.028	KI3054	34.67	1.055

*KI3054 is suspected to have an error and is scheduled for repeat analysis

The mean quadratic elongation is nearly the same for both the M1 and M2 sites with the exception of KI3054. See **Table 1.3.3-2**.

Table 1.3.3-2: Mean quadratic elongation (λoct) for M1 and M2

Sample	%Fe	M1 Volume	M1 λ oct	M2 Volume	M2 λ oct
DH101D	6.50	11.926	1.028	12.537	1.027
San Carlos	7.00	11.924	1.028	12.543	1.027
H30B4	6.50	11.898	1.028	12.512	1.027
H30B1 R2	7.00	11.887	1.028	12.516	1.027
DH101E	7.00	11.900	1.028	12.522	1.027
H30B1	7.00	11.915	1.028	12.535	1.027
DH101C R2	7.00	11.896	1.028	12.517	1.027
DH101C	7.50	11.933	1.028	12.546	1.027
EP3139D R2	7.50	11.899	1.028	12.526	1.027
EP3139C	8.46	11.916	1.028	12.534	1.027
EP3139C R2	8.46	11.914	1.028	12.534	1.027
DH101D R2	7.00	11.899	1.028	12.526	1.027
DH101B	9.00	11.920	1.028	12.536	1.027
KBH941	16.00	12.011	1.029	12.599	1.028
KBH941 R2	16.00	12.005	1.029	12.594	1.028
KI3648	27.50	12.107	1.030	12.661	1.029
NWA2737 R2	27.00	12.104	1.030	12.652	1.029
KI3054 R2	35.00	12.175	1.031	12.688	1.030
KI3362	39.50	12.227	1.031	12.736	1.031
KI4143	58.00	12.433	1.033	12.871	1.033
KI4143 R2	60.00	12.461	1.033	12.898	1.033
85540	91.50	12.761	1.037	13.196	1.036
90613	93.50	12.784	1.037	13.289	1.036
LLV	97.00	12.761	1.037	13.087	1.037
112085	95.00	12.791	1.037	13.290	1.037
LFC	98.00	12.775	1.037	13.106	1.037
Mourne	97.51	12.785	1.037	13.174	1.037
85539	94.50	12.884	1.038	13.414	1.037
Rockport	98.51	12.790	1.037	13.184	1.037
KI3054*	34.67	12.210	1.030	12.278	1.055

*KI3054 is suspected to have an error and is scheduled for repeat analysis

The polyhedron volumes of the Si tetrahedron, the M1 octahedron, and the M2 octahedron in general increase with increasing iron content in the sample (see **Figure 1.3.3-1)**.

Figure 1.3.3-1 Increase of polyhedron volumes with increased %Fe in sample

a) Slight increase of Si tetrahedron volume with increased %Fe in sample

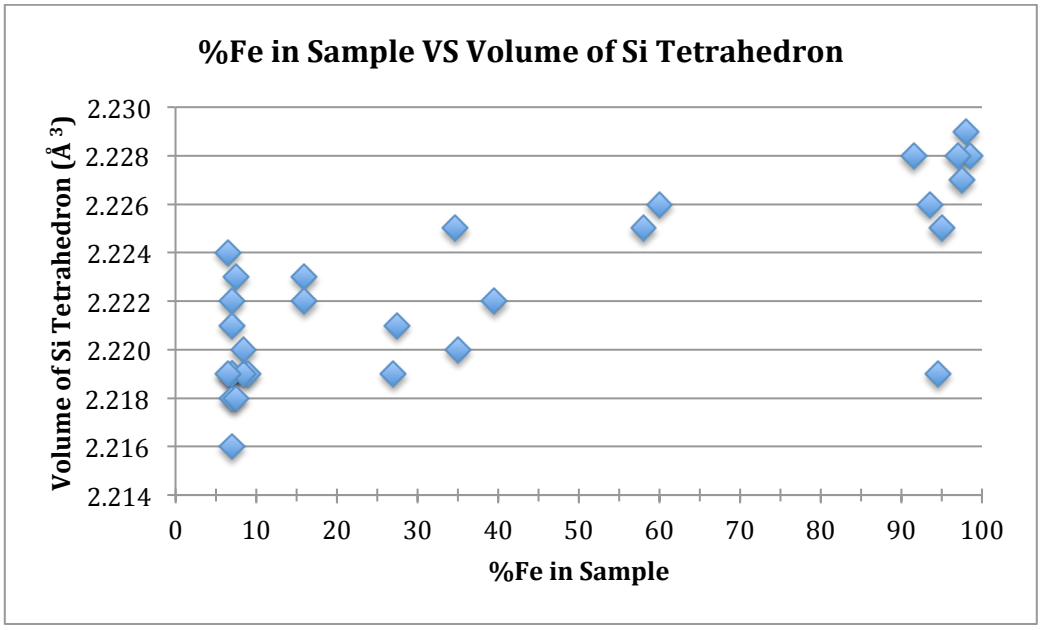

b) Increase of M1 octahedron volume with increased %Fe in sample

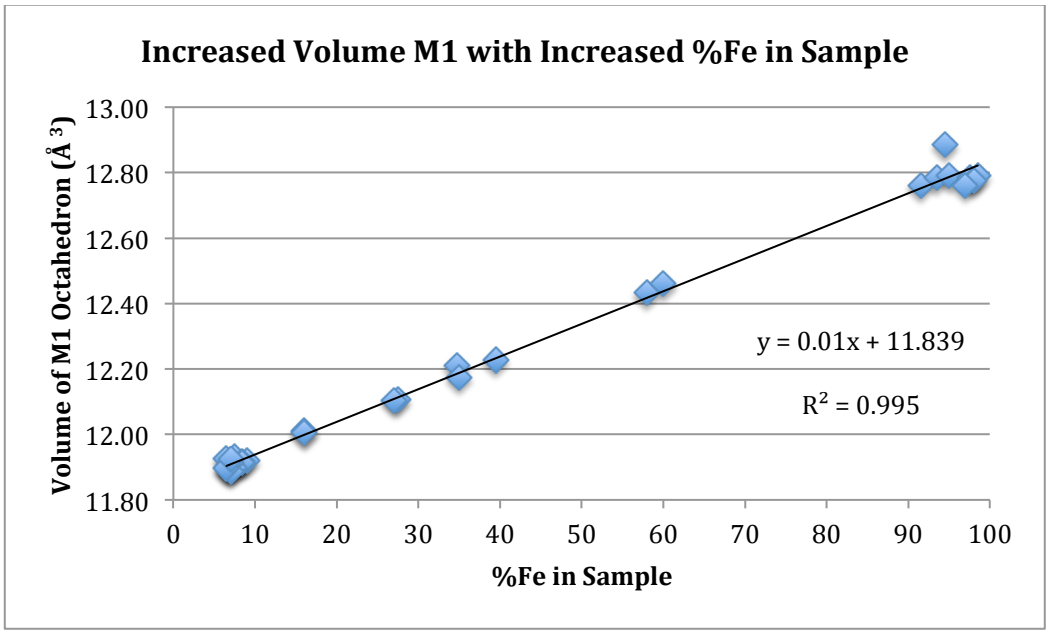

c) Increase of M2 octahedron volume with increased %Fe in sample

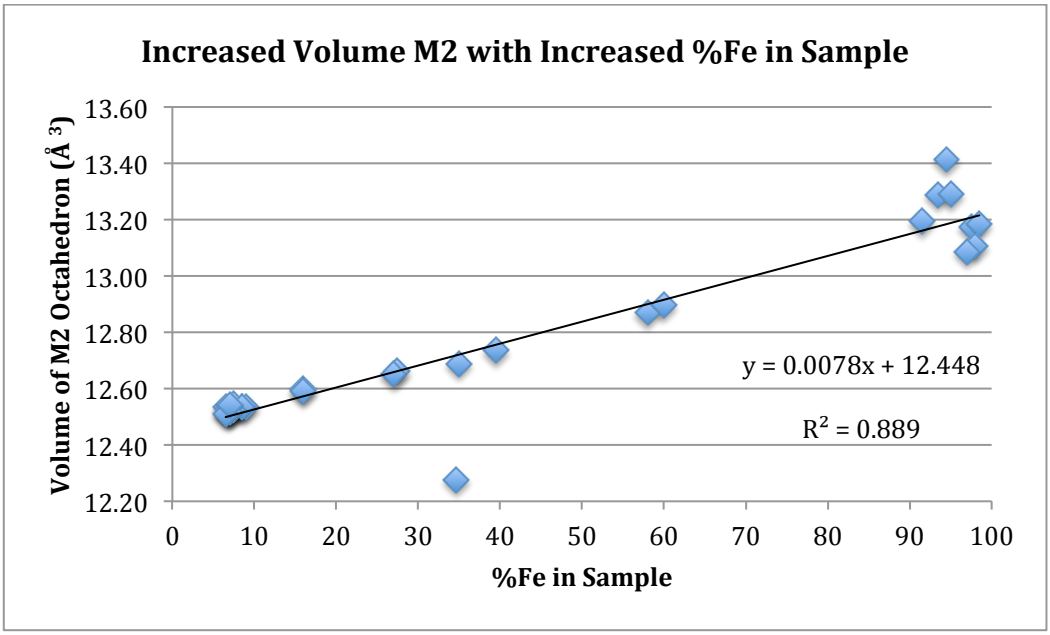

The outlier point in 1.3.8c is KI3054, the same point that was an outlier for the λ_{oct} value.

1.3.4 Compositional analysis

The Fe^{3+} content of each sample was obtained with Mössbauer spectroscopy. For seventeen samples, it was possible to collect compositional data from electron probe microanalysis (EPMA) on the same samples that were used for crystal structure refinement. The results are summarized in **Table 1.3.4-1**. The composition determined by single crystal X-ray diffraction (SCXRD) matches the composition from electron microprobe analysis (see **Table 1.3.4-2**), which strengthens the conclusions drawn from increasing iron content.

The laihunite samples have vacancies in the structure (Xu et al., 2014), and therefore a value for M1+M2 below 2.0. It should also be noted that Sample 112085 from Red Rock Ridge has a significant manganese content. A partitioning of Fe into the M1 and Mg into the M2 positions was observed for most samples and is discussed in detail in Chapter Two.

Table **1.3.4-1**: EPMA chemical analysis of crystals used for SCXRD

Sample	Mg	Fe2+	Fe3+	ΣFe	Mn	Si	M1+M2
85539	0.007	1.933	0.000	1.933	0.063	0.997	2.003
112085 RRR	0.060	1.595	0.049	1.644	0.268	0.998	1.972
BA-2-1 WR1	1.715	0.271	0.003	0.274	0.006	1.001	1.995
DH101B	1.767	0.216	0.009	0.224	0.004	0.999	1.996
DH101C	1.808	0.175	0.009	0.184	0.003	0.999	1.995
DH101D	1.809	0.172	0.008	0.180	0.003	1.001	1.992
DH101E	1.813	0.168	0.011	0.179	0.003	0.999	1.994
EP3139C	1.787	0.203	0.000	0.203	0.003	1.001	1.993
EP3139D	1.795	0.194	0.000	0.194	0.003	1.001	1.992
H30B1	1.812	0.176	0.005	0.182	0.003	1.000	1.997
H30B4	1.820	0.169	0.003	0.172	0.003	1.001	1.994
KBH941	1.639	0.356	0.000	0.356	0.005	0.997	2.000
KI 3054	1.280	0.724	0.000	0.724	0.009	0.993	2.014
KI 4143	0.785	1.178	0.024	1.202	0.020	0.987	2.008
NWA 2737	1.419	0.552	0.023	0.575	0.011	0.991	2.005
LF China ✚	0.036	0.724	1.000	1.725	0.002	0.868	1.763
LL Village ✚	0.047	0.555	1.127	1.682	0.002	0.853	1.731

✚ Laihunite Samples

Table 1.3.4-2: Comparison of composition from SCXRD and EPMA

	Refinement Composition		EPMA Composition	
Sample ID	Mg	Fe	Mg	ΣFe
NMNH85539	0.11	1.89	0.01	1.93
85540	0.17	1.83		
90035	0.01	1.99		
90613	0.13	1.87		
104576	0.02	1.98		
112085	0.10	1.90	0.06	1.64
DH101B	1.82	0.18	1.77	0.22
DH101C	1.85	0.15	1.81	0.18
DH101C R2	1.86	0.14	1.81	0.18
DH101D	1.87	0.13	1.81	0.18
DH101D R2	1.86	0.14	1.81	0.18
DH101E	1.86	0.14	1.81	0.18
EP3139C	1.84	0.17	1.79	0.20
EP3139C R2	1.84	0.17	1.79	0.20
EP3139D	1.84	0.17	1.80	0.19
EP3139D R2	1.85	0.15	1.80	0.19
H30B1	1.86	0.14	1.81	0.18
H30B1 R2	1.86	0.14	1.81	0.18
H30B4	1.87	0.13	1.82	0.17
KBH941	1.68	0.32	1.64	0.36
KBH941 R2	1.68	0.32	1.64	0.36
KI3054	1.30	0.69	1.28	0.72
KI3054 R2	1.30	0.70	1.28	0.72
KI3362	1.21	0.79		
KI3648	1.45	0.55		
KI4143	0.84	1.16	0.79	1.20
KI4143 R2	0.80	1.20	0.79	1.20
Mourne	0.05	1.96		
NWA2737 R2	1.46	0.54	1.42	0.58
Rockport	0.03	1.98		
SanCarlos	1.86	0.14		
LLV ✚	0.06	1.94	0.05	1.68
LFC ✚	0.04	1.96	0.04	1.72

refinement and electron microprobe analysis

✚ Laihunite Samples

CHAPTER ONE REFERENCES

Birle, J.D., Gibbs, G.V., Moore, P.B., and Smith, J.V. (1968) Crystal structures of natural olivines. American Mineralogist, 53, 807-824.

Bragg, W.L. (1929) Atomic arrangements in the silicates. Transactions of the Faraday Society, 25, 291-314.

Bragg, W.L. (1930) The structure of Silicates. Nature, 3152, 125, 510-511.

Bragg, W.L. and Brown, G.B. (1929) Die Struktur des Olivins. Zeitschrift für Kristallographie, 63, 538.

Bragg, W.L. and West, J. (1927) The Structure of Certain Silicates. Proceedings of the Royal Society of London, Series A, 114, 768, 450-473.

Bruker (2012). APEX2. Buker AXS Inc., Madison, Wisconsin, USA.

Hazen, R.M. (1976) Effects of temperature and pressure on the crystal structure of forsterite. American Mineralogist, 61, 1280-1293.

International Tables for Crystallography (2016) Volume A: Space Group Symmetry, 896 p. Wiley, New York.

Müller, P. (2009) Practical suggestions for better crystal structures. Crystallography Reviews, 15:1, 57-83.

Robinson, K., Gibbs, G.V., and Ribbe, P.H. (1971) Quadratic Elongation: A Quantitative Measure of Distortion in Coordination Polyhedra. Science, 172, 567-570.

Sheldrick, G.M. (2007) A short history of SHELX. Acta Crystallographica Section A, A64, 112-122.

Sheldrick, G.M. (2014) Crystal structure refinement with SHELXL. Acta Crystallographica Section C, C71, 3-8.

Sheldrick, G.M. (2015) SHELXT- Integrated space-group and crystal-structure determination. Acta Crystallographica Section A, A71, 3-8.

Smyth, J.R. and Hazen, R.M. (1973) The crystal structures of forsterite and hortonolite at several temperatures up to 900 °C. American Mineralogist, 58, 588-593.

CHAPTER TWO: OBSERVED PARTITIONING OF Mg INTO THE M2 SITE IN OLIVINE GROUP MINERALS

2.1 Abstract

Previous studies have found partitioning of Fe^{2+} into the M1 site in olivine. This single crystal X-ray diffraction analysis of 30 new olivine samples further strengthens this observation. The partitioning, however, seems far more dependent on the available Mg^{2+} entering the M2 site than on a preferential partitioning of Fe^{2+} into the M1 site. In most samples studied, the percent of total magnesium in the sample that occupies the M2 position is significantly higher than the percent of total iron in the sample that occupies the M1 position. The calculated distribution coefficient (K_D) values are presented for all samples.

2.2 Introduction

Several different techniques have been employed to study the Fe^{2+}-Mg^{2+} partitioning in olivine between the two octahedral sites, M1 and M2. The primary techniques have been single crystal X-ray diffraction (e.g. Finger and Virgo, 1971) and Mössbauer spectroscopy (e.g. Takashima and Ohashi, 1968). Much of the early interest in possible partitioning involved work on lunar samples (e.g. Brown and Prewitt, 1973; Ghose et al., 1976). The majority of samples studied to date were found to have slight partitioning with more Fe^{2+} occupying the M1 site and more Mg^{2+} occupying the M2 site. Some notable exceptions include samples studied by Shinno et al. (1974) and Wenk and Raymond (1973).

The authors of these studies have offered various ideas to explain this partitioning, but it is generally agreed upon that the partitioning is an effect of temperature and bonding environment (see Kroll et al., 2006 and references therein). It is less clear whether composition influences the partitioning (Wenk and Raymond, 1973; Brown and Prewitt, 1973). The effect of temperature on Fe^{2+}-Mg^{2+} partitioning has been studied through Mössbauer spectroscopy (see Virgo and Hafner, 1972; Shinno et al., 1974; Morozov et al., 2005; and Abdu et al., 2008) and through optical absorption spectroscopy (Taran and Koch-Müller, 2006), where it has been observed that Fe^{2+} preferentially enters the M1 site with

increased temperature. Artioli et al. (1995) observed a reversal in this partitioning between 880-960 °C using single crystal neutron diffraction. Contrary to this observation, Heinemann et al. (2006) did not see Fe^{2+} entering the M2 position as temperature increases above 900°C. The calculated distribution coefficient (K_D) values given in this paper, however, do not match the values that come from the K_D formula that is given, which puts these results in question.

This study looks at previously published crystal structures of olivine and the partitioning of Fe^{2+} and Mg^{2+} between the two octahedral metal sites before comparing past results to thirty new refinements.

2.3 Experimental Methods

The site occupancies of M1 and M2 were refined using a free variable as detailed in Chapter 1. This type of refinement only allows for characterizing Fe^{2+} and Mg^{2+}. The percent of total Fe in the sample that was in the M1 site was calculated using the occupancy from the free variables and the associated estimated standard deviation (ESD) values, as was the percent of total Mg in the sample that was in the M2 site. An explanation of the calculation and the error propagation is in **Appendix E**. In addition, the calculated distribution coefficient, K_D, was calculated using the occupancy from refinement with the free variables. The calculated distribution coefficient (K_D) is determined by the formula $K_D = \frac{M2Mg * M1Fe}{M1Mg * M2Fe}$ which is equivalent to $K_D = \frac{M2Mg/M2Fe}{M1Mg/M1Fe}$. A K_D value greater than 1.0 indicates a degree of ordering of Fe^{2+} in the M1 site. Likewise, a K_D value less than 1.0 indicates a degree of ordering of Fe^{2+} in the M2 site.

2.4 Results and Discussion

2.4.1 Site occupancy

The results of the site occupancy refinements are in **Appendix F**. The percent of total iron in the sample that is in the M1 octahedron (%ΣFe M1) does not appear to be correlated to the volume of the M1 octahedron. Likewise, the percent of total magnesium in the sample that is in the M2 octahedron (%ΣMg M2) does not appear to be correlated to the volume of the M2 octahedron. See **Figure 2.4.1-1** and **Figure 2.4.1-2**.

Figure 2.4.1-1: Percent of total iron in sample in the M1 octahedral site VS polyhedron volumes

a) %ΣFe M1 VS volume of M1 octahedron

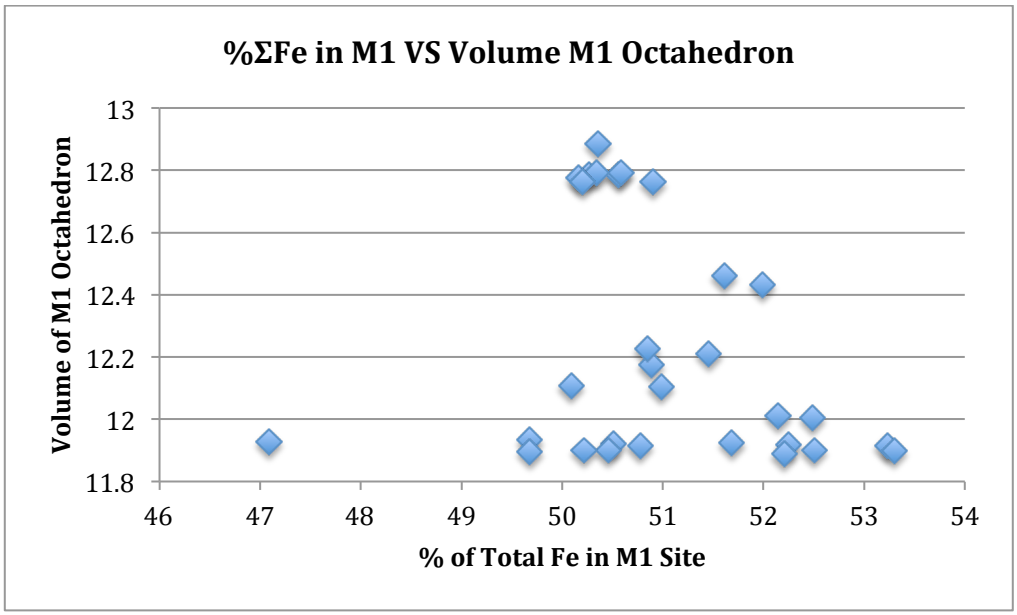

b) %ΣFe M1 VS volume of M2 octahedron

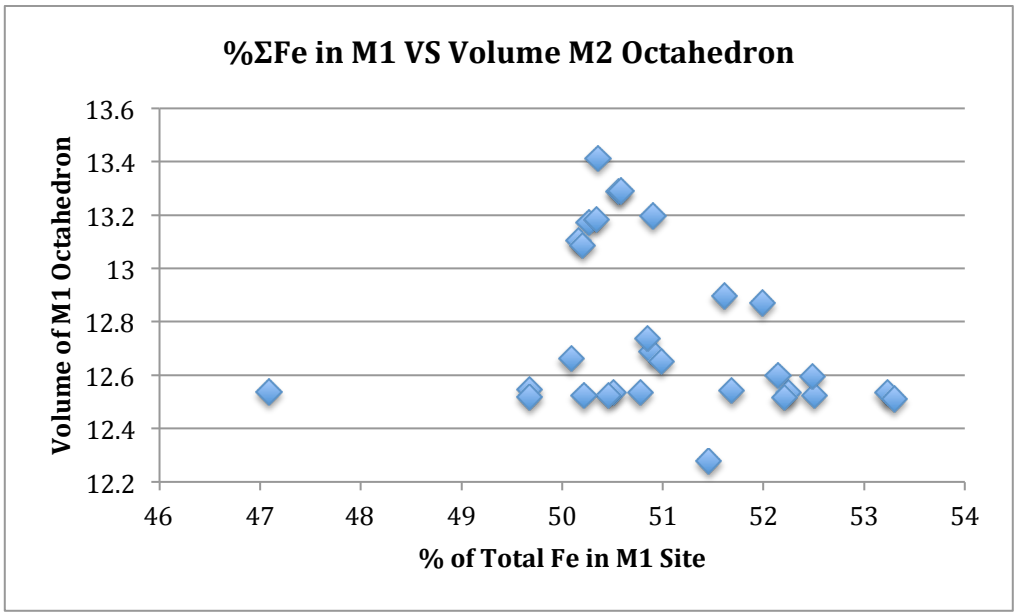

c) %ΣFe M1 VS volume of Si tetrahedron

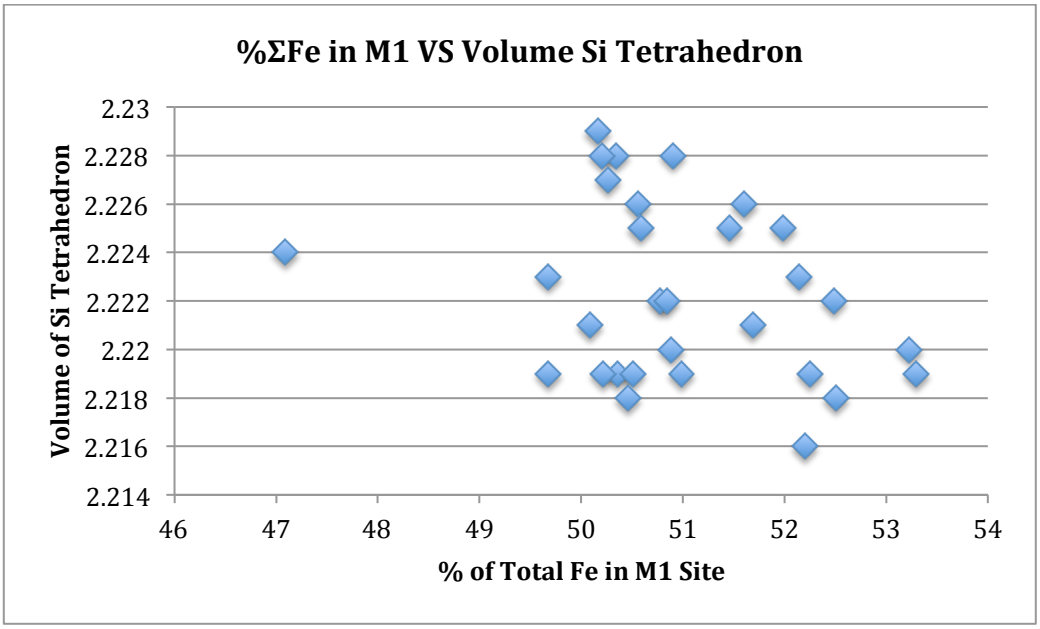

Figure 2.4.1-2: Percent of total magnesium in sample in the M2 octahedral site VS polyhedron volumes

a) %ΣMg M2 VS volume of M1 octahedron

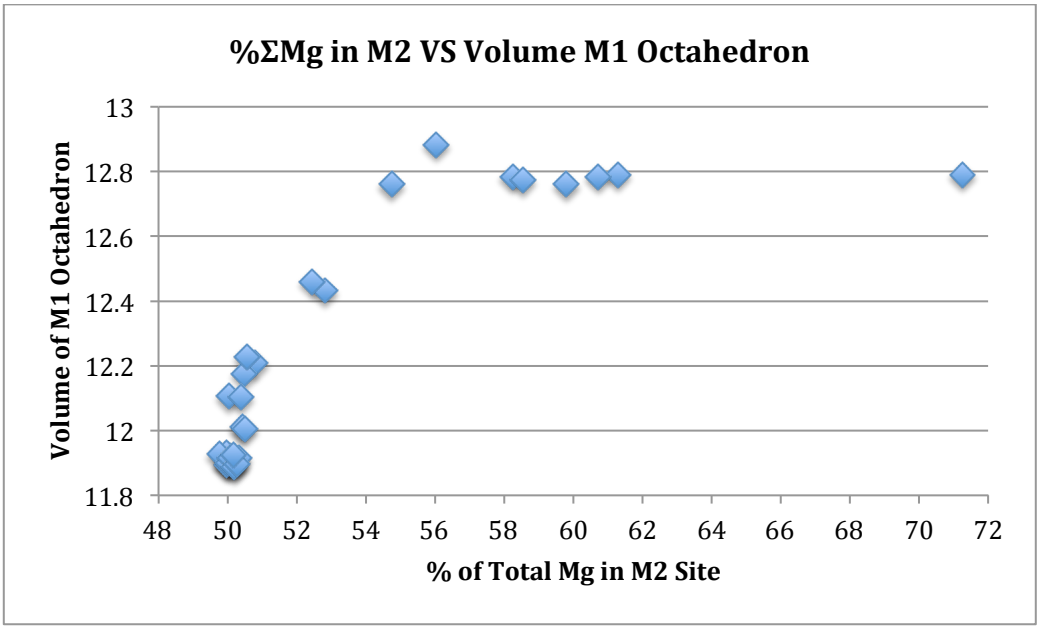

b) %ΣMg M2 VS volume of M2 octahedron

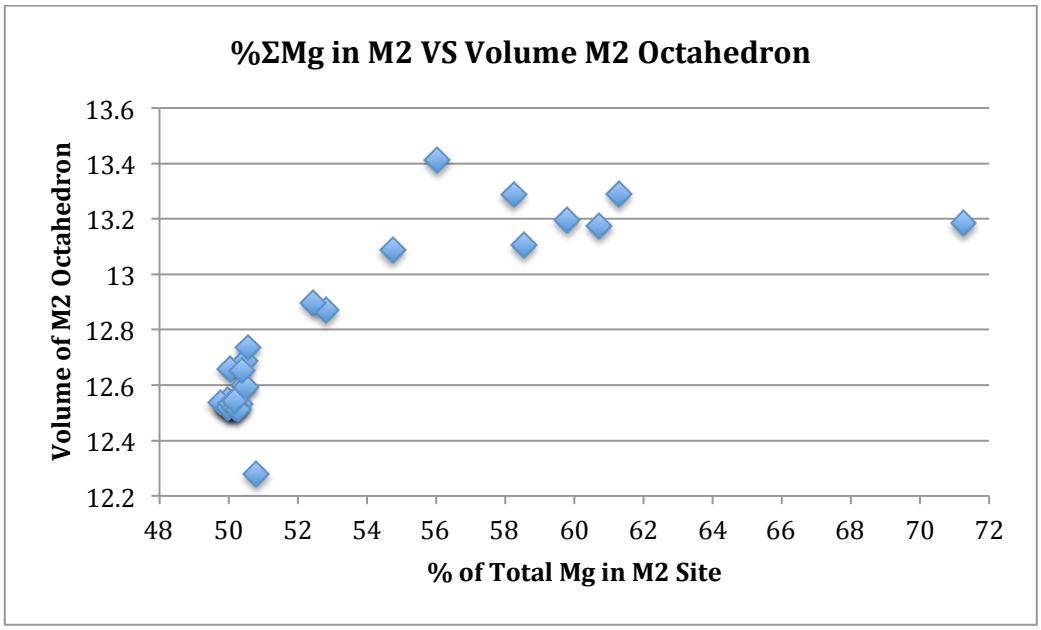

c) %ΣMg M2 VS volume of Si tetrahedron

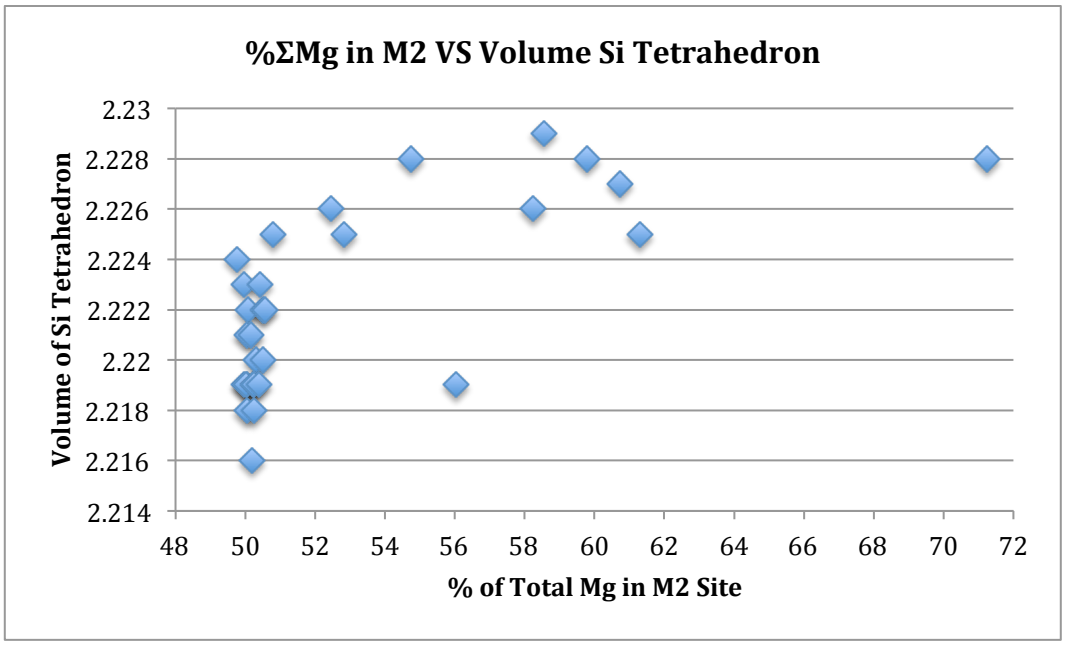

The partitioning of Fe^{2+} and Mg^{2+} in olivine is often expressed in terms of Fe^{2+} in the M1 site, though the correlation is stronger between Mg^{2+} and the M2 site. At low levels of total Mg in the sample, the %ΣMg values are consistently above 50% for Mg in the M2 site. For low levels of iron, however, the %ΣFe values are not as consistently above 50% for Fe in the M1 site. See **Figure 2.4.1-3**.

A convincing line of best fit cannot be drawn for the iron preferentially entering the M1 site, however some of the samples with low iron, and therefore high magnesium, content showed the most preference even within experimental error. These observations align with previous conclusions by Bush et al. (1970) where Mössbauer data was used to show iron-rich olivine to have nearly no ordering while magnesium-rich olivine had approximately 10% more iron in one of the metal sites. The samples in this study, however, did not show iron preference in the M1 site on the order of 10%. The highest points were at 53.30% and 53.23% of the total iron in the sample occupying the M1 site, which is approximately 6% more iron in the M1 site vs the M2 site. Brown and Prewitt (1973) suggested this pattern is a result of Mg-rich olivine minerals crystallizing earlier than Fe-rich olivine minerals, which are more ordered.

At very low levels of total magnesium, the ESD of the free variable was too high to use two of the samples. The percent uncertainty for sample 90035 was 104.1%, and the percent uncertainty for sample 104576 was 94.1%. These samples are removed from **Figure 2.4.1-3b** and the Rockport sample with a percent uncertainty of 45.0% is removed from **Figure 2.4.1-4** for the discussion of a trendline and from **Figure 2.4.1-4** for the discussion of the distribution coefficient values (K_D).

An attempt was made to model the Mg partitioning in the M2 site in order to predict what the partitioning may be for samples in the missing composition range of 70-85% Fe that was discussed in Chapter 1. This corresponds to the compositional gap of 15-30% Mg in **Figure 2.4.1-3b**. A power regression model was chosen, and in order to determine the uncertainty in Microsoft Excel, the power regression was converted to a linear function by taking the natural logarithm of the equation (**Figure 2.4.1-4**).

Figure 2.4.1-3: Iron Partitioning in the M1 site and Mg partitioning in the M2 site
a) %Fe in sample VS %ΣFe in M1

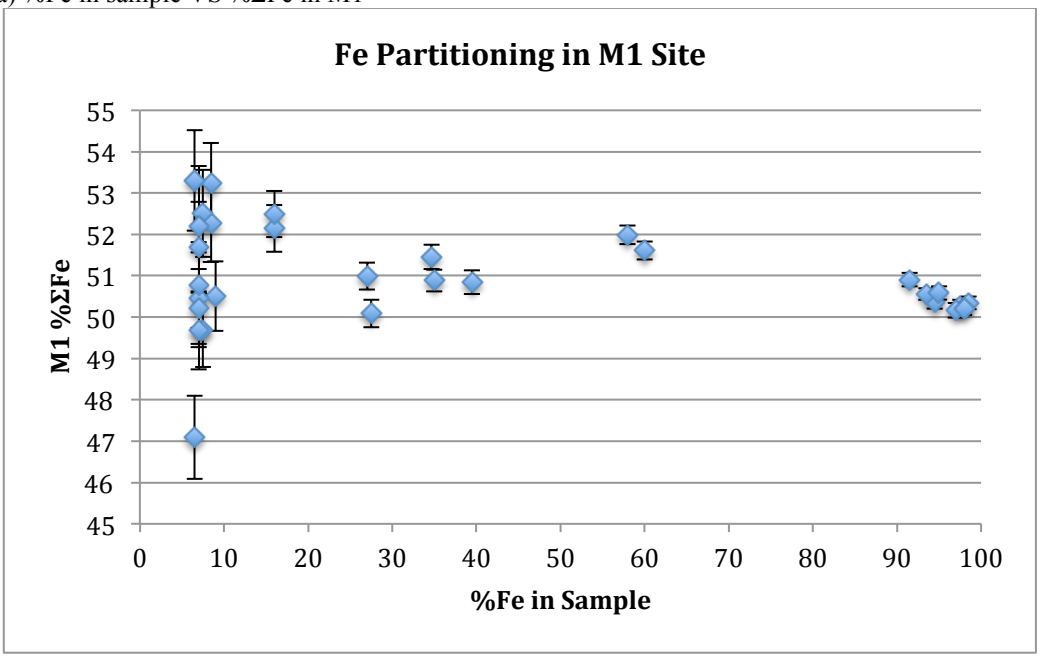

b) %Mg in sample VS %ΣMg in M2

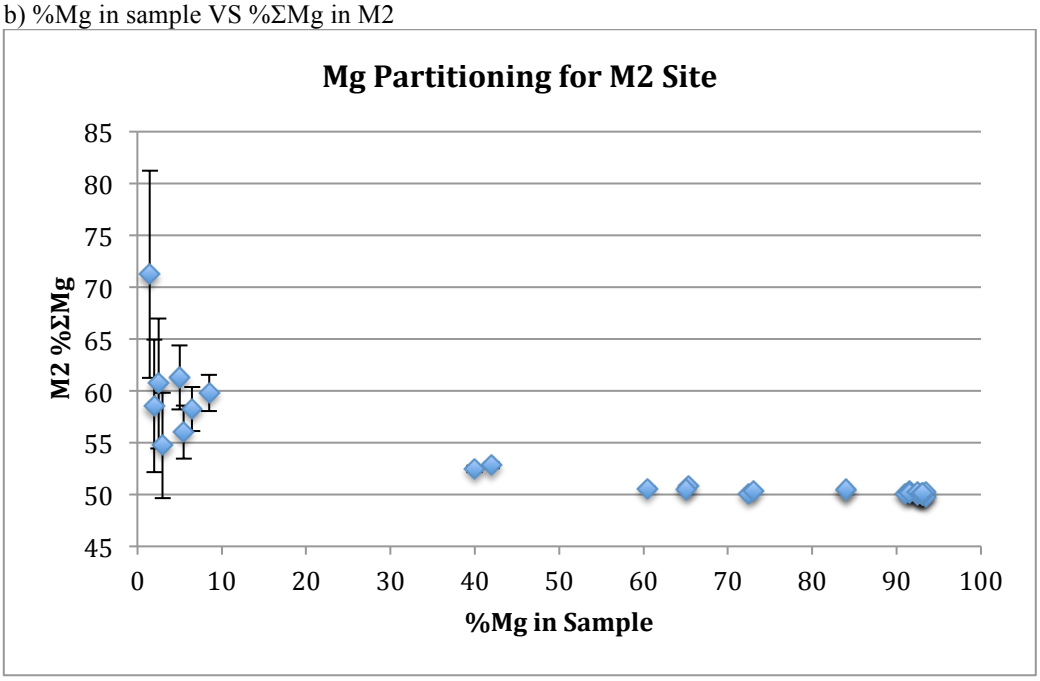

Figure 2.4.1-4: Mg partitioning in the M2 site with a power regression fit
a) M2%ΣMg with a power regression fit

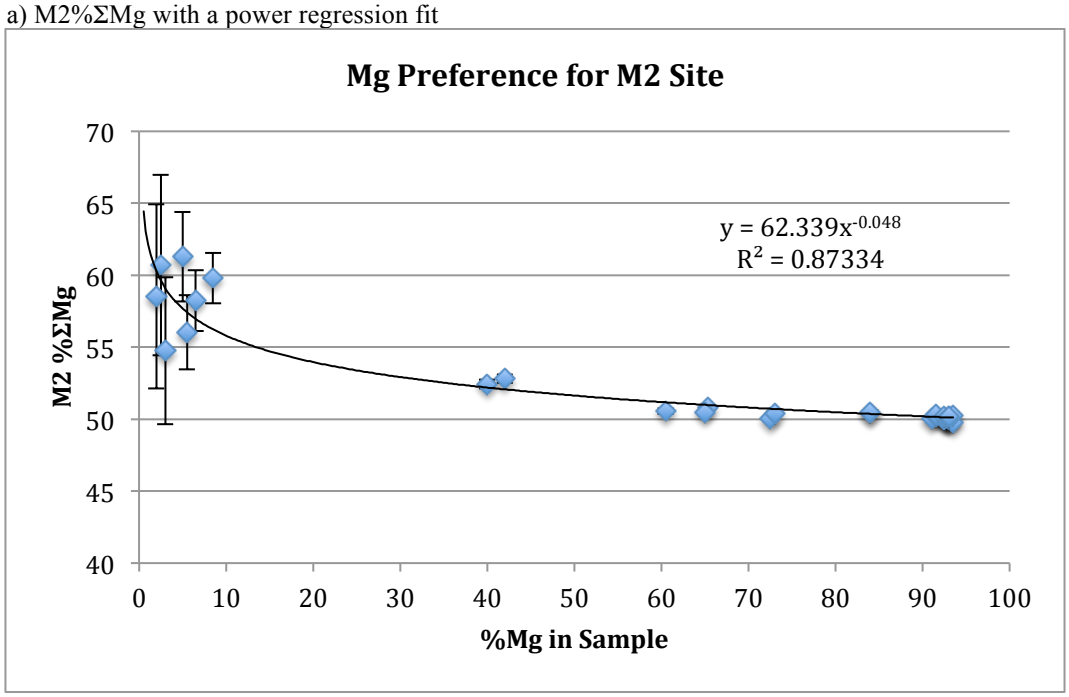

b) Natural log of power regression fit

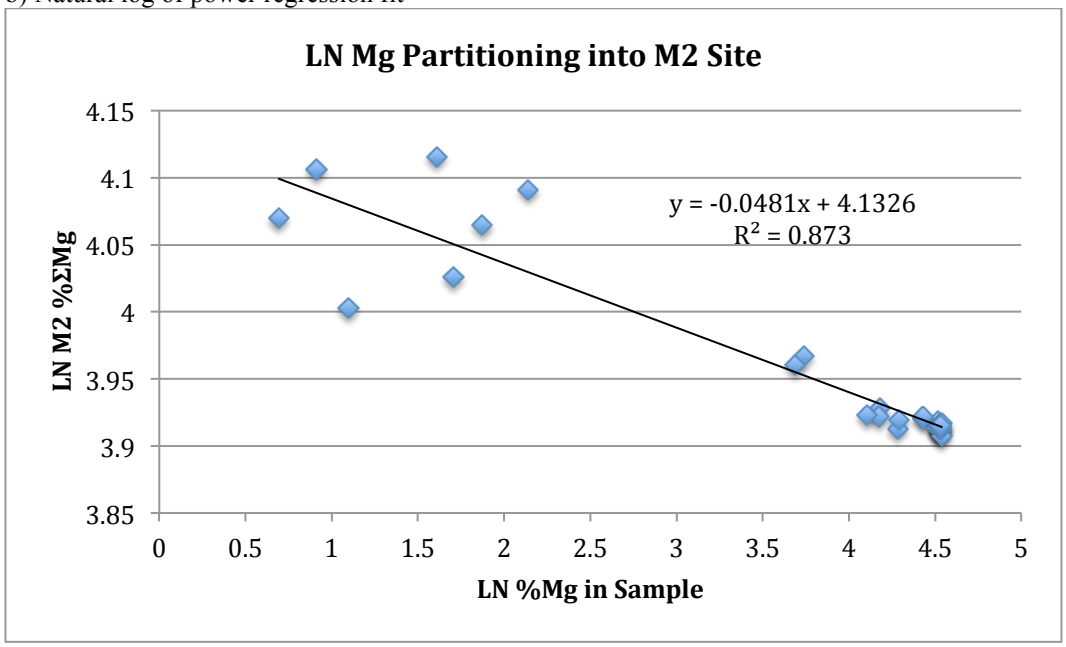

The equation for the natural log function is shown below with the uncertainties of the last digit(s) in parenthesis.

$$y = 0.0481(35)x + 4.13(1)$$

The value of such a fit is only predictive, and it will be interesting to see if samples from the missing composition ranges match the prediction once more samples are analyzed.

The distribution coefficient values (K_D) for previously published olivine structures as well as 30 new refinements are summarized in **Table 2.4.1-1** and **Table 2.4.1-2**. The M1 and M2 site occupancy refinement is sensitive to a number of factors in the refinement such as the secondary extinction coefficient (Merli et al., 2000) and the concentration of trace elements. The trace elements will affect the value of K_D, however only one sample, 112085 from Red Rock Ridge, had any significant amounts of Mn present.

Table 2.4.1-1: K_D values from past publications

Reference	**Sample Composition**		**Temp**	Occupancy							
				M1				M2			
	%Mg	**%Fe**	**°C**	Mg		Fe		Mg		Fe	
Artioli et al., 1995: N1RT	88	12	RT	0.879		0.121	(11)	0.881		0.119	(11)
Brown and Prewitt, 1973: Lunar Rock 12052	69	31	RT 24	0.675		0.325		0.705		0.285	
Brown and Prewitt, 1973: Lunar Rock 12018	82	18	RT	0.814		0.186		0.826		0.164	
Brown and Prewitt, 1973: Metamorphic OG2B	71	29	RT	0.708		0.292		0.712		0.288	
Finger, 1971: 10020	73.15	26.45	RT	0.729	(5)	0.271	(5)	0.734	(5)	0.258	(5)
Finger, 1971: C15-64	49.00	50.65	RT	0.477	(4)	0.523	(4)	0.503	(4)	0.490	(4)
Finger and Virgo 1971: Lunar Olivine B1/12018	82.5	16.5	RT 24	0.807	(4)	0.192	(4)	0.846	(4)	0.147	(4)
Ghose et al., 1976: Anorthosite 67075	49.73	49.49	RT	0.475	(2)	0.525	(2)	0.520		0.480	
Heinemann et al., 2006: Bo-2-1	52	48	"as is"	0.4954	(6)	0.5046	(6)	0.5695	(6)	0.4305	(6)
Heinemann et al., 2006: Bo-5-1	52	48	"as is"	0.4915	(9)	0.5085	(9)	0.5734	(9)	0.4266	(9)
Heinemann et al., 2006: Bo-8-1	52	48	"as is"	0.4931	(7)	0.5069	(7)	0.5718	(7)	0.4282	(7)
Heinemann et al., 2006: Bo-10-1	52	48	20	0.4874	(7)	0.5126	(7)	0.5775	(7)	0.4225	(7)
Heinemann et al., 2007: Fa 11.6	88.4	11.6	"as is"	0.8834	(10)	0.1166	(10)	0.8766	(10)	0.1134	(10)
Heinemann et al., 2007: Fa 22.3	77.7	22.3	20	0.7636	(8)	0.2364	(8)	0.7805	(8)	0.2073	(8)
Heinemann et al., 2007: Fa 27.8	72.2	27.8	"as is"	0.7055	(7)	0.2945	(7)	0.7265	(7)	0.2573	(7)
Liang and Hawthorne, 1994: Ol SC	88.50	11.85	RT	0.904	(3)	0.096	(3)	0.912	(3)	0.088	(3)
Smyth and Hazen, 1973: Hortonolite	37.5	55.0	RT 20	0.361		0.639	(2)	0.389		0.611	
Wenk and Raymond, 1973				0.895	(8)	0.104	(2)	0.891	(9)	0.108	(2)
Wenk and Raymond, 1973				0.665	(6)	0.334	(4)	0.678	(4)	0.311	(6)
Wenk and Raymond, 1973				0.625	(8)	0.374	(2)	0.648	(2)	0.341	(8)

Reference	Sample Composition		KD *	
	%Mg	%Fe		
Artioli et al., 1995: N1RT	88	12	1.02	(13)
Brown and Prewitt, 1973: Lunar Rock 12052	69	31	1.19	(3)
Brown and Prewitt, 1973: Lunar Rock 12018	82	18	1.15	(3)
Brown and Prewitt, 1973: Metamorphic OG2B	71	29	1.02	(4)
Finger, 1971: 10020	73.15	26.45	1.06	(5)
Finger, 1971: C15-64	49.00	50.65	1.13	(4)
Finger and Virgo 1971: Lunar Olivine B1/12018	82.5	16.5	1.37	(4)
Ghose et al., 1976: Anorthosite 67075	49.73	49.49	1.20	
Heinemann et al., 2006: Bo-2-1	52	48	1.35	
Heinemann et al., 2006: Bo-5-1	52	48	1.39	
Heinemann et al., 2006: Bo-8-1	52	48	1.37	
Heinemann et al., 2006: Bo-10-1	52	48	1.44	
Heinemann et al., 2007: Fa 11.6	88.4	11.6	1.020	
Heinemann et al., 2007: Fa 22.3	77.7	22.3	1.166	
Heinemann et al., 2007: Fa 27.8	72.2	27.8	1.179	
Liang and Hawthorne, 1994: Ol SC	88.50	11.85	1.10	
Smyth and Hazen, 1973: Hortonolite	37.5	55.0	1.13	
Wenk and Raymond, 1973			0.96	
Wenk and Raymond, 1973			1.09	
Wenk and Raymond, 1973			1.14	

* KD for exchange reaction Mg(M2) + Fe(M1) <=> Mg(M1) + Fe(M2)
Notes for these samples are found in **Appendix G**.

Table 2.4.1-2: K_D values from new refinements

Reference		Sample Composition		Sample Temp	Occupancy							
					M1				M2			
		%Mg	%Fe	°C	Mg	ESD	Fe	ESD	Mg	ESD	Fe	ESD
Valdez Samples	85539	5.50	94.50	RT 18	0.049	0.004	0.951	0.004	0.063	0.004	0.937	0.004
	85540	8.50	91.50	RT 18	0.068	0.004	0.932	0.004	0.101	0.004	0.899	0.004
	90613	6.50	93.50	RT 18	0.053	0.004	0.947	0.004	0.074	0.004	0.926	0.004
	112085	5.00	95.00	RT 18	0.038	0.004	0.962	0.004	0.060	0.004	0.940	0.004
	DH101B	91.00	9.00	RT 18	0.899	0.002	0.101	0.002	0.901	0.002	0.099	0.002
	DH101C	92.50	7.50	RT 18	0.908	0.002	0.092	0.002	0.906	0.003	0.094	0.003
	DH101C R2	93.00	7.00	RT 18	0.914	0.002	0.086	0.002	0.913	0.002	0.087	0.002
	DH101D	93.50	6.50	RT 18	0.928	0.002	0.072	0.002	0.919	0.003	0.081	0.003
	DH101D R2	93.00	7.00	RT 18	0.912	0.002	0.088	0.002	0.914	0.003	0.086	0.003
	DH101E	93.00	7.00	RT 18	0.913	0.002	0.087	0.002	0.914	0.002	0.086	0.002
	EP3139C	91.54	8.46	RT 18	0.904	0.002	0.096	0.002	0.913	0.002	0.087	0.002
	EP3139C R2	91.54	8.46	RT 18	0.905	0.002	0.095	0.002	0.916	0.002	0.084	0.002
	EP3139D R2	92.50	7.50	RT 18	0.911	0.002	0.089	0.002	0.919	0.002	0.081	0.002
	H30B1	93.00	7.00	RT 18	0.913	0.002	0.087	0.002	0.915	0.003	0.085	0.003
	H30B1 R2	93.00	7.00	RT 18	0.918	0.003	0.082	0.003	0.925	0.003	0.075	0.003
	H30B4	93.50	6.50	RT 18	0.920	0.002	0.080	0.002	0.930	0.002	0.070	0.002
	KBH941	84.00	16.00	RT 18	0.826	0.002	0.174	0.002	0.841	0.003	0.159	0.003
	KBH941 R2	84.00	16.00	RT 18	0.825	0.002	0.175	0.002	0.841	0.002	0.159	0.002
	KI3054	65.33	34.67	RT 18	0.636	0.003	0.364	0.003	0.656	0.003	0.344	0.003
	KI3054 R2	65.00	35.00	RT 18	0.638	0.002	0.362	0.002	0.650	0.003	0.350	0.003
	KI3362	60.50	39.50	RT 18	0.598	0.003	0.402	0.003	0.612	0.003	0.388	0.003
	KI3648	72.50	27.50	RT 18	0.720	0.002	0.280	0.002	0.721	0.003	0.279	0.003
	KI4143	42.00	58.00	RT 18	0.390	0.003	0.610	0.003	0.437	0.004	0.563	0.004
	KI4143 R2	40.00	60.00	RT 18	0.377	0.003	0.623	0.003	0.415	0.004	0.585	0.004
	Mourne	2.49	97.51	RT 18	0.019	0.004	0.981	0.004	0.029	0.004	0.971	0.004
	NWA2737 R2	73.00	27.00	RT 18	0.713	0.002	0.287	0.002	0.725	0.003	0.275	0.003
	Rockport	1.49	98.51	RT 18	0.009	0.004	0.991	0.004	0.023	0.004	0.977	0.004
	SanCarlos	93.00	7.00	RT 18	0.910	0.002	0.090	0.002	0.916	0.003	0.084	0.003
	LLV ✚	3.00	97.00	RT 18	0.030	0.005	0.970	0.005	0.037	0.005	0.963	0.005
	LFC ✚	2.00	98.00	RT 18	0.019	0.004	0.981	0.004	0.027	0.004	0.973	0.004

* K_D for exchange reaction Mg(M2) + Fe(M1) <=> Mg(M1) + Fe(M2)

✚ Laihunite Samples

Reference		Sample Composition		KD *
		%Mg	%Fe	
Valdez Samples	85539	5.50	94.50	1.293
	85540	8.50	91.50	1.542
	90613	6.50	93.50	1.426
	112085	5.00	95.00	1.621
	DH101B	91.00	9.00	1.023
	DH101C	92.50	7.50	0.986
	DH101C R2	93.00	7.00	0.986
	DH101D	93.50	6.50	0.881
	DH101D R2	93.00	7.00	1.020
	DH101E	93.00	7.00	1.010
	EP3139C	91.54	8.46	1.104
	EP3139C R2	91.54	8.46	1.153
	EP3139D R2	92.50	7.50	1.116
	H30B1	93.00	7.00	1.035
	H30B1 R2	93.00	7.00	1.100
	H30B4	93.50	6.50	1.154
	KBH941	84.00	16.00	1.109
	KBH941 R2	84.00	16.00	1.127
	KI3054	65.33	34.67	1.094
	KI3054 R2	65.00	35.00	1.057
	KI3362	60.50	39.50	1.057
	KI3648	72.50	27.50	1.005
	KI4143	42.00	58.00	1.212
	KI4143 R2	40.00	60.00	1.176
	Mourne	2.49	97.51	1.562
	NWA2737 R2	73.00	27.00	1.056
	Rockport	1.49	98.51	2.512
	SanCarlos	93.00	7.00	1.077
	LLV ✚	3.00	97.00	1.218
	LFC ✚	2.00	98.00	1.424

* KD for exchange reaction Mg(M2) + Fe(M1) <=> Mg(M1) + Fe(M2)
✚ Laihunite Samples

2.4.2 Calculated distribution coefficients

There is a general trend of less site preference for magnesium-rich olivine group minerals, as was shown in **Figure 2.4.1-3b**. This is also reflected by the K_D values, shown in **Figure 2.4.2-1**. The K_D values in general decrease as the percent of magnesium in the sample increases. It is possible that the distribution of K_D values at low levels of total magnesium represents the same break in linear trends that was observed in Chapter 1 for high levels of total iron. There is, however, a broad distribution of K_D values at both low and high levels of total magnesium, which could make drawing that conclusion difficult, even with more data in the 15-30% total magnesium range.

Figure 2.4.2-1: K_D VS %Mg in sample

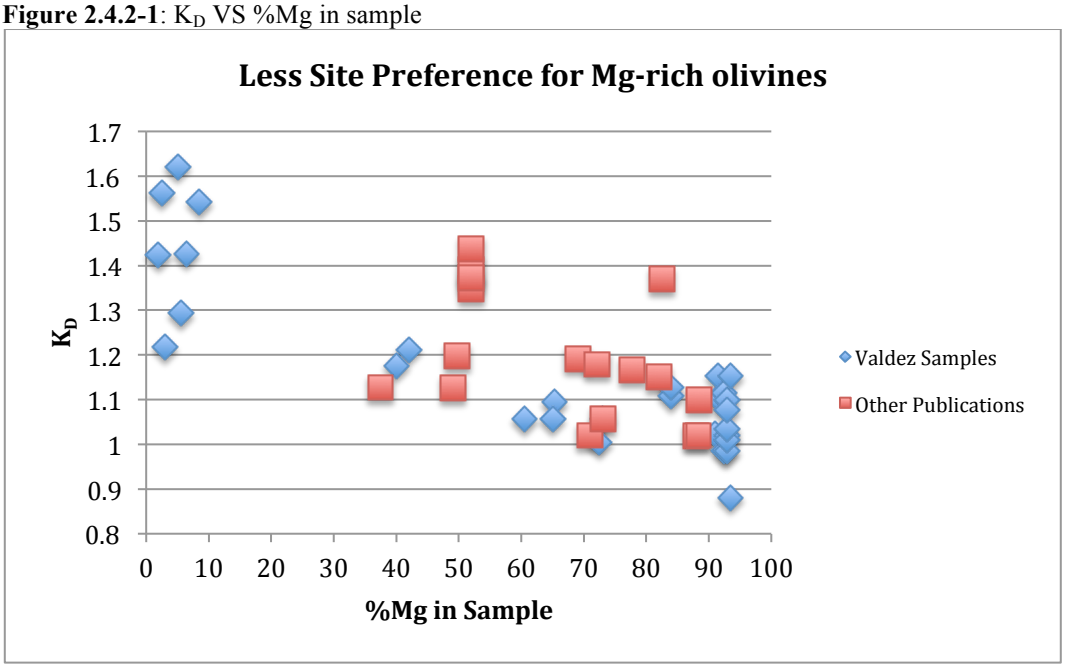

A few K_D values stand out from the set and belong to samples from the Dish Hill, California region. DH101C, DH101C_R2, and DH101D all have a K_D value below 1.0, indicating ordering of Fe^{2+} in the M2 site. This is possibly due to Fe^{3+} content. DH101C has 4.7% Fe^{3+} and DH101D has 4.5% Fe^{3+}, which is not unusually high or low for the set of samples, however Banfield (1992) described thin layers of laihunite in a Dish Hill olivine, and the laihunite structure has vacancies, which can alter the K_D value.

2.4.3 Bonding environment

It has been suggested that Fe^{2+} might fit better into the M1 site because it is of a smaller ionic radius than Mg^{2+} (Grum Grizhimailo et al., 1969). Some papers, however, state that Fe^{2+} has the larger ionic radius in octahedral coordination (Brown and Prewitt, 1973; Ghose et al., 1976). These claims have been made about the relative ionic radius of Fe^{2+} and Mg^{2+} in olivine without any measurements, and it would be prudent to measure the ionic radii using an electron density map per Gibbs et al. (1992). The presence of more than one element in the metal sites would disrupt these calculations, so a synthetic forsterite such as the one used by Hazen (1976) would be ideal, as would a fayalite sample with no Fe^{3+}.

There is also disagreement in the literature about which site is more distorted. Brown and Prewitt (1973) and Ghose et al. (1976) determined M1 to be the more distorted site. However, Grum-Grzhimailo et al. (1969) indicate the M1 site is less distorted. The extent of distortion can be quantified by the mean quadratic elongation (λ_{oct}), but it was shown in Chapter 1 that this was not significantly different between the two octahedral sites. Robinson et al. (1971) provide a second means of quantification, the bond angle variance (σ^2), which will be investigated in future work.

If the bond angle variance proves to be correlated to Fe^{2+} partitioning into the more distorted M1 site, there is one possible explanation. Bush et al. (1970) give the examples of the orthopyroxene system, $(Mg,Fe)SiO_3$, and the cummingtonite-grunerite system, $(Mg,Fe)_7Si_8O_{22}(OH)_2$, where octahedrally-coordinated Fe^{2+} is preferentially located in the more distorted octahedral site and Mg^{2+} is predominately in the more symmetrical octahedral site. The two octahedral sites in olivine, however, are not as different as the octahedral sites in the two other systems (Bush et al. 1970), which might be the reason some samples do not show a site preference within experimental error.

CHAPTER TWO REFERENCES

Abdu, Y.A., Annersten, H., Ericsson, T., Hawthorne, F.C. (2008) High-temperature cation ordering in olivine: an *in situ* Mössbauer study of synthetic $(Mg_{0.55}Fe_{0.45})_2$ SiO_4. Hyperfine Interact, 186, 99-103.

Artioli, G., Rinaldi, R., Wilson, C.C., and Zanazzi, P.F. (1995) High-temperature Fe-Mg cation partitioning in olivine: In-situ single-crystal neutron diffraction study. American Mineralogist, 80, 197-200.

Banfield, J.F., Dyar, M.D., McGuire, A.V. (1992) The defect microstructure of oxidized mantle olivine from Dish Hill, California. American Mineralogist, 77, 977-986.

Brown, G.E., and Prewitt, C.T. (1973) High-temperature crystal chemistry of hortonolite. American Mineralogist, 58, 577-587.

Bush, W.R., Hafner, S.S., Virgo, D. (1970) Some Ordering of Iron and Magnesium at the Octahedrally Coordinated Sites in a Magnesium-rich Olivine. Nature, 227, 1339-1341.

Finger, L.W. (1970) Fe/Mg ordering in olivines. Carnegie Institution of Washington Yearbook 1969-1970, 302-305.

Finger, L.W. and Virgo, D. (1971) Confirmation of Fe.Mg ordering in olivines. Carnegie Institution of Washington Yearbook 1969-1970, 221-225.

Ghose, S., Wan, C., McCallum, I.S. (1976) Fe^{2+}-Mg^{2+} order in an olivine from the lunar anorthosite 67075 and the significance of cation order in lunar and terrestrial olivines. Indian Journal of Earth Sciences, 3, 1, 1-8.

Gibbs, G.V., Spackman, M.A., Boisen, M.B., Jr. (1992) Bonded and promolecule radii for molecules and crystals. American Mineralogist, 77, 741-750.

Grum-Grzhimailo, S.V., Boksha, O.N., and Varina, T.M. (1969) The absorption spectrum of olivine. Soviet Physics- Crystallography, 14, 2, 272-274.

Hazen, R.M. (1976) Effects of temperature and pressure on the crystal structure of forsterite. American Mineralogist, 61, 1280-1293.

Heinemann, R., Kroll, H., Kirfel, A., and Barbier, B. (2006) Order and anti-order in olivine I: Structural response to temperature. European Journal of Mineralogy, 18, 673-689.

Heinemann, R., Kroll, H., Kirfel, A., and Barbier, B. (2007) Order and anti-order in olivine III: Variation of the cation distribution in the Fe,Mg olivine solid solution series with temperature and composition. European Journal of Mineralogy, 19, 15-27.

Kroll, H., Kirfel, A., Heinemann, R. (2006) Order and anti-order in olivine II: Thermodynamic analysis and crystal-chemical modeling. European Journal of Mineralogy, 18, 691-704.

Liang, J. and Hawthorne, F.C. (1994) Characterization of fine-grained mixtures of rock-forming minerals by Rietveld structure refinement: olivine + pyroxene. The Canadian Mineralogist, 32, 541-552.

Merli, M., Oberti, R., Caucia, F., Ungaretti, L. (2000) Determination of site population in olivine: Warnings on X-ray data treatment and refinement. American Mineralogist, 85, 55-65.

Morozov, M., Brinkmann, C., Lottermoser, W., Tippelt, G., Amthauer, G., and Kroll, H. (2005) Octahedral cation partitioning in Mg,Fe^{2+}-olivine. Mössbauer spectroscopic study of synthetic $(Mg_{0.5}\ Fe^{2+}{}_{0.5})_2SiO_4$ (Fa_{50}). European Journal of Mineralogy, 17, 495-500.

Robinson, K., Gibbs, G.V., and Ribbe, P.H. (1971) Quadratic Elongation: A quantitative measure of distortion in coordination polyhedra. Science, 172, 567-570.

Shinno, I., Hayashi, M., Kuroda, Y. (1974) Mössbauer studies of natural olivines. Mineralogical Journal, 7, 4, 344-358.

Smyth, J.R. and Hazen, R.M. (1973) The crystal structures of forsterite and hortonolite at several temperatures up to 900 °C. American Mineralogist, 58, 588-593.

Takashima, Y., and Ohashi, S. (1968) The Mössbauer Spectra of Various Natural Minerals. Bulletin of the Chemical Society of Japan, 41, 88-93.

Taran, M.N., Matsyuk, S.S. (2013) Fe^{2+}, Mg-distribution among non-equivalent structural sites M1 and M2 in natural olivines: an optical spectroscopy study. Physical Chemistry of Minerals, 40, 309-318.

Virgo, D., Hafner, S.S. (1972) Temperature-dependent Mg, Fe distribution in a lunar olivine. Earth and Planetary Science Letters, 14, 305-312.

Wenk, H.R. and Raymond, K.N. (1973) Four new structure refinements of olivine. Zeitschrift für Kristallographie, 137, 86-105.

CHAPTER THREE: CHARACTERIZATION OF XANES SPECTRA FOR OLIVINE GROUP MINERALS AS A FUNCTION OF ORIENTATION AND COMPOSITION

3.1 Abstract

X-ray absorption near edge structure (XANES) spectra have been shown to be dependent on crystal orientation. This study characterizes the variation in spectra along the a, b, and c crystallographic axes for the orthorhombic olivine group minerals. Samples with varying compositions were used with the formula $Mg_xFe_{1-x}SiO_4$. The bulk mineral samples were analyzed with electron microprobe analysis to determine chemical composition, and with Mössbauer spectroscopy to determine Fe^{3+} content. Single crystal samples were analyzed with X-ray diffraction to determine the unit cell parameters, and were then oriented optically using a spindle stage prior to X-ray absorption spectroscopy. Where possible, the composition of each single crystal was then determined with electron microprobe analysis. The composition of the single crystals was nearly identical to the bulk analysis.

X-ray absorption spectroscopy results show the three crystallographic axes are visually distinct in the XANES region; however samples with lower iron are more easily distinguishable, possibly due to self-absorption. There is a correlation at the pre-edge between peak intensity and higher total iron content, and $\%Fe^{3+}$ does not influence this trend. The background was removed in the pre-edge region to allow for comparison of peak position relative to composition and orientation.

3.2 Introduction

The ratio of Fe^{2+} to Fe^{3+} can be calculated from synchrotron X-ray absorption data by focusing on the Fe *K*-absorption edge while using a technique known as X-ray absorption near edge structure (XANES) spectroscopy. The pre-edge peaks are caused by iron cations in different valence states and coordination polyhedra (Dyar et al., 2016), and these peaks can be fit with a calibration curve to characterize the iron in the sample (Bajt et al., 1994). This analysis, however, was developed for powdered samples and was therefore independent of crystal orientation. A separate curve is also required for each mineral group due to differences

in the coordination polyhedra (Wilke et al., 2001). See also Dyar et al. (2016) and references therein.

There are multiple appeals to developing an analogous technique for single crystal samples. For one, is not always possible to acquire enough bulk sample to perform Mössbauer analysis, and synchrotron radiation is not limited to only examining iron. Perhaps more importantly, a XANES technique that can be applied to a randomly oriented single crystal can be used for studying thin sections. This would allow the examination of zoning in individual crystals.

Previous work in X-ray absorption spectroscopy by our group has shown that features in the pre-edge and main edge regions are dependent on crystallographic orientation (Dyar et al., 2001). Thus far, orientational effects have been studied systematically for pyroxene and mica group minerals (Dyar et al., 2002b) as well as garnet group minerals (Dyar et al., 2012) and amphibole group minerals (Dyar et al., 2016). This study begins to characterize olivine group minerals, which have two distorted octahedral sites in which Fe^{2+} and Fe^{3+} can be found.

Samples for this study were oriented along the a,b, and c crystallographic axes, which correspond to one of the principal vibration directions X, Y, and Z, as olivine group minerals are orthorhombic. The optical orientation is used for three reasons: 1) it is the only way to ensure that all possible transitions are represented in the XANES spectra, 2) it is the historical convention for collecting visible and infrared spectra along the principal vibration directions, and 3) the vibration directions of mineral grains can be found in a thin section using a polarized light microscope (Dyar et al., 2016).

3.3 Experimental Methods

The same samples that were used for single crystal X-ray diffraction were optically oriented using a polarized light microscope and the program EXCALIBR (Dyar et al., 2002a; Bloss, 1981; Gunter and Twamley, 2001). X-ray absorption near edge structure (XANES) data was collected at Argonne National Laboratory Beamline 13 IDE at the Fe *K*-edge, which is at about 7,000 electron volts (eV). The XANES data were processed through an online platform operated by the University of Massachusetts (2017). The baseline was removed through the

AirPLS algorithm with a smoothness set at 1.000. The pre-edge peaks between 7109-7111 eV were fit with a Gaussian curve that calculated the height, center, and area of each peak. These data are in **Appendix H** .The samples from X-ray absorption spectroscopy (XAS) were then analyzed by electron microprobe and compared to the chemistry from single crystal X-ray diffraction refinement as outlined in Chapter 1.

3.4 Results and Discussion

3.4.1 Optical orientation

The EXCALIBR program finds the orientation of a single crystal with the use of extinction data from the polarized light microscope. The output from processing this data provides the two optic axes (for the biaxial olivine group minerals), as well as the acute angle between them, 2*V*. The 2*V* values from optical orientation are shown in **Table 3.4.1-1**. The 2V value is known to increase with increasing mole percent forsterite (%Fo), and is plotted in **Figure 3.4.1-1**.

Table 3.4.1-1: 2*V* from optical orientation

Sample	**R-squared**	**2*V* (°)**	**(ese)**
85540	0.99691	54.737	2.419
104576	0.96361	46.549	2.739
DH101B	0.96191	82.069	1.241
H30B4	0.99365	86.801	1.306
H36628	0.98913	88.538	2.169
KI3362	0.97891	85.745	0.919
KI3648	0.99224	82.961	1.418
Mourne	0.94187	58.794	2.214
Rockport	0.93118	42.801	4.986
SanCarlos	0.98643	85.546	0.701
LFC	0.98740	62.956	1.916
LLV	0.98446	61.699	1.150

Figure 3.4.1-1: %Fo VS 2*V*

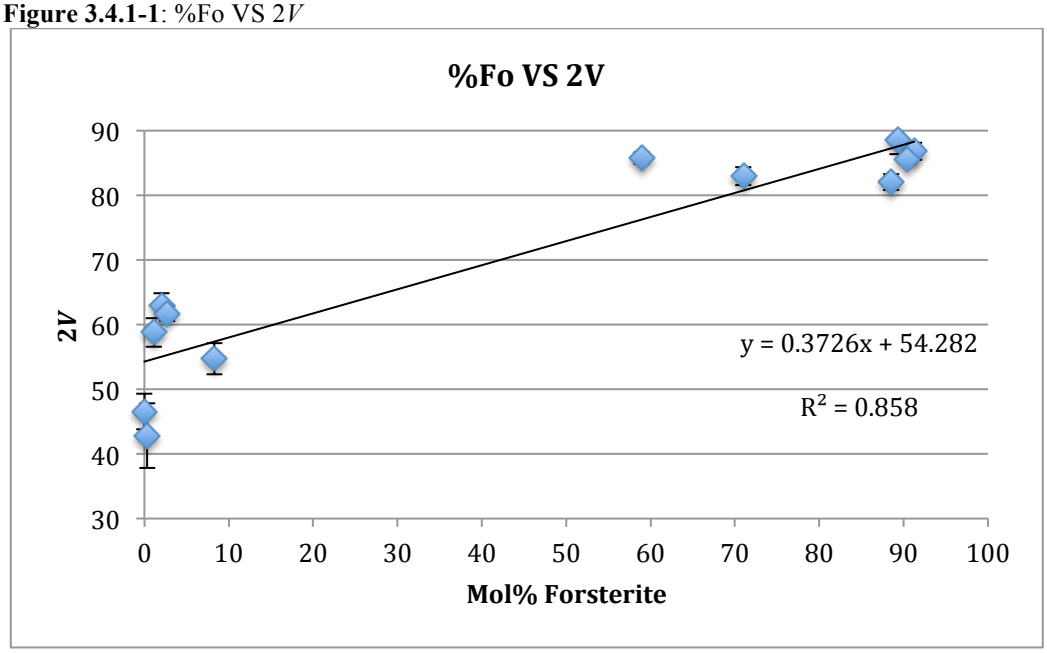

The samples ended up being oriented using X-ray data at the synchrotron, but this step is necessary for minerals that do not have an optical axis parallel to a crystallographic axis.

3.4.2 Visually distinct XANES main region

The XANES spectra proved to be dependent on orientation, both in the pre-edge and in the main region. The general shape of each orientation is visually distinct. See **Figure 3.4.2-1**. In general, the samples with lower iron have higher intensities in the main region (shown in green). This is possibly due to self-absorption.

The a crystallographic axis has a single narrow peak at around 7125 eV. The b crystallographic axis is the most distinct with two peaks. The lowest eV peak is taller than the higher eV peak. The c crystallographic orientation has a single peak with a steep slope on the left side. It is also broader than the peak in the a crystallographic orientation.

Figure 3.4.2-1: Visually distinct XANES spectra along each crystallographic axis

a) Along the a crystallographic axis

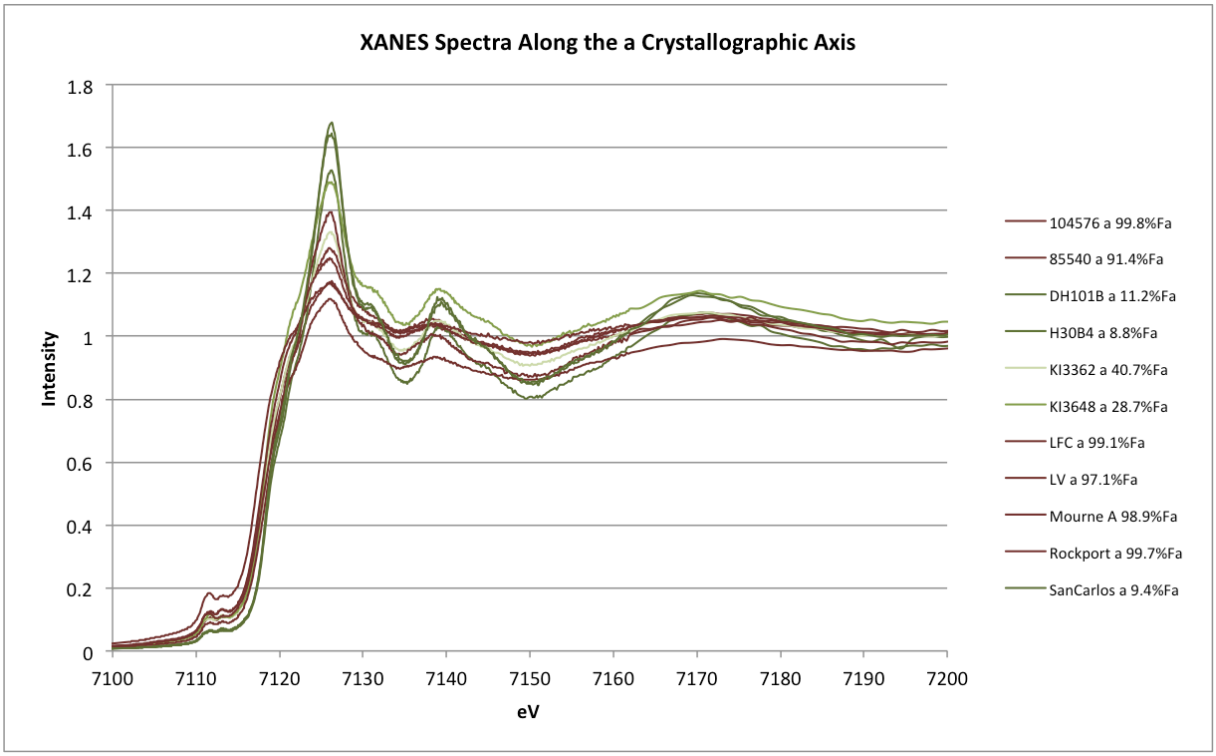

b) Along the b crystallographic axis

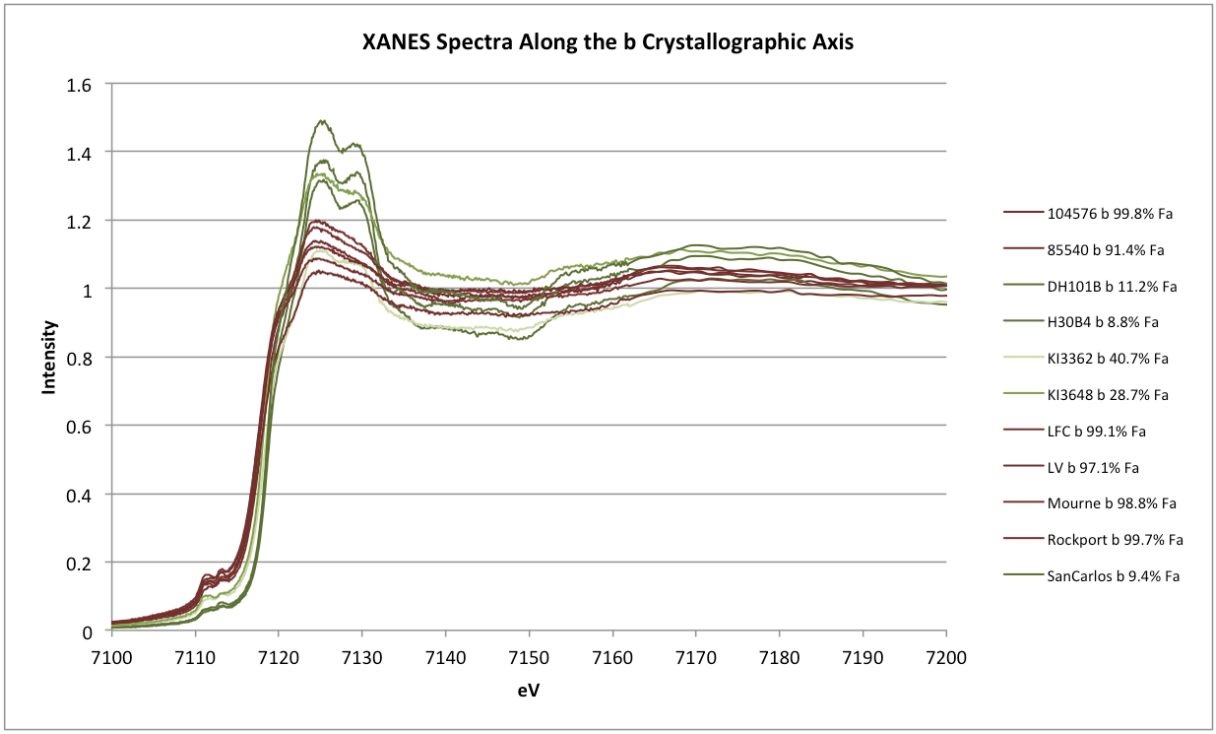

c) Along the c crystallographic axis

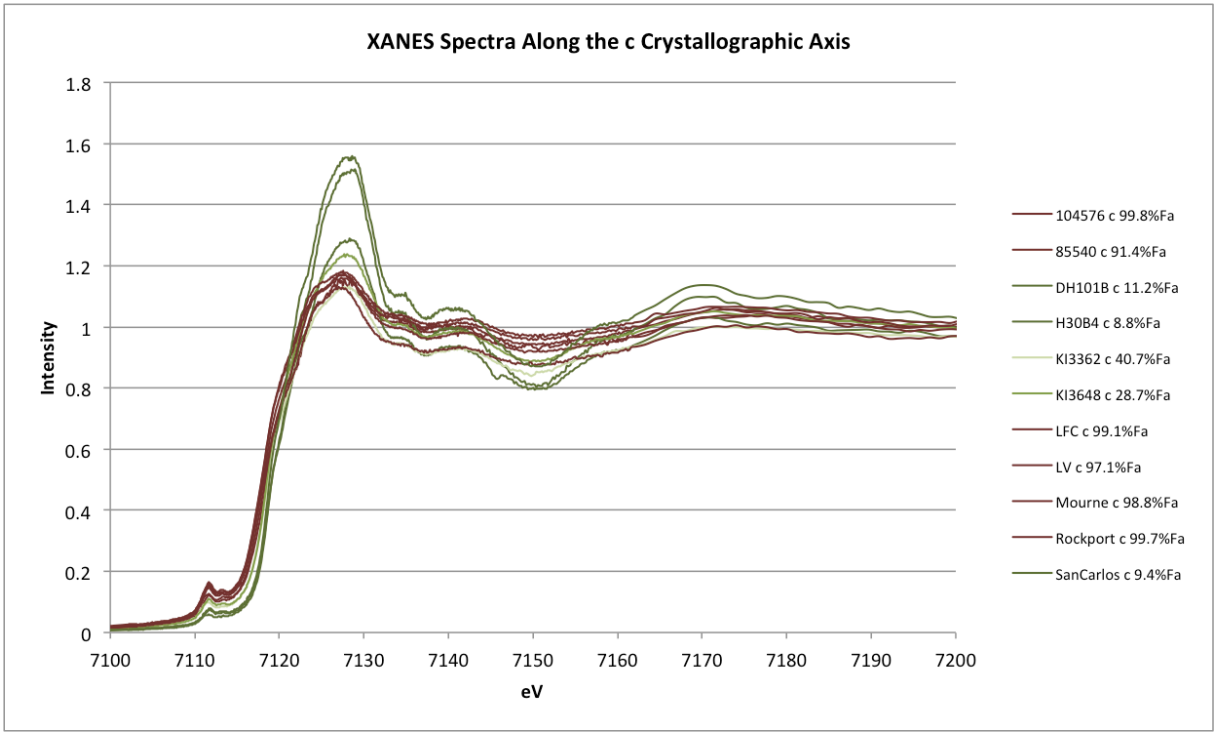

3.4.3 The pre-edge region

In contrast to the main edge region, the samples with higher total iron have higher intensity peaks in the pre-edge region (see **Figure 3.4.3-1**, shown in red). Similarly, the samples with higher Fe^{3+} content have a slight trend of higher intensity. This might be an artifact of samples with high iron having the highest $\%Fe^{3+}$ (see **Figure 3.4.3-2**).

Figure 3.4.3-1: Pre-edge region with %Fa

a) Along the a crystallographic axis

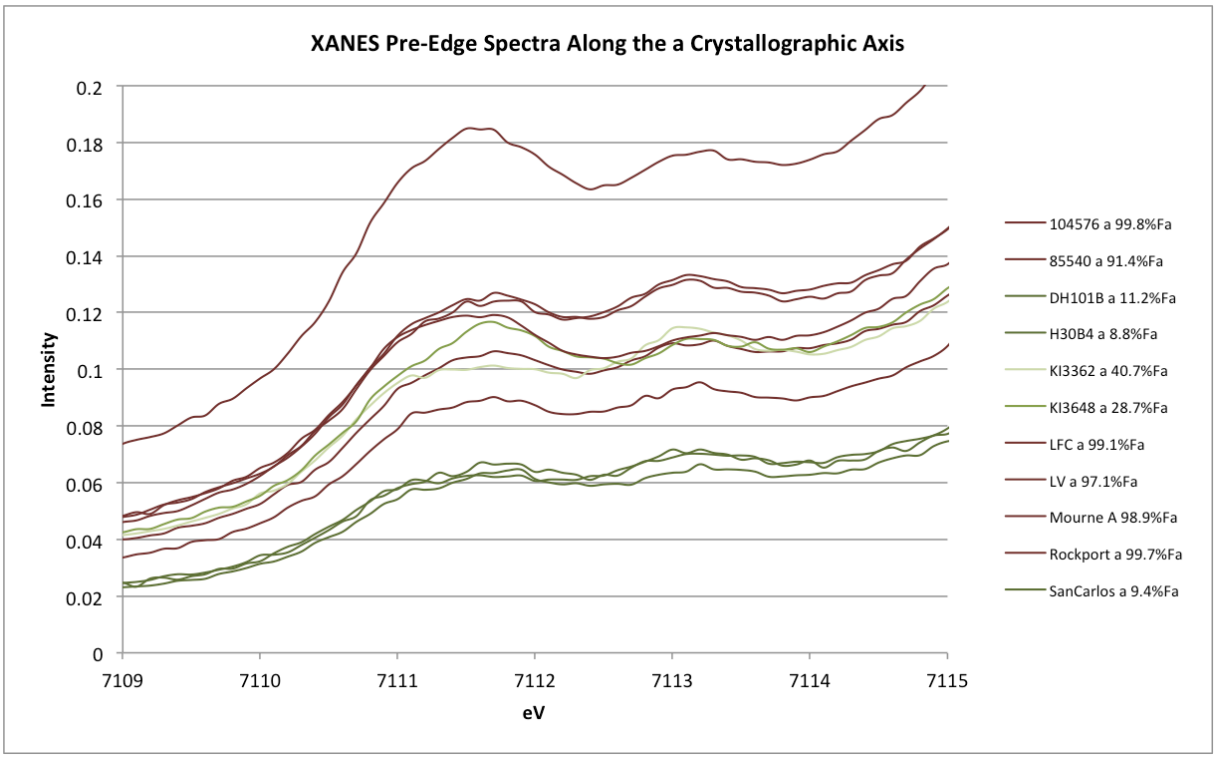

b) Along the b crystallographic axis

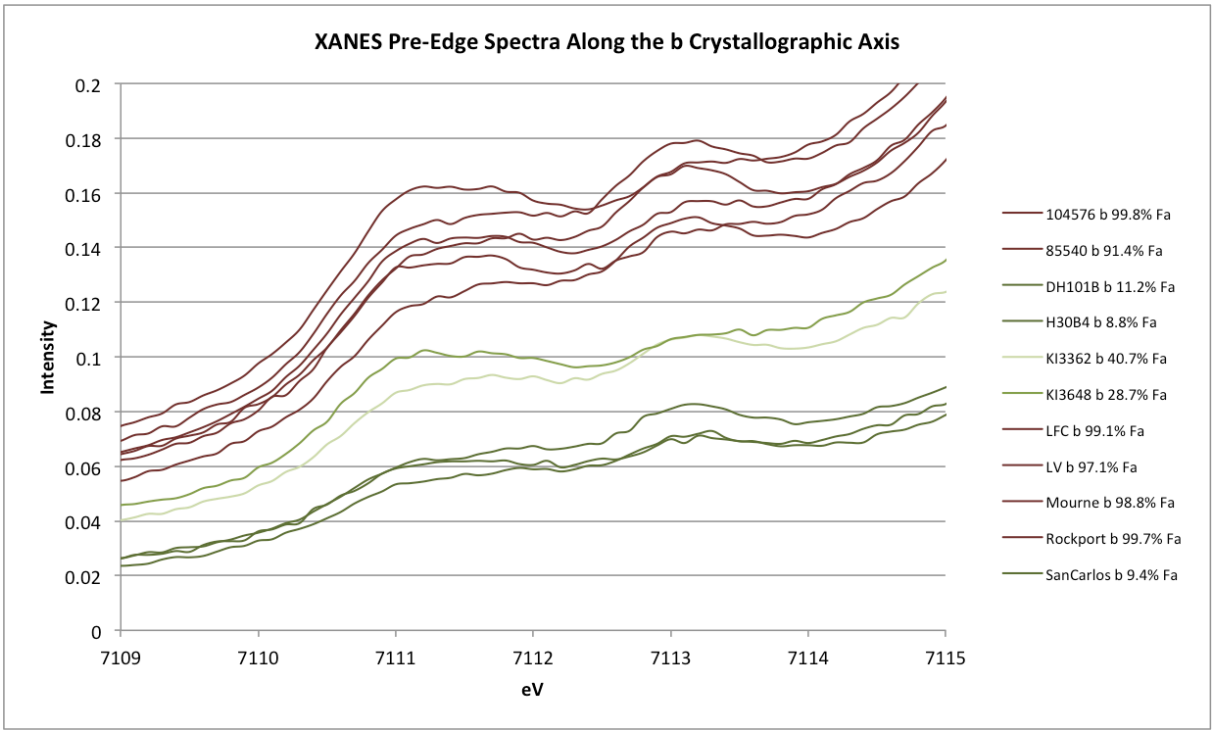

c) Along the c crystallographic axis

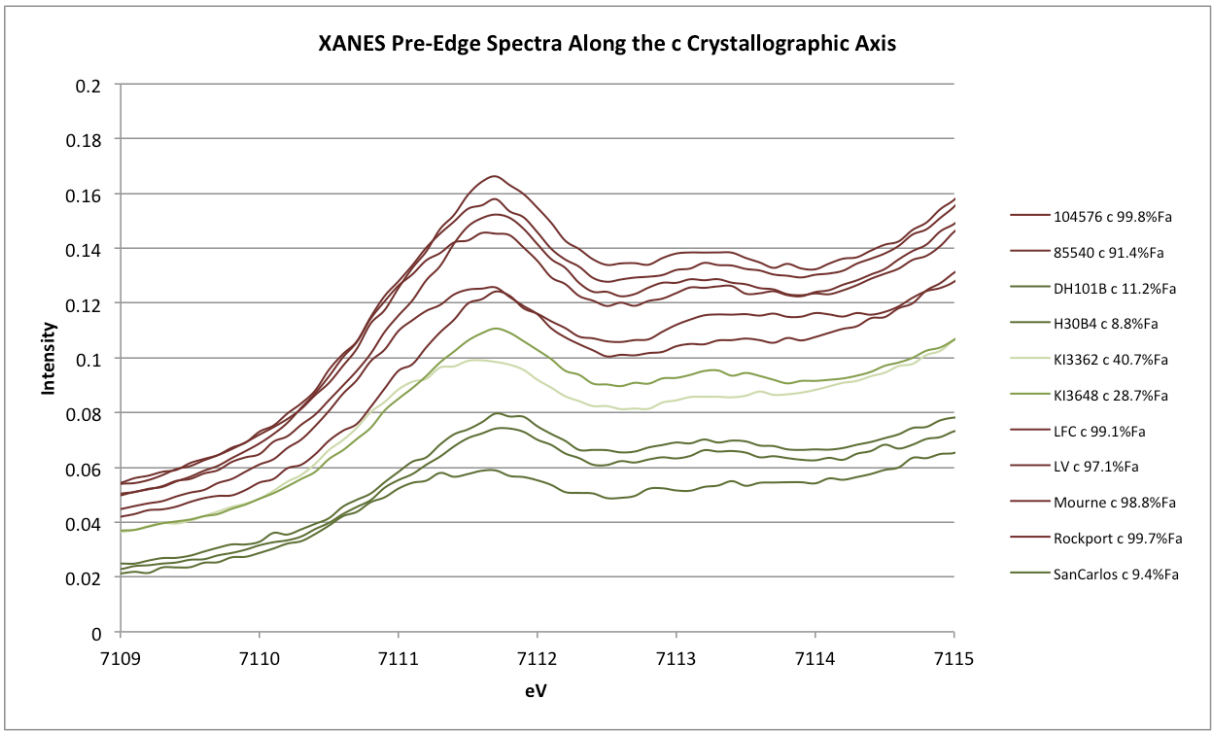

Figure 3.4.3-2: Pre-edge region with $\%Fe^{3+}$

a) Along the a crystallographic direction

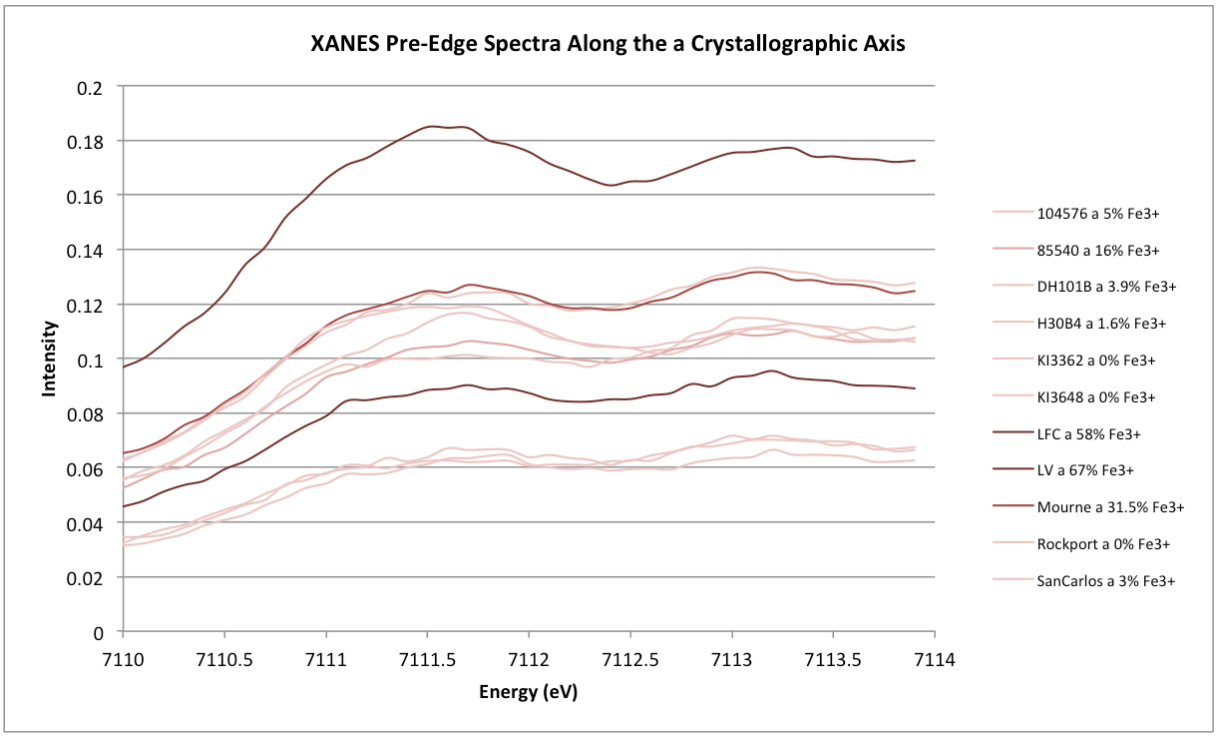

b) Along the b crystallographic direction

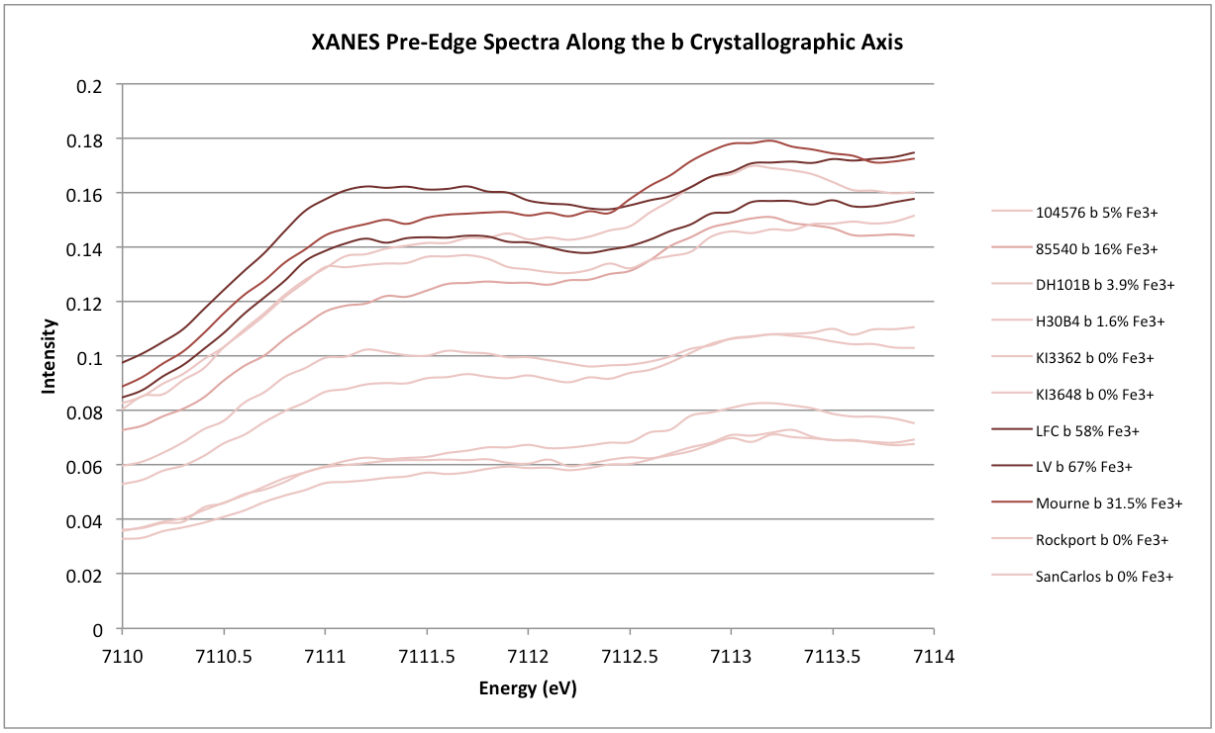

c) Along the c crystallographic direction

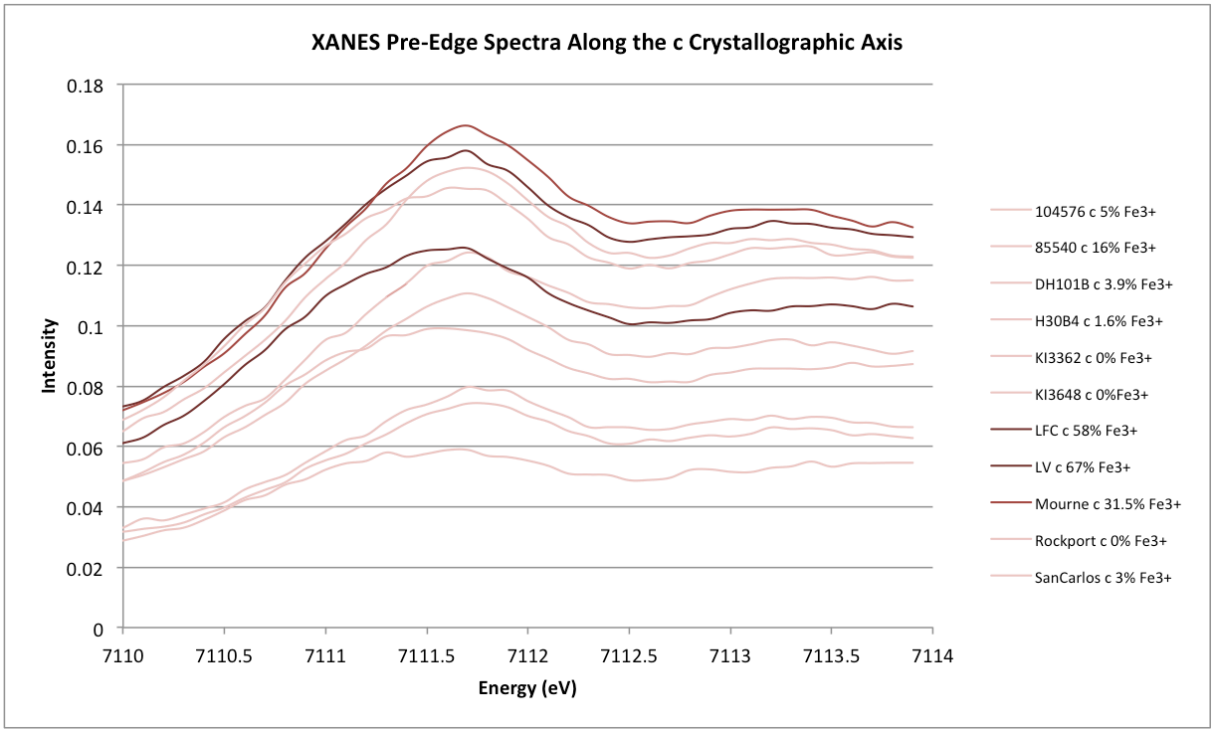

3.4.4 Pre-edge peak shifts

The centers of the pre-edge peaks shift with changing orientation of the crystallographic axes. The lowest eV peak positions are seen when the crystals are aligned along the b crystallographic axis, and the highest are seen along the c crystallographic axis. The centers of the a orientations are about midway between the other two. The shift of the center of the pre-edge peaks is not correlated to the amount of total iron in the sample (see **Figure 3.4.4-1)**, the amount of Fe^{3+} in the sample (see **Figure 3.4.4-2**), or the K_D value (see **Figure 4.4.4-3**).

The lack of a correlation between the amount of iron in the sample and the centers of the peaks suggests a systematic error in the background removal process, as the pre-edge peak fitting technique is widely accepted and has been shown to have high accuracy (Dyar et al., 2016). The results presented in this section will likely prove to have been precise, though not accurate, when the data is reprocessed using a more sophisticated background removal and peak fitting technique as described in Dyar et al. (2016). It is expected that upon reprocessing the data with a multivariate approach, the influence that the total amount of iron in the sample has on the pre-edge will be visible. This should allow a model to be constructed in the future, but three individual calibration curves will be necessary because of the separation of values along the a, b, and c crystallographic axes is a real effect.

Figure 3.4.4-1: Shift of pre-edge peaks and %Fe in sample

a) Center of peak 1

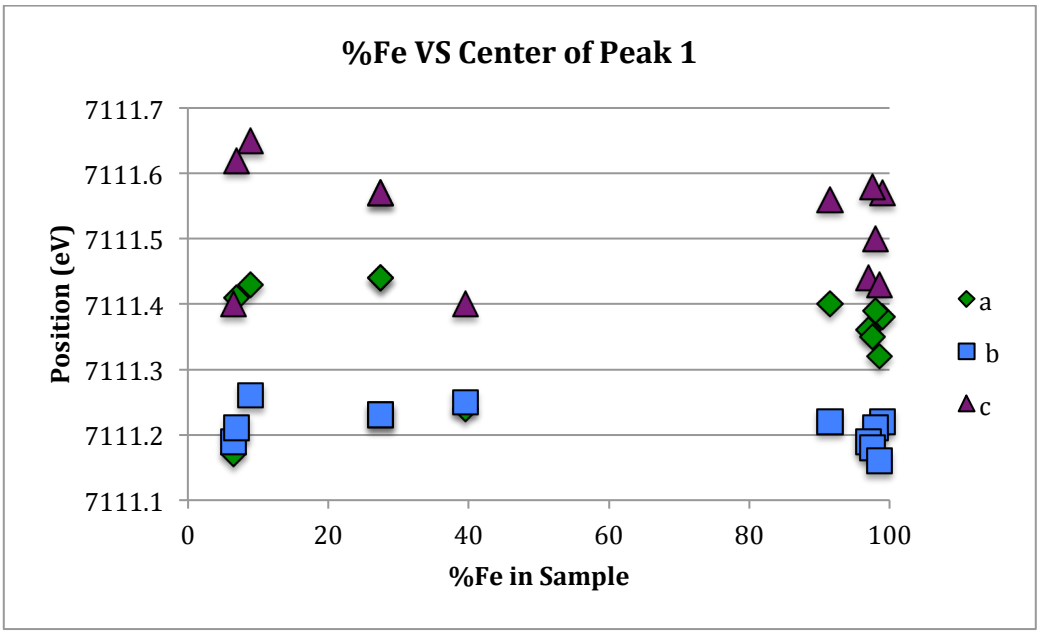

b) Center of peak 2

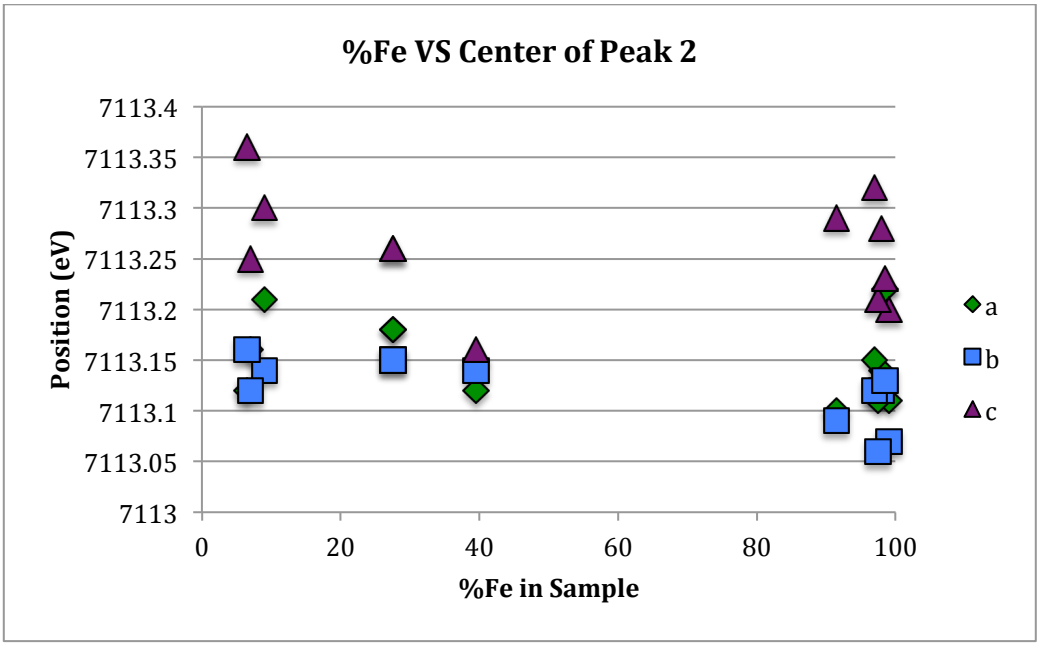

Figure 3.4.4-2: shift of pre-edge peaks and %Fe^{3+} in sample

a) Center of peak 1

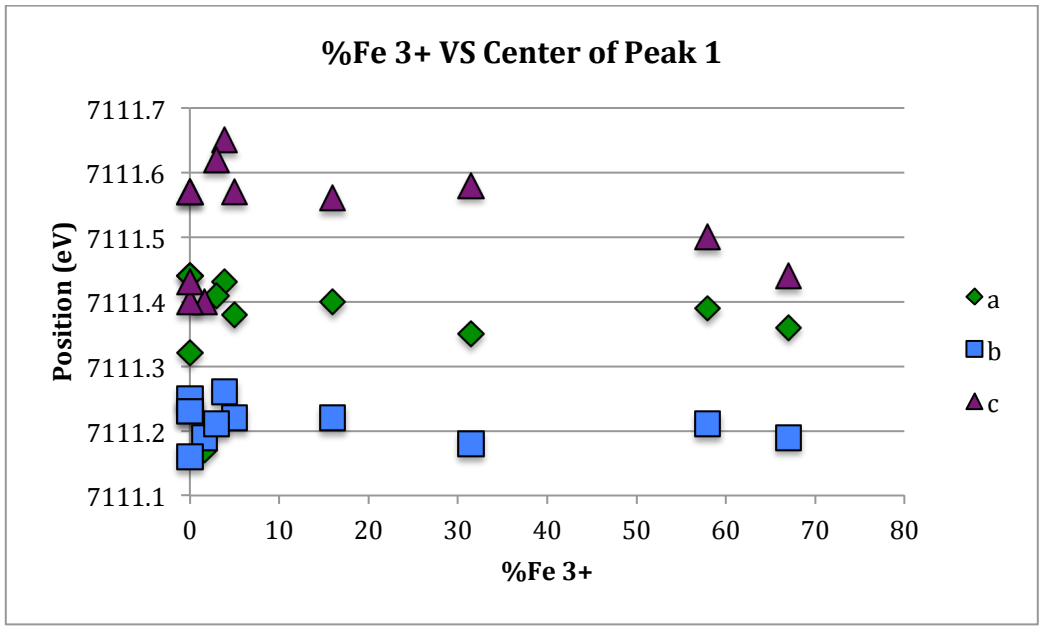

b) Center of peak 2

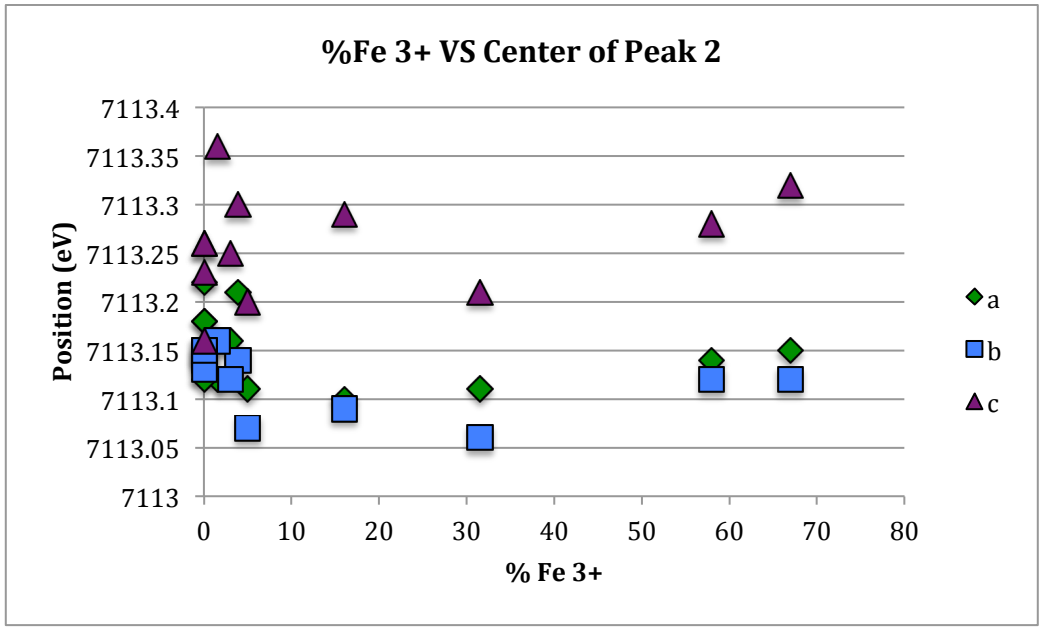

Figure 3.4.4-3: shift of pre-edge peaks and K_D of sample

a) Center of peak 1

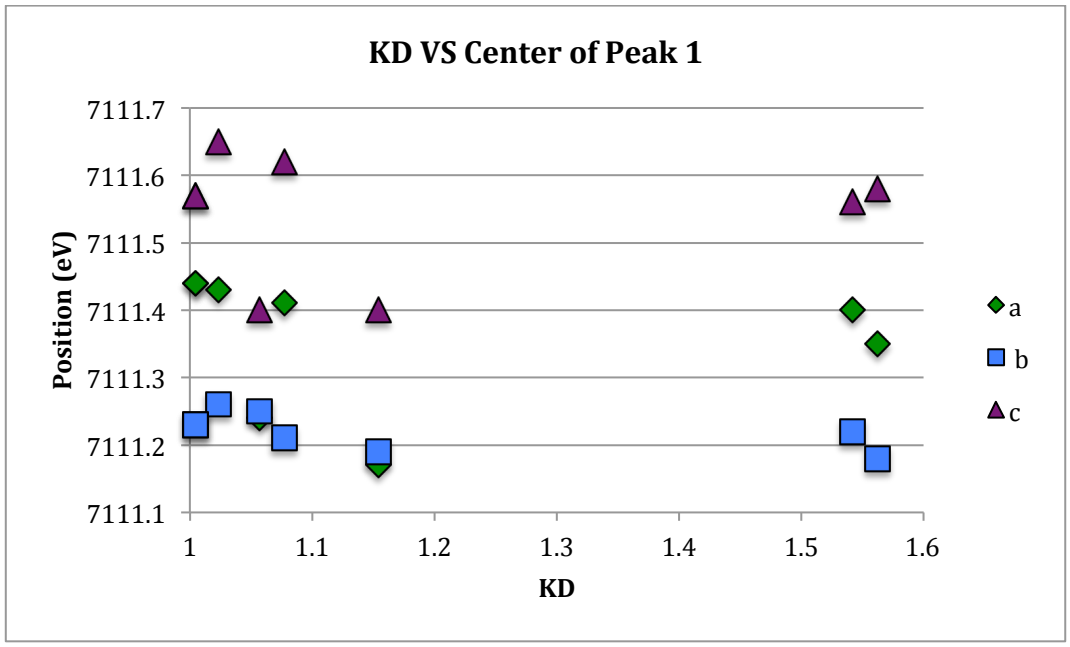

b) Center of peak 2

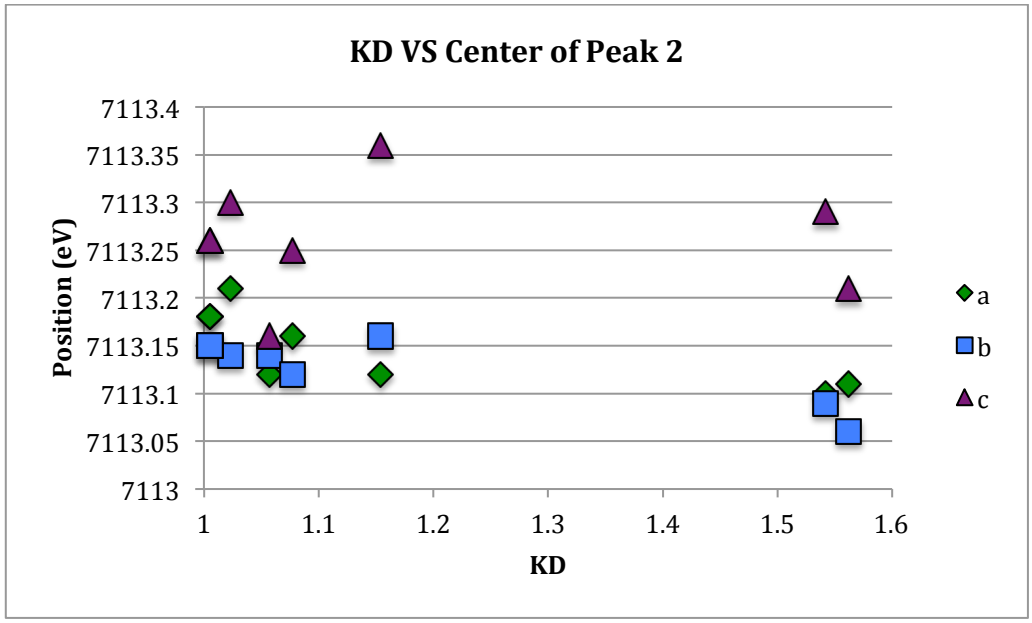

3.4.5 Randomly-oriented samples

In order to be sure that the observed effects of orientation on the spectra were valid, a number of samples were randomly oriented for data collection and are shown in **Figure 3.4.5-1**.

Figure 3.4.5-1: Spectra of randomly-oriented samples

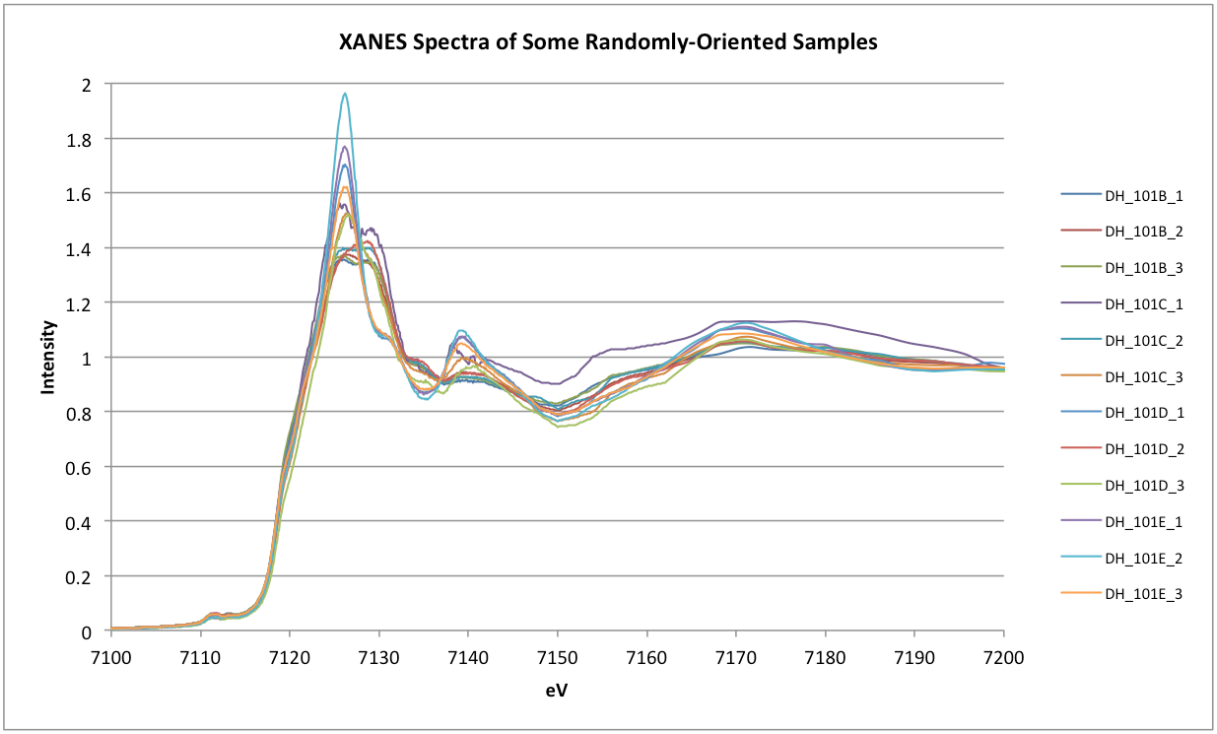

The samples are not intentionally oriented along any axis, but some features of each of the three axes can be seen. A future study will involve samples at a "known random" orientation. It may then be possible to visually identify the axis that the randomly-oriented sample is closest to, and then compare it to what the known orientation is.

The main edge peaks are very different along the a, b, and c crystallographic axes, so it would also be of interest to further study the changing shape of the peaks as a crystal is rotated from one axis, through random orientations, and into another axis. It is expected that one can watch the main edge features "grow" and "split" as the crystal is rotated.

CHAPTER THREE REFERENCES

Bajt, S., Sutton, S.R., and Delaney, J.S. (1994) Microanalysis of iron oxidation nstates in silicates and oxides using X-ray absorption near edge structure (XANES). Geochmical et Cosmochemica Acta, 58, 5209-5214.

Bloss, F.D. (1981) The Spindle Stage: Principles and Practice. Cambridge University Press, U.K.

Dyar, M.D., Breves, E.A., Emerson, E., Bell, S.W., Nelms, M., Ozanne, M.V., Peel, S.E., Carmosino, M.L., Tucker, J.M., Gunter, M.E., Delaney, J.S., Lanzirotti, A., and Woodland, A.B. (2012) Accurate determination of ferric iron in garnets by bulk Mössbauer spectroscopy and synchrotron micro-XANES. American Mineralogist, 97, 1726-1740.

Dyar, M.D., Breves, E.A., Gunter, M.E., Lanzirotti, A., Tucker, J.M., Carey, C.J., Peel, S.E., Brown, E.B., Oberti, R., Lerotic, M., and Delaney, J.S. (2016) Use of multivariate analysis for synchrotron micro-XANES analysis of iron valence state in amphiboles. American Mineralogist, 101, 1171-1189.

Dyar, M.D., Delaney, J.S., and Sutton, S.R. (2001) Fe XANES spectra of iron-rich micas. European Journal of Mineralogy, 13, 1079-1098.

Dyar, M.D., Delaney, J.S., Sutton, S.R., and Schaeffer, M.W. (1998) Fe^{3+} distribution in oxidized olivine: A synchrotron micro-XANES study. American Mineralogist, 83, 1361-1365.

Dyar, M.D., Gunter, M.E., Delaney, J.S., Lanzirotti, A., and Sutton, S.R. (2002a) Use of the spindle stage for orientation of single crystals for microXAS: Isotropy and anisotropy in Fe-XANES spectra. American Mineralogist, 87, 1500-1504.

Dyar, M.D., Gunter, M.E., Delaney, J.S., Lanzarotti, A., and Sutton, S.R. (2002b) Systematics in the structure and XANES spectra of pyroxenes, amphiboles, and micas as derived from oriented single crystals. The Canadian Mineralogist, 40, 1375-1393.

Gunter, M.E., and Twamley, B. (2001) A new method to determine the optical orientation of biaxial minerals: A mathematical approach. Canadian Mineralogist, 39, 1701-1711.

University of Massachusetts. (2017) Project Superman: Web Interface. http://nemo.cs.umass.edu:54321

Wilke, M. Farges, F., Petit, P.-E., Brown, G.E., Jr., and Martin, F. (2001) Oxidation state and coordination of Fe in minerals: An Fe K-XANES spectroscopic study. American Mineralogist, 86, 714-730.

APPENDIX A: UNIT CELL PARAMETERS

Samples in Pbnm			85539		85540		90613		112085	
Chemistry	Mg		0.11		0.17		0.13		0.10	
	Fe		1.89		1.83		1.87		1.90	
	%Mg		5.50		8.50		6.50		5.00	
	%Fe		94.50		91.50		93.50		95.00	
	Formula Weight (g/mol)		200.24		198.51		199.69		200.64	
Cell Parameters	a (Å)		4.8423	(5)	4.8266	(2)	4.8319	(2)	4.8320	(2)
	b (Å)		10.5425	(11)	10.4964	(5)	10.5137	(3)	10.5169	(4)
	c (Å)		6.1249	(7)	6.1004	(3)	6.1088	(2)	6.1095	(2)
	α=β=γ		90		90		90		90	
	Volume (Å^3)		312.68	(6)	309.06	(2)	310.334	(19)	310.47	(2)
	Density (g/cm^3)		4.254		4.266		4.274		4.292	
	Z		4		4		4		4	
Refinement Details	Average Redundancy		10.565		10.381		10.487		10.503	
	Completeness (%)		99.8		99.8		99.5		99.8	
	Resolution (Å)		0.66		0.66		0.66		0.66	
	R1(%)		1.14		1.13		1.08		1.23	
	wR2 (%)		2.93		2.85		2.67		3.08	
	Goodness-of-fit		1.110		1.110		1.118		1.146	
Atomic Coordinates	M1	x/a	0.00		0.00		0.00		0.00	
		y/b	0.00		0.00		0.00		0.00	
		z/c	0.00		0.00		0.00		0.00	
		U(eq)	0.00676	(8)	0.00641	(8)	0.00628	(7)	0.00626	(8)
	M2	x/a	0.98749	(4)	0.98638	(4)	0.98697	(4)	0.98694	(4)
		y/b	0.28020	(2)	0.28008	(2)	0.28008	(2)	0.28011	(2)
		z/c	0.25		0.25		0.25		0.25	
		U (eq)	0.00593	(8)	0.00564	(9)	0.00564	(8)	0.00563	(9)
	Si	x/a	0.42939	(7)	0.43002	(7)	0.42976	(7)	0.42984	(8)
		y/b	0.09642	(3)	0.09694	(3)	0.09661	(3)	0.09665	(3)
		z/c	0.25		0.25		0.25		0.25	
		U(eq)	0.00475	(9)	0.00483	(9)	0.00460	(9)	0.00460	(10)
	O1	x/a	0.7646	(2)	0.76659	(19)	0.76585	(19)	0.7661	(2)
		y/b	0.09175	(9)	0.09181	(9)	0.09160	(9)	0.09159	(10)
		z/c	0.25		0.25		0.25		0.25	
		U(eq)	0.00758	(17)	0.00701	(17)	0.00672	(17)	0.00680	(18)
	O2	x/a	0.2109	(2)	0.2108	(2)	0.2114	(2)	0.2112	(2)
		y/b	0.45342	(9)	0.45305	(9)	0.45307	(9)	0.45318	(9)
		z/c	0.25		0.25		0.25		0.25	
		U(eq)	0.00719	(17)	0.00689	(17)	0.00672	(17)	0.00655	(18)
	O3	x/a	0.28806	(14)	0.28786	(14)	0.28782	(14)	0.28798	(14)
		y/b	0.16422	(6)	0.16495	(6)	0.16449	(6)	0.16458	(7)
		z/c	0.03793	(11)	0.03661	(11)	0.03698	(11)	0.03713	(12)
		U(eq)	0.00817	(13)	0.00788	(13)	0.00757	(13)	0.00764	(14)

Samples in Pbnm			DH101B		DH101C		DH101C R2		DH101D	
Chemistry	Mg		1.82		1.85		1.86		1.87	
	Fe		0.18		0.15		0.14		0.13	
	%Mg		91.00		92.50		93.00		93.50	
	%Fe		9.00		7.50		7.00		6.50	
	Formula Weight (g/mol)		146.39		145.52		145.13		144.89	
Cell Parameters	a (Å)		4.7669	(3)	4.7693	(2)	4.7642	(4)	4.7695	(5)
	b (Å)		10.2398	(6)	10.2395	(4)	10.2330	(8)	10.2388	(10)
	c (Å)		5.9991	(3)	6.0021	(3)	5.9972	(5)	5.9992	(6)
	α=β=γ		90		90		90		90	
	Volume (Å^3)		292.83	(3)	293.11	(2)	292.48	(4)	292.96	(5)
	Density (g/cm^3)		3.320		3.298		3.297		3.285	
	Z		4		4		4		4	
Refinement Details	Average Redundancy		10.183		10.220		10.455		9.383	
	Completeness (%)		99.3		99.3		99.5		99.6	
	Resolution (Å)		0.66		0.66		0.66		0.66	
	R1(%)		1.39		1.24		1.24		1.54	
	wR2 (%)		3.86		3.51		3.68		4.35	
	Goodness-of-fit		1.197		1.268		1.250		1.206	
Atomic Coordinates	M1	x/a	0.00		0.00		0.00		0.00	
		y/b	0.00		0.00		0.00		0.00	
		z/c	0.00		0.00		0.00		0.00	
		U(eq)	0.00488	(13)	0.00542	(12)	0.00499	(12)	0.00550	(14)
	M2	x/a	0.98974	(7)	0.98991	(7)	0.98999	(7)	0.99012	(8)
		y/b	0.27772	(3)	0.27766	(3)	0.27767	(3)	0.27758	(4)
		z/c	0.25		0.25		0.25		0.25	
		U (eq)	0.00486	(13)	0.00551	(13)	0.00516	(3)	0.00568	(15)
	Si	x/a	0.42680	(6)	0.42676	(6)	0.42675	(6)	0.42681	(7)
		y/b	0.09440	(3)	0.09438	(3)	0.09435	(3)	0.09432	(3)
		z/c	0.25		0.25		0.25		0.25	
		U(eq)	0.00386	(10)	0.00411	(9)	0.00374	(9)	0.00448	(11)
	O1	x/a	0.76616	(17)	0.76617	(16)	0.76618	(16)	0.76620	(19)
		y/b	0.09165	(8)	0.09171	(7)	0.09165	(7)	0.09172	(8)
		z/c	0.25		0.25		0.25		0.25	
		U(eq)	0.00546	(15)	0.00568	(14)	0.00527	(14)	0.00601	(16)
	O2	x/a	0.22027	(17)	0.22044	(16)	0.22053	(16)	0.22042	(19)
		y/b	0.44778	(7)	0.44763	(7)	0.44761	(7)	0.44763	(8)
		z/c	0.25		0.25		0.25		0.25	
		U(eq)	0.00551	(15)	0.00576	(14)	0.00535	(14)	0.00607	(16)
	O3	x/a	0.27852	(12)	0.27852	(11)	0.27830	(11)	0.27828	(13)
		y/b	0.16325	(5)	0.16322	(5)	0.16318	(5)	0.16326	(6)
		z/c	0.03347	(10)	0.03345	(9)	0.03338	(9)	0.03336	(10)
		U(eq)	0.00598	(12)	0.00625	(11)	0.00579	(11)	0.00659	(13)

Samples in Pbnm			DH101D R2		DH101E		EP3139C		EP3139C R2	
Chemistry	Mg		1.86		1.86		1.84		1.84	
	Fe		0.14		0.14		0.17		0.17	
	%Mg		93.00		93.00		91.54		91.54	
	%Fe		7.00		7.00		8.46		8.46	
	Formula Weight (g/mol)		145.05		145.05		145.91		145.91	
Cell Parameters	a (Å)		4.7667	(3)	4.7653	(2)	4.7675	(2)	4.76710	(10)
	b (Å)		10.2331	(6)	10.2320	(4)	10.2365	(4)	10.2374	(3)
	c (Å)		5.9990	(4)	5.9979	(2)	5.9993	(2)	5.9992	(2)
	α=β=γ		90		90		90		90	
	Volume (Å^3)		292.62	(3)	292.449	(19)	292.781	(19)	292.777	(14)
	Density (g/cm^3)		3.292	(3)	3.294		3.310		3.31	
	Z		4		4		4		4	
Refinement Details	Average Redundancy		10.106		10.120		10.552		10.455	
	Completeness (%)		99.6		99.3		99.8		99.8	
	Resolution (Å)		0.66		0.66		0.66		0.66	
	R1(%)		1.45		1.24		1.30		1.26	
	wR2 (%)		4.18		3.39		3.83		3.74	
	Goodness-of-fit		1.241		1.285		1.201		1.206	
Atomic Coordinates	M1	x/a	0.00		0.00		0.00		0.00	
		y/b	0.00		0.00		0.00		0.00	
		z/c	0.00		0.00		0.00		0.00	
		U(eq)	0.00528	(14)	0.00508	(12)	0.00486	(12)	0.00493	(12)
	M2	x/a	0.99004	(8)	0.99003	(7)	0.98991	(7)	0.98988	(7)
		y/b	0.27765	(4)	0.27765	(3)	0.27772	(3)	0.27771	(3)
		z/c	0.25		0.25		0.25		0.25	
		U (eq)	0.00537	(15)	0.00514	(13)	0.00493	(13)	0.00492	(13)
	Si	x/a	0.42674	(7)	0.42674	(6)	0.42674	(6)	0.42679	(6)
		y/b	0.09434	(3)	0.09433	(3)	0.09438	(3)	0.09436	(3)
		z/c	0.25		0.25		0.25		0.25	
		U(eq)	0.00389	(11)	0.00369	(9)	0.00390	(10)	0.00396	(9)
	O1	x/a	0.76603	(18)	0.76609	(16)	0.76613	(16)	0.76618	(16)
		y/b	0.09165	(8)	0.09165	(7)	0.09164	(7)	0.09164	(7)
		z/c	0.25		0.25		0.25		0.25	
		U(eq)	0.00538	(16)	0.00530	(14)	0.00557	(15)	0.00553	(14)
	O2	x/a	0.22061	(18)	0.22057	(16)	0.22037	(16)	0.22046	(16)
		y/b	0.44755	(8)	0.44759	(7)	0.44774	(7)	0.44774	(7)
		z/c	0.25		0.25		0.25		0.25	
		U(eq)	0.00542	(16)	0.00526	(14)	0.00551	(14)	0.00555	(14)
	O3	x/a	0.27825	(12)	0.27832	(11)	0.27842	(11)	0.27841	(11)
		y/b	0.16314	(6)	0.16316	(5)	0.16325	(5)	0.16326	(5)
		z/c	0.03341	(10)	0.03336	(9)	0.03349	(9)	0.03349	(9)
		U(eq)	0.00595	(13)	0.00576	(11)	0.00606	(12)	0.00604	(11)

Samples in Pbnm			EP3139D R2		H30B1		H30B1 R2		H30B4	
Chemistry	Mg		1.85		1.86		1.86		1.87	
	Fe		0.15		0.14		0.14		0.13	
	%Mg		92.50		93.00		93.00		93.50	
	%Fe		7.50		7.00		7.00		6.50	
	Formula Weight (g/mol)		145.52		145.13		145.28		144.89	
Cell Parameters	a (Å)		4.7657	(2)	4.7674	(3)	4.7654	(4)	4.7657	(3)
	b (Å)		10.2333	(4)	10.2357	(6)	10.2285	(8)	10.2278	(7)
	c (Å)		5.9980	(2)	5.9997	(3)	5.9956	(5)	5.9974	(4)
	α=β=γ		90		90		90		90	
	Volume (Å^3)		292.515	(19)	292.77	(3)	292.24	(4)	292.33	(3)
	Density (g/cm^3)		3.304		3.292		3.302		3.292	
	Z		4		4		4		4	
Refinement Details	Average Redundancy		10.466		9.924		10.555		10.420	
	Completeness (%)		99.6		99.6		99.6		99.6	
	Resolution (Å)		0.66		0.67		0.67		0.66	
	R1(%)		1.48		1.41		2.10		1.32	
	wR2 (%)		4.18		3.76		5.61		3.88	
	Goodness-of-fit		1.205		1.255		1.161		1.191	
Atomic Coordinates	M1	x/a	0.00		0.00		0.00		0.00	
		y/b	0.00		0.00		0.00		0.00	
		z/c	0.00		0.00		0.00		0.00	
		U(eq)	0.00489	(13)	0.00544	(13)	0.00534	(17)	0.00492	(12)
	M2	x/a	0.98993	(7)	0.99000	(7)	0.98993	(9)	0.99012	(7)
		y/b	0.27769	(3)	0.27766	(3)	0.27765	(4)	0.27765	(3)
		z/c	0.25		0.25		0.25		0.25	
		U (eq)	0.00494	(14)	0.00551	(14)	0.00514	(19)	0.00496	(13)
	Si	x/a	0.42676	(6)	0.42677	(6)	0.42678	(8)	0.42676	(6)
		y/b	0.09436	(3)	0.09438	(3)	0.09435	(4)	0.09435	(3)
		z/c	0.25		0.25		0.25		0.25	
		U(eq)	0.00391	(11)	0.00409	(9)	0.00411	(14)	0.00386	(9)
	O1	x/a	0.76615	(17)	0.76609	(18)	0.7661	(2)	0.76614	(17)
		y/b	0.09166	(8)	0.09164	(8)	0.09161	(10)	0.09167	(8)
		z/c	0.25		0.25		0.25		0.25	
		U(eq)	0.00547	(15)	0.00574	(15)	0.0056	(2)	0.00541	(15)
	O2	x/a	0.22059	(17)	0.22052	(17)	0.2206	(2)	0.22054	(17)
		y/b	0.44773	(7)	0.44757	(8)	0.44771	(9)	0.44762	(7)
		z/c	0.25		0.25		0.25		0.25	
		U(eq)	0.00545	(15)	0.00567	(15)	0.0057	(2)	0.00547	(15)
	O3	x/a	0.27833	(12)	0.27835	(12)	0.27829	(15)	0.27831	(12)
		y/b	0.16320	(5)	0.16317	(5)	0.16319	(7)	0.16325	(5)
		z/c	0.03344	(9)	0.03332	(10)	0.03337	(12)	0.03339	(10)
		U(eq)	0.00600	(13)	0.00616	(12)	0.00616	(17)	0.00596	(12)

Samples in Pbnm			KBH941		KBH941 R2		KI3054		KI3054 R2	
Chemistry	Mg		1.68		1.68		1.30		1.30	
	Fe		0.32		0.32		0.69		0.70	
	%Mg		84.00		84.00		65.33		65.00	
	%Fe		16.00		16.00		34.67		35.00	
	Formula Weight (g/mol)		150.72		150.72		162.63		162.79	
Cell Parameters	a (Å)		4.7749	(3)	4.7737	(2)	4.7886	(4)	4.78360	(10)
	b (Å)		10.2614	(6)	10.2614	(4)	10.3163	(8)	10.3061	(3)
	c (Å)		6.0107	(3)	6.0099	(3)	6.0318	(4)	6.0268	(2)
	α=β=γ		90		90		90		90	
	Volume (Å^3)		294.51	(3)	294.39	(2)	297.97	(4)	297.123	(15)
	Density (g/cm^3)		3.399		3.401		3.625		3.639	
	Z		4		4		4		4	
Refinement Details	Average Redundancy		10.023		10.272		9.712		10.439	
	Completeness (%)		99.8		99.7		99.7		99.5	
	Resolution (Å)		0.66		0.66		0.66		0.66	
	R1(%)		1.24		1.25		1.21		1.07	
	wR2 (%)		3.65		3.69		3.63		3.16	
	Goodness-of-fit		1.287		1.238		1.199		1.208	
Atomic Coordinates	M1	x/a	0.00		0.00		0.00		0.00	
		y/b	0.00		0.00		0.00		0.00	
		z/c	0.00		0.00		0.00		0.00	
		U(eq)	0.00515	(11)	0.00514	(11)	0.00589	(10)	0.00539	(9)
	M2	x/a	0.98905	(7)	0.98902	(7)	0.98734	(6)	0.98735	(5)
		y/b	0.27791	(3)	0.27794	(3)	0.27845	(3)	0.27845	(2)
		z/c	0.25		0.25		0.25		0.25	
		U (eq)	0.00525	(12)	0.00514	(12)	0.00565	(11)	0.00533	(10)
	Si	x/a	0.42707	(7)	0.42707	(6)	0.42786	(7)	0.42781	(6)
		y/b	0.09469	(3)	0.09469	(3)	0.09537	(3)	0.09540	(3)
		z/c	0.25		0.25		0.25		0.25	
		U(eq)	0.00418	(9)	0.00411	(9)	0.00457	(9)	0.00415	(9)
	O1	x/a	0.76617	(18)	0.76621	(17)	0.76608	(18)	0.76635	(16)
		y/b	0.09174	(8)	0.09176	(8)	0.09193	(8)	0.09192	(7)
		z/c	0.25		0.25		0.25		0.25	
		U(eq)	0.00587	(15)	0.00580	(15)	0.00651	(15)	0.00598	(14)
	O2	x/a	0.21932	(18)	0.21926	(17)	0.21683	(18)	0.21671	(16)
		y/b	0.44820	(8)	0.44824	(7)	0.44938	(8)	0.44935	(7)
		z/c	0.25		0.25		0.25		0.25	
		U(eq)	0.00591	(15)	0.00584	(15)	0.00640	(15)	0.00590	(14)
	O3	x/a	0.27931	(12)	0.27929	(12)	0.28127	(12)	0.28142	(11)
		y/b	0.16344	(6)	0.16343	(5)	0.16396	(6)	0.16397	(5)
		z/c	0.03372	(10)	0.03370	(9)	0.03437	(10)	0.03438	(9)
		U(eq)	0.00650	(12)	0.00640	(12)	0.00705	(12)	0.00658	(11)

Samples in Pbnm			KI3362		KI3648		KI4143		KI4143 R2	
Chemistry	Mg		1.21		1.45		0.84		0.80	
	Fe		0.79		0.55		1.16		1.20	
	%Mg		60.50		72.50		42.00		40.00	
	%Fe		39.50		27.50		58.00		60.00	
	Formula Weight (g/mol)		165.63		157.98		177.38		178.48	
Cell Parameters	a (Å)		4.7884	(2)	4.7812	(4)	4.8030	(2)	4.8051	(3)
	b (Å)		10.3219	(4)	10.2892	(9)	10.3804	(3)	10.3877	(7)
	c (Å)		6.0343	(3)	6.0202	(5)	6.0551	(2)	6.0598	(4)
	α=β=γ		90		90		90		90	
	Volume (Å^3)		298.25	(2)	296.16	(4)	301.889	(18)	302.47	(3)
	Density (g/cm^3)		3.689		3.543		3.903		3.919	
	Z		4		4		4		4	
Refinement Details	Average Redundancy		10.186		10.247		10.428		9.928	
	Completeness (%)		99.7		99.8		99.7		99.7	
	Resolution (Å)		0.66		0.66		0.66		0.66	
	R1(%)		1.33		1.17		1.25		1.24	
	wR2 (%)		3.88		3.60		3.24		3.23	
	Goodness-of-fit		1.338		1.308		1.253		1.175	
Atomic Coordinates	M1	x/a	0.00		0.00		0.00		0.00	
		y/b	0.00		0.00		0.00		0.00	
		z/c	0.00		0.00		0.00		0.00	
		U(eq)	0.00651	(11)	0.00655	(10)	0.00700	(9)	0.00635	(9)
	M2	x/a	0.98704	(6)	0.98786	(6)	0.98645	(5)	0.98634	(5)
		y/b	0.27856	(3)	0.27825	(3)	0.27909	(2)	0.27917	(2)
		z/c	0.25		0.25		0.25		0.25	
		U (eq)	0.00634	(12)	0.00650	(11)	0.00660	(10)	0.00604	(10)
	Si	x/a	0.42797	(7)	0.42750	(6)	0.42888	(7)	0.42895	(7)
		y/b	0.09553	(3)	0.09509	(3)	0.09622	(3)	0.09621	(3)
		z/c	0.25		0.25		0.25		0.25	
		U(eq)	0.00540	(10)	0.00541	(9)	0.00562	(9)	0.00491	(9)
	O1	x/a	0.76631	(19)	0.76622	(17)	0.76650	(19)	0.76628	(19)
		y/b	0.09192	(9)	0.09179	(8)	0.09212	(9)	0.09213	(9)
		z/c	0.25		0.25		0.25		0.25	
		U(eq)	0.00720	(16)	0.00715	(15)	0.00761	(16)	0.00710	(16)
	O2	x/a	0.21625	(18)	0.21796	(16)	0.21386	(18)	0.21373	(19)
		y/b	0.44961	(8)	0.44884	(7)	0.45085	(8)	0.45093	(8)
		z/c	0.25		0.25		0.25		0.25	
		U(eq)	0.00724	(17)	0.00710	(15)	0.00765	(16)	0.00687	(16)
	O3	x/a	0.28174	(13)	0.28056	(12)	0.28405	(13)	0.28417	(13)
		y/b	0.16402	(6)	0.16370	(5)	0.16457	(6)	0.16456	(6)
		z/c	0.03456	(11)	0.03414	(9)	0.03523	(11)	0.03527	(11)
		U(eq)	0.00780	(13)	0.00774	(12)	0.00841	(12)	0.00774	(13)

Samples in Pbnm			Mourne		NWA2737 R2		Rockport		San Carlos	
Chemistry	Mg		0.05		1.46		0.03		1.86	
	Fe		1.96		0.54		1.98		0.14	
	%Mg		2.49		73.00		1.49		93.00	
	%Fe		97.51		27.00		98.51		7.00	
	Formula Weight (g/mol)		202.37		157.90		203.00		145.13	
Cell Parameters	a (Å)		4.8273	(3)	4.7795	(2)	4.8276	(6)	4.7682	(3)
	b (Å)		10.4989	(7)	10.2879	(3)	10.5044	(14)	10.2366	(6)
	c (Å)		6.0979	(4)	6.0198	(2)	6.0983	(8)	6.0011	(4)
	α=β=γ		90		90		90		90	
	Volume (Å^3)		309.05	(3)	296.000	(18)	309.25	(7)	292.91	(3)
	Density (g/cm^3)		4.349		3.543		4.36		3.291	
	Z		4		4		4		4	
Refinement Details	Average Redundancy		10.388		10.445		10.466		9.894	
	Completeness (%)		99.7		99.7		99.8		99.6	
	Resolution (Å)		0.66		0.66		0.66		0.66	
	R1(%)		1.17		1.14		1.17		1.51	
	wR2 (%)		2.89		3.38		2.88		3.90	
	Goodness-of-fit		1.121		1.229		1.128		1.159	
Atomic Coordinates	M1	x/a	0.00		0.00		0.00		0.00	
		y/b	0.00		0.00		0.00		0.00	
		z/c	0.00		0.00		0.00		0.00	
		U(eq)	0.00625	(8)	0.00535	(10)	0.00634	(8)	0.00586	(14)
	M2	x/a	0.98637	(4)	0.98796	(6)	0.98637	(4)	0.99003	(7)
		y/b	0.28023	(2)	0.27826	(3)	0.28025	(2)	0.27766	(3)
		z/c	0.25		0.25		0.25		0.25	
		U (eq)	0.00563	(8)	0.00528	(10)	0.00568	(8)	0.00586	(15)
	Si	x/a	0.43054	(8)	0.42755	(6)	0.43065	(8)	0.42675	(6)
		y/b	0.09727	(4)	0.09512	(3)	0.09727	(4)	0.09435	(3)
		z/c	0.25		0.25		0.25		0.25	
		U(eq)	0.00464	(10)	0.00409	(9)	0.00463	(10)	0.00447	(10)
	O1	x/a	0.7671	(2)	0.76620	(16)	0.7672	(2)	0.76602	(18)
		y/b	0.09187	(10)	0.09184	(7)	0.09184	(10)	0.09168	(8)
		z/c	0.25		0.25		0.25		0.25	
		U(eq)	0.00659	(18)	0.00599	(14)	0.00656	(18)	0.00613	(16)
	O2	x/a	0.2100	(2)	0.21781	(16)	0.2098	(2)	0.22048	(17)
		y/b	0.45338	(9)	0.44895	(7)	0.45342	(9)	0.44759	(8)
		z/c	0.25		0.25		0.25		0.25	
		U(eq)	0.00664	(18)	0.00585	(14)	0.00677	(19)	0.00610	(16)
	O3	x/a	0.28863	(15)	0.28057	(11)	0.28867	(15)	0.27833	(12)
		y/b	0.16532	(7)	0.16375	(5)	0.16527	(7)	0.16316	(5)
		z/c	0.03666	(12)	0.03416	(9)	0.03657	(12)	0.03345	(10)
		U(eq)	0.00746	(14)	0.00647	(11)	0.00752	(14)	0.00664	(13)

Samples in Pbnm			LFC		LLV	
Chemistry	Mg		0.04		0.06	
	Fe		1.96		1.94	
	%Mg		2.00		3.00	
	%Fe		98.00		97.00	
	Formula Weight (g/mol)		202.45		201.98	
Cell Parameters	a (Å)		4.8233	(5)	4.8229	(2)
	b (Å)		10.4865	(10)	10.4785	(5)
	c (Å)		6.0929	(6)	6.0903	(3)
	α=β=γ		90		90	
	Volume (Å^3)		308.18	(5)	307.78	(2)
	Density (g/cm^3)		4.363		4.359	
	Z		4		4	
Refinement Details	Average Redundancy		10.276		10.344	
	Completeness (%)		99.7		100.0	
	Resolution (Å)		0.66		0.66	
	R1(%)		1.18		1.22	
	wR2 (%)		2.64		3.37	
	Goodness-of-fit		1.177		1.185	
Atomic Coordinates	M1	x/a	0.00		0.00	
		y/b	0.00		0.00	
		z/c	0.00		0.00	
		U(eq)	0.00607	(7)	0.00588	(9)
	M2	x/a	0.98603	(4)	0.98601	(4)
		y/b	0.28023	(2)	0.28021	(2)
		z/c	0.25		0.25	
		U (eq)	0.00546	(8)	0.00538	(9)
	Si	x/a	0.43092	(8)	0.43086	(8)
		y/b	0.09754	(3)	0.09755	(4)
		z/c	0.25		0.25	
		U(eq)	0.00426	(9)	0.00425	(11)
	O1	x/a	0.7677	(2)	0.7676	(2)
		y/b	0.09202	(10)	0.09204	(10)
		z/c	0.25		0.25	
		U(eq)	0.00627	(18)	0.00616	(19)
	O2	x/a	0.2095	(2)	0.2095	(2)
		y/b	0.45338	(9)	0.45326	(10)
		z/c	0.25		0.25	
		U(eq)	0.00632	(18)	0.00630	(19)
	O3	x/a	0.28879	(14)	0.28859	(16)
		y/b	0.16570	(7)	0.16569	(7)
		z/c	0.03634	(12)	0.03624	(13)
		U(eq)	0.00703	(13)	0.00699	(15)

APPENDIX B: BOND LENGTHS AND POLYHEDRON VOLUMES

Sample			85539	85540	90613	112085
%Mg			5.50	8.50	6.50	5.00
%Fe			94.50	91.50	93.50	95.00
M2 %ΣMg			56.03165	59.79864	58.24089	61.29163
ESD			(4.58530)	(2.92169)	(3.63430)	(5.07564)
Bond Lengths	M1	O1 (Å)	2.1399 (7)	2.1269 (7)	2.1307 (7)	2.1304 (7)
		O1 (Å)	2.1399 (7)	2.1269 (7)	2.1307 (7)	2.1304 (7)
		O2 (Å)	2.1319 (7)	2.1254 (7)	2.1262 (7)	2.1268 (7)
		O2 (Å)	2.1319 (7)	2.1254 (7)	2.1262 (7)	2.1268 (7)
		O3 (Å)	2.2354 (7)	2.2311 (7)	2.2307 (7)	2.2324 (7)
		O3 (Å)	2.2354 (7)	2.2311 (7)	2.2307 (7)	2.2324 (7)
		Vol (Å3)	12.884	12.761	12.784	12.791
	M2	O1 (Å)	2.2609 (10)	2.2429 (10)	2.2513 (10)	2.2517 (10)
		O2 (Å)	2.1227 (10)	2.1141 (9)	2.1175 (9)	2.1182 (10)
		O3 (Å)	2.0943 (7)	2.0756 (7)	2.0830 (7)	2.0833 (7)
		O3 (Å)	2.0943 (7)	2.0756 (7)	2.0830 (7)	2.0833 (7)
		O3' (Å)	2.3023 (7)	2.2962 (7)	2.2985 (7)	2.2986 (7)
		O3' (Å)	2.3023 (7)	2.2962 (7)	2.2985 (7)	2.2986 (7)
		Vol (Å3)	13.414	13.196	13.289	13.290
	Si	O1 (Å)	1.6241 (10)	1.654 (10)	1.6248 (10)	1.6255 (10)
		O2 (Å)	1.6536 (10)	1.6562 (10)	1.6561 (10)	1.6555 (11)
		O3 (Å)	1.6329 (7)	1.6355 (7)	1.6349 (7)	1.6345 (7)
		O3 (Å)	1.6329 (7)	1.6355 (7)	1.6350 (7)	1.6345 (7)
		Vol (Å3)	2.219	2.228	2.226	2.225

Sample			DH101B		DH101C		DH101C R2		DH101D	
%Mg			91.00		92.50		93.00		93.50	
%Fe			9.00		7.50		7.00		6.50	
M2 %ΣMg			50.05610		49.96665		49.96906		49.75790	
ESD			(0.18191)		(0.18486)		(0.18134)		(0.18987)	
Bond Lengths	M1	O1 (Å)	2.0911	(6)	2.0922	(5)	2.0901	(5)	2.0916	(6)
		O1 (Å)	2.0911	(6)	2.0922	(5)	2.0901	(5)	2.0916	(6)
		O2 (Å)	2.0768	(6)	2.0777	(5)	2.0756	(5)	2.0773	(6)
		O2 (Å)	2.0768	(6)	2.0777	(5)	2.0756	(5)	2.0773	(6)
		O3 (Å)	2.1442	(6)	2.1443	(5)	2.1416	(5)	2.1438	(6)
		O3 (Å)	2.1442	(6)	2.1443	(5)	2.1416	(5)	2.1438	(6)
		Vol (Å3)	11.920		11.933		11.896		11.926	
	M2	O1 (Å)	2.1831	(9)	2.1827	(8)	2.1818	(8)	2.1822	(10)
		O2 (Å)	2.0592	(8)	2.0586	(8)	2.0569	(8)	2.0586	(9)
		O3 (Å)	2.0666	(6)	2.0681	(3)	2.0668	(6)	2.0682	(7)
		O3 (Å)	2.0666	(6)	2.0681	(3)	2.0668	(6)	2.0682	(7)
		O3' (Å)	2.2262	(6)	2.2265	(6)	2.2241	(6)	2.2245	(7)
		O3' (Å)	2.2262	(6)	2.2265	(6)	2.2241	(6)	2.2245	(7)
		Vol (Å3)	12.536		12.546		12.517		12.537	
	Si	O1 (Å)	1.6179	(9)	1.6189	(8)	1.6173	(8)	1.6190	(10)
		O2 (Å)	1.6570	(8)	1.6585	(8)	1.6574	(8)	1.6580	(9)
		O3 (Å)	1.6383	(6)	1.6389	(6)	1.6383	(6)	1.6399	(7)
		O3 (Å)	1.6383	(6)	1.6390	(6)	1.6383	(6)	1.6399	(7)
		Vol (Å3)	2.219		2.223		2.219		2.224	

Sample			DH101D R2		DH101E		EP3139C		EP3139C R2	
%Mg			93.00		93.00		91.54		91.54	
%Fe			7.00		7.00		8.46		8.46	
M2 %ΣMg			50.04353		50.02053		50.22703		50.31800	
ESD			(0.20592)		(0.17781)		(0.16730)		(0.16575)	
Bond Lengths	M1	O1 (Å)	2.0911	(6)	2.0905	(5)	2.0911	(5)	2.0909	(5)
		O1 (Å)	2.0911	(6)	2.0905	(5)	2.0911	(5)	2.0909	(5)
		O2 (Å)	2.0763	(6)	2.0758	(5)	2.0767	(5)	2.0764	(5)
		O2 (Å)	2.0763	(6)	2.0758	(5)	2.0767	(5)	2.0764	(5)
		O3 (Å)	2.1416	(6)	2.1415	(5)	2.1436	(5)	2.1437	(5)
		O3 (Å)	2.1416	(6)	2.1416	(5)	2.1436	(5)	2.1437	(5)
		Vol (Å3)	11.899		11.900		11.916		11.914	
	M2	O1 (Å)	2.1824	(9)	2.1819	(8)	2.1833	(8)	2.1831	(8)
		O2 (Å)	2.0568	(9)	2.0569	(8)	2.0582	(8)	2.0587	(8)
		O3 (Å)	2.0680	(6)	2.0672	(6)	2.0674	(6)	2.0673	(6)
		O3 (Å)	2.0680	(6)	2.0672	(6)	2.0674	(6)	2.0673	(6)
		O3' (Å)	2.2246	(7)	2.2244	(6)	2.2253	(6)	2.2253	(6)
		O3' (Å)	2.2246	(7)	2.2244	(6)	2.2253	(6)	2.2253	(6)
		Vol (Å3)	12.526		12.522		12.534		12.534	
	Si	O1 (Å)	1.6175	(9)	1.6173	(8)	1.6183	(8)	1.6181	(8)
		O2 (Å)	1.6582	(9)	1.6574	(8)	1.6568	(2)	1.6570	(8)
		O3 (Å)	1.6386	(6)	1.6385	(6)	1.6384	(6)	1.6386	(6)
		O3 (Å)	1.6386	(6)	1.6385	(6)	1.6384	(6)	1.6386	(6)
		Vol (Å3)	2.218		2.219		2.219		2.220	

Sample			EP3139D R2	H30B1	H30B1 R2	H30B4
%Mg			92.50	93.00	93.00	93.50
%Fe			7.50	7.00	7.00	6.50
M2 %ΣMg			50.23309	50.07304	50.18744	50.26611
ESD			(0.17511)	(0.18916)	(0.22346)	(0.16893)
Bond Lengths	M1	O1 (Å)	2.0905 (6)	2.0912 (6)	2.0898 (7)	2.0903 (6)
		O1 (Å)	2.0905 (6)	2.0912 (6)	2.0898 (7)	2.0903 (6)
		O2 (Å)	2.0755 (5)	2.0768 (6)	2.0749 (7)	2.0757 (6)
		O2 (Å)	2.0755 (5)	2.0768 (6)	2.0749 (7)	2.0757 (6)
		O3 (Å)	2.1421 (6)	2.1425 (6)	2.1412 (7)	2.1418 (6)
		O3 (Å)	2.1421 (6)	2.1425 (6)	2.1412 (7)	2.1418 (6)
		Vol (Å3)	11.899	11.915	11.887	11.898
	M2	O1 (Å)	2.1820 (9)	2.1829 (9)	2.1815 (11)	2.1812 (9)
		O2 (Å)	2.0582 (8)	2.0573 (9)	2.0577 (11)	2.0563 (8)
		O3 (Å)	2.0672 (6)	2.0675 (6)	2.0664 (8)	2.0671 (6)
		O3 (Å)	2.0672 (6)	2.0675 (6)	2.0664 (8)	2.0671 (6)
		O3' (Å)	2.2247 (6)	2.2256 (7)	2.2239 (8)	2.2233 (6)
		O3' (Å)	2.2247 (6)	2.2256 (7)	2.2239 (8)	2.2233 (6)
		Vol (Å3)	12.526	12.535	12.516	12.512
	Si	O1 (Å)	1.6177 (9)	1.6179 (9)	1.6171 (12)	1.6176 (9)
		O2 (Å)	1.6567 (8)	1.6586 (9)	1.6563 (11)	1.6568 (8)
		O3 (Å)	1.6382 (6)	1.6390 (6)	1.6381 (8)	1.6385 (6)
		O3 (Å)	1.6382 (6)	1.6390 (6)	1.6381 (8)	1.6385 (6)
		Vol (Å3)	2.218	2.222	2.216	2.219

Sample			KBH941		KBH941 R2		KI3054		KI3054 R2	
%Mg			84.00		84.00		65.33		65.00	
%Fe			16.00		16.00		34.67		35.00	
M2 %ΣMg			50.42896		50.49781		50.79897		50.48997	
ESD			(0.20532)		(0.19882)		(0.30383)		(0.27849)	
Bond Lengths	M1	O1 (Å)	2.0954	(6)	2.0951	(6)	2.1043	(6)	2.1016	(5)
		O1 (Å)	2.0954	(6)	2.0951	(6)	2.1043	(6)	2.1016	(5)
		O2 (Å)	2.0825	(6)	2.0822	(6)	2.0941	(6)	2.0926	(5)
		O2 (Å)	2.0825	(6)	2.0822	(6)	2.0941	(6)	2.0926	(5)
		O3 (Å)	2.1524	(6)	2.1520	(6)	2.1721	(6)	2.1704	(5)
		O3 (Å)	2.1524	(6)	2.1520	(6)	2.1721	(6)	2.1704	(5)
		Vol (Å3)	12.011		12.005		12.210		12.175	
	M2	O1 (Å)	2.1868	(9)	2.1866	(9)	2.1966	(9)	2.1939	(8)
		O2 (Å)	2.0645	(9)	2.0644	(8)	2.0778	(8)	2.0751	(8)
		O3 (Å)	2.0672	(6)	2.0667	(6)	2.0662	(6)	2.0640	(5)
		O3 (Å)	2.0672	(6)	2.0667	(6)	2.0662	(6)	2.0640	(5)
		O3' (Å)	2.2339	(7)	2.2339	(6)	2.2511	(6)	2.2494	(6)
		O3' (Å)	2.2339	(7)	2.2339	(6)	2.2511	(6)	2.2494	(6)
		Vol (Å3)	12.599		12.594		12.278		12.688	
	Si	O1 (Å)	1.6195	(9)	1.6192	(9)	1.6200	(9)	1.6199	(8)
		O2 (Å)	1.6578	(9)	1.6573	(8)	1.6579	(9)	1.6563	(8)
		O3 (Å)	1.6387	(6)	1.6386	(6)	1.6386	(6)	1.6366	(6)
		O3 (Å)	1.6387	(6)	1.6386	(6)	1.6386	(6)	1.6366	(6)
		Vol (Å3)	2.223		2.222		2.225		2.220	

Sample			KI3362		KI3648		KI4143		KI4143 R2	
%Mg			60.50		72.50		42.00		40.00	
%Fe			39.50		27.50		58.00		60.00	
M2 %ΣMg			50.55124		50.03402		52.81826		52.44968	
ESD			(0.36490)		(0.25749)		(0.55485)		(0.58877)	
Bond Lengths	M1	O1 (Å)	2.1043	(6)	2.0992	(6)	2.1128	(6)	2.1147	(6)
		O1 (Å)	2.1043	(6)	2.0992	(6)	2.1128	(6)	2.1147	(6)
		O2 (Å)	2.0958	(6)	2.0882	(6)	2.1073	(6)	2.1088	(6)
		O2 (Å)	2.0958	(6)	2.0882	(6)	2.1073	(6)	2.1088	(6)
		O3 (Å)	2.1748	(6)	2.1630	(6)	2.1966	(6)	2.1982	(6)
		O3 (Å)	2.1748	(6)	2.1630	(6)	2.1966	(6)	2.1982	(6)
		Vol (Å3)	12.227		12.107		12.433		12.461	
	M2	O1 (Å)	2.1974	(9)	2.1918	(9)	2.2097	(9)	2.2120	(9)
		O2 (Å)	2.0788	(9)	2.0715	(8)	2.0909	(9)	2.0922	(9)
		O3 (Å)	2.0654	(6)	2.0652	(6)	2.0664	(6)	2.0673	(6)
		O3 (Å)	2.0654	(6)	2.0652	(6)	2.0664	(6)	2.0673	(6)
		O3' (Å)	2.2537	(7)	2.2442	(6)	2.2688	(7)	2.2712	(7)
		O3' (Å)	2.2537	(7)	2.2442	(6)	2.2688	(7)	2.2712	(7)
		Vol (Å3)	12.736		12.661		12.871		12.898	
	Si	O1 (Å)	1.6205	(10)	1.6198	(9)	1.6221	(10)	1.6215	(10)
		O2 (Å)	1.6570	(9)	1.6577	(8)	1.6574	(9)	1.6576	(9)
		O3 (Å)	1.6372	(7)	1.6373	(6)	1.6366	(7)	1.6375	(7)
		O3 (Å)	1.6372	(7)	1.6373	(6)	1.6366	(7)	1.6375	(7)
		Vol (Å3)	2.222		2.221		2.225		2.226	

Sample			Mourne		NWA2737 R2		Rockport		San Carlos	
%Mg			2.49		73.00		1.49		93.00	
%Fe			97.51		27.00		98.51		7.00	
M2 %ΣMg			60.71874		50.38597		71.24450		50.16073	
ESD			(10.33861)		(0.23970)		(14.02525)		(0.19440)	
Bond Lengths	M1	O1 (Å)	2.1257	(7)	2.0991	(5)	2.1255	(7)	2.0920	(6)
		O1 (Å)	2.1257	(7)	2.0991	(5)	2.1255	(7)	2.0920	(6)
		O2 (Å)	2.1268	(7)	2.0880	(5)	2.1275	(7)	2.0773	(6)
		O2 (Å)	2.1268	(7)	2.0880	(5)	2.1275	(7)	2.0773	(6)
		O3 (Å)	2.2370	(7)	2.1630	(5)	2.2373	(7)	2.1427	(6)
		O3 (Å)	2.2370	(7)	2.1630	(5)	2.2373	(7)	2.1427	(6)
		Vol (Å3)	12.785		12.104		12.790		11.924	
	M2	O1 (Å)	2.2430	(10)	2.1912	(8)	2.2442	(11)	2.1830	(9)
		O2 (Å)	2.1142	(10)	2.0714	(8)	2.1148	(10)	2.0574	(9)
		O3 (Å)	2.0720	(7)	2.0651	(6)	2.0719	(8)	2.0687	(6)
		O3 (Å)	2.0720	(7)	2.0651	(6)	2.0719	(8)	2.0687	(6)
		O3' (Å)	2.2972	(8)	2.2432	(6)	2.2984	(8)	2.2253	(7)
		O3' (Å)	2.2972	(8)	2.2432	(6)	2.2984	(8)	2.2253	(7)
		Vol (Å3)	13.174		12.652		13.184		12.543	
	Si	O1 (Å)	1.6256	(11)	1.6189	(8)	1.6258	(11)	1.6179	(9)
		O2 (Å)	1.6561	(11)	1.6565	(8)	1.6563	(11)	1.6583	(9)
		O3 (Å)	1.6347	(8)	1.6371	(6)	1.6352	(8)	1.6388	(6)
		O3 (Å)	1.6347	(8)	1.6371	(6)	1.6352	(8)	1.6388	(6)
		Vol (Å3)	2.227		2.219		2.228		2.221	

Sample			LFC		LLV	
%Mg			2.00		3.00	
%Fe			98.00		97.00	
M2 %ΣMg			58.54077		54.74802	
ESD			(10.93977)		(9.30750)	
Bond Lengths	M1	O1 (Å)	2.1229	(7)	2.1224	(8)
		O1 (Å)	2.1229	(7)	2.1224	(8)
		O2 (Å)	2.1268	(7)	2.1263	(8)
		O2 (Å)	2.1268	(7)	2.1263	(8)
		O3 (Å)	2.2379	(7)	2.2361	(8)
		O3 (Å)	2.2379	(7)	2.2361	(8)
		Vol (Å3)	12.775		12.761	
	M2	O1 (Å)	2.2370	(10)	2.2355	(11)
		O2 (Å)	2.1114	(10)	2.1095	(11)
		O3 (Å)	2.0665	(7)	2.0657	(8)
		O3 (Å)	2.0665	(7)	2.0657	(8)
		O3' (Å)	2.2956	(7)	2.2944	(8)
		O3' (Å)	2.2956	(7)	2.2944	(8)
		Vol (Å3)	13.106		13.087	
	Si	O1 (Å)	1.6255	(11)	1.6251	(11)
		O2 (Å)	1.6565	(11)	1.6565	(11)
		O3 (Å)	1.6357	(7)	1.6357	(8)
		O3 (Å)	1.6357	(7)	1.6357	(8)
		Vol (Å3)	2.229		2.228	

APPENDIX C: DETERMINING BOND LENGTH IN AN IDEAL OCTAHEDRAL COMPLEX

The length of a bond in an ideal octahedral complex is the distance from the center of symmetry to each of the six corners. If one has the volume of the octahedron, the side length can be calculated, and then the side length can be used to calculate the bond length.

The side length, *a*, is calculated for an ideal octahedron with the following equation: $a = 2^{5/6}\left(3\frac{V}{8}\right)^{1/3}$, where *V* is the volume; see **Figure B.1**. The length *a* can then be used as the hypotenuse of a right isosceles triangle, where the two equal lengths, *l*, correspond to the ideal bond length in a perfect octahedron where: $l = \frac{a}{\sqrt{2}}$; see **Figure B.2**.

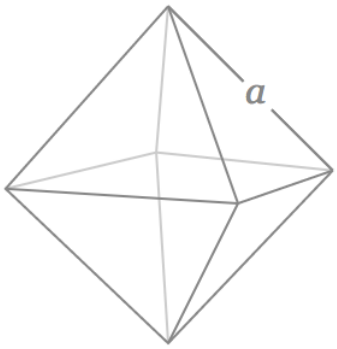

Figure B.1: Side length, a, of a perfect octahedron. Open source image from Google Equation Solver.

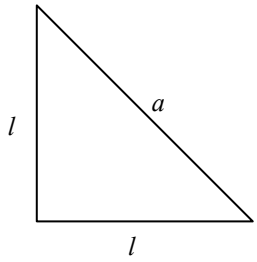

Figure B.2: Isosceles triangle with hypotenuse *a* and equal side lengths *l*.

APPENDIX D: MEAN QUADRATIC ELONGATION (λ_{oct}) FOR OCTAHEDRAL M1 AND M2 SITES

Sample	Composition		M1 Volume	Ideal Side Length	Ideal Bond Length	λ oct
	%Mg	%Fe				
85539	5.50	94.50	12.884	3.012	2.130	1.038
85540	8.50	91.50	12.761	3.003	2.123	1.037
90613	6.50	93.50	12.784	3.004	2.124	1.037
112085	5.00	95.00	12.791	3.005	2.125	1.037
DH101B	91.00	9.00	11.920	2.935	2.075	1.028
DH101C	92.50	7.50	11.933	2.936	2.076	1.028
DH101C R2	93.00	7.00	11.896	2.933	2.074	1.028
DH101D	93.50	6.50	11.926	2.936	2.076	1.028
DH101D R2	93.00	7.00	11.899	2.933	2.074	1.028
DH101E	93.00	7.00	11.900	2.933	2.074	1.028
EP3139C	91.54	8.46	11.916	2.935	2.075	1.028
EP3139C R2	91.54	8.46	11.914	2.935	2.075	1.028
EP3139D R2	92.50	7.50	11.899	2.933	2.074	1.028
H30B1	93.00	7.00	11.915	2.935	2.075	1.028
H30B1 R2	93.00	7.00	11.887	2.932	2.074	1.028
H30B4	93.50	6.50	11.898	2.933	2.074	1.028
KBH941	84.00	16.00	12.011	2.943	2.081	1.029
KBH941 R2	84.00	16.00	12.005	2.942	2.080	1.029
KI3054	65.33	34.67	12.210	2.959	2.092	1.030
KI3054 R2	65.00	35.00	12.175	2.956	2.090	1.031
KI3362	60.50	39.50	12.227	2.960	2.093	1.031
KI3648	72.50	27.50	12.107	2.950	2.086	1.030
KI4143	42.00	58.00	12.433	2.977	2.105	1.033
KI4143 R2	40.00	60.00	12.461	2.979	2.106	1.033
Mourne	2.49	97.51	12.785	3.004	2.124	1.037
NWA2737 R2	73.00	27.00	12.104	2.950	2.086	1.030
Rockport	1.49	98.51	12.790	3.005	2.125	1.037
San Carlos	93.00	7.00	11.924	2.935	2.076	1.028
LFC	2.00	98.00	12.775	3.004	2.124	1.037
LLV	3.00	97.00	12.761	3.003	2.123	1.037
					Total	1.031

Sample	Composition		M2 Volume	Ideal Side Length	Ideal Bond Length	λ oct
	%Mg	%Fe				
85539	5.50	94.50	13.414	3.053	2.159	1.037
85540	8.50	91.50	13.196	3.036	2.147	1.036
90613	6.50	93.50	13.289	3.043	2.152	1.036
112085	5.00	95.00	13.290	3.044	2.152	1.037
DH101B	91.00	9.00	12.536	2.985	2.111	1.027
DH101C	92.50	7.50	12.546	2.986	2.111	1.027
DH101C R2	93.00	7.00	12.517	2.983	2.110	1.027
DH101D	93.50	6.50	12.537	2.985	2.111	1.027
DH101D R2	93.00	7.00	12.526	2.984	2.110	1.027
DH101E	93.00	7.00	12.522	2.984	2.110	1.027
EP3139C	91.54	8.46	12.534	2.985	2.110	1.027
EP3139C R2	91.54	8.46	12.534	2.985	2.110	1.027
EP3139D R2	92.50	7.50	12.526	2.984	2.110	1.027
H30B1	93.00	7.00	12.535	2.985	2.111	1.027
H30B1 R2	93.00	7.00	12.516	2.983	2.109	1.027
H30B4	93.50	6.50	12.512	2.983	2.109	1.027
KBH941	84.00	16.00	12.599	2.990	2.114	1.028
KBH941 R2	84.00	16.00	12.594	2.989	2.114	1.028
KI3054	65.33	34.67	12.278	2.964	2.096	1.055
KI3054 R2	65.00	35.00	12.688	2.997	2.119	1.030
KI3362	60.50	39.50	12.736	3.001	2.122	1.031
KI3648	72.50	27.50	12.661	2.995	2.118	1.029
KI4143	42.00	58.00	12.871	3.011	2.129	1.033
KI4143 R2	40.00	60.00	12.898	3.013	2.131	1.033
Mourne	2.49	97.51	13.174	3.035	2.146	1.037
NWA2737 R2	73.00	27.00	12.652	2.994	2.117	1.029
Rockport	1.49	98.51	13.184	3.035	2.146	1.037
San Carlos	93.00	7.00	12.543	2.985	2.111	1.027
LFC	2.00	98.00	13.106	3.029	2.142	1.037
LLV	3.00	97.00	13.087	3.028	2.141	1.037
					Total	1.031

Sample	λ oct M1	λ oct M2
85539	1.038	1.037
85540	1.037	1.036
90613	1.037	1.036
112085	1.037	1.037
DH101B	1.028	1.027
DH101C	1.028	1.027
DH101C R2	1.028	1.027
DH101D	1.028	1.027
DH101D R2	1.028	1.027
DH101E	1.028	1.027
EP3139C	1.028	1.027
EP3139C R2	1.028	1.027
EP3139D R2	1.028	1.027
H30B1	1.028	1.027
H30B1 R2	1.028	1.027
H30B4	1.028	1.027
KBH941	1.029	1.028
KBH941 R2	1.029	1.028
KI3054	1.030	1.055
KI3054 R2	1.031	1.030
KI3362	1.031	1.031
KI3648	1.030	1.029
KI4143	1.033	1.033
KI4143 R2	1.033	1.033
Mourne	1.037	1.037
NWA2737 R2	1.030	1.029
Rockport	1.037	1.037
San Carlos	1.028	1.027
LFC	1.037	1.037
LLV	1.037	1.037

APPENDIX E: ERROR PROPAGATION FOR M1 %ΣFe AND M2 %ΣMg

A trend was observed where a higher percent of total iron is found in the M1 site, and a higher percent of total magnesium is found in the M2 site. This was observed with the following calculations: $M1_{\%\Sigma Fe} = \frac{M1FE}{M1FE+M2FE}$ and $M2_{\%\Sigma Mg} = \frac{M2MG}{M1MG+M2MG}$. The error propagation is complicated by the fact that the values M1FE and M2MG appear twice in the equations, respectively. This means that the values are correlated, so one cannot simply apply the addition rule followed by the quotient rule. Instead, the relationships have to be rewritten as $M1_{\%\Sigma Fe} = \frac{1}{1+{M2FE}/{M1FE}}$ and $M2_{\%\Sigma Mg} = \frac{1}{1+{M1MG}/{M2MG}}$ to avoid the same value appearing twice. The error is then propagated in three steps: First for ${M1MG}/{M2MG}$ and ${M2FE}/{M1FE}$, then for $1 + {M1MG}/{M2MG}$ and $1 + {M2FE}/{M1FE}$, and lastly for $\left(1 + {M1MG}/{M2MG}\right)^{-1}$ and $\left(1 + {M2FE}/{M1FE}\right)^{-1}$. For the first step, the quotient rule is applied to determine the uncertainty for ${M1MG}/{M2MG}$ as $U_{M1MG/M2MG} = \sqrt{\left(\frac{U_{M1MG}}{M1MG}\right)^2 + \left(\frac{U_{M2MG}}{M2MG}\right)^2}$ and for ${M2FE}/{M1FE}$, as $U_{M2Fe/M1Fe} = \sqrt{\left(\frac{U_{M2FE}}{M2FE}\right)^2 + \left(\frac{U_{M1FE}}{M1FE}\right)^2}$. The error does not need to be propagated for adding $1 + {M1MG}/{M2MG}$ and $1 + {M2FE}/{M1FE}$ because one is an exact number. Furthermore, no error propagation is necessary in the last step $\left(1 + {M1MG}/{M2MG}\right)^{-1}$ and $\left(1 + {M2FE}/{M1FE}\right)^{-1}$, as the percent uncertainty is unchanged when the reciprocal of a quantity is taken.

APPENDIX F: PERCENT OF TOTAL Fe IN M1 SITE AND PERCENT OF TOTAL Mg IN M2 SITE

Sample ID	%Mg	%Fe	M1MG	M1FE	M1 ESD	%Uncertainty
NMNH85539	5.50	94.50	0.04946	0.95054	0.00400	8.08734
85540	8.50	91.50	0.06788	0.93212	0.00405	5.96641
90035 •	0.50	99.50	0.00534	0.99466	0.00556	104.11985
90613	6.50	93.50	0.05308	0.94692	0.00372	7.00829
104576 •	1.00	99.00	0.00542	0.99458	0.00510	94.09594
112085	5.00	95.00	0.03812	0.96188	0.00418	10.96537
DH101B	91.00	9.00	0.89924	0.10076	0.00218	0.24243
DH101C ◆	92.50	7.50	0.90761	0.09239	0.00222	0.24460
DH101C R2 ◆	93.00	7.00	0.91369	0.08631	0.00218	0.23859
DH101D ◆	93.50	6.50	0.92763	0.07237	0.00230	0.24794
DH101D R2	93.00	7.00	0.91246	0.08754	0.00246	0.26960
DH101E	93.00	7.00	0.91282	0.08718	0.00219	0.23992
EP3139C	91.54	8.46	0.90435	0.09565	0.00200	0.22115
EP3139C R2	91.54	8.46	0.90460	0.09540	0.00201	0.22220
EP3139D	91.54	8.46	0.90996	0.09004	0.00258	0.28353
EP3139D R2	92.50	7.50	0.91060	0.08940	0.00208	0.22842
H30B1	93.00	7.00	0.91256	0.08744	0.00231	0.25313
H30B1 R2	93.00	7.00	0.91818	0.08182	0.00267	0.29079
H30B4	93.50	6.50	0.92044	0.07956	0.00209	0.22707
KBH941	84.00	16.00	0.82626	0.17374	0.00233	0.28199
KBH941 R2	84.00	16.00	0.82486	0.17514	0.00224	0.27156
KI3054	65.33	34.67	0.63551	0.36449	0.00268	0.42171
KI3054 R2	65.00	35.00	0.63761	0.36239	0.00243	0.38111
KI3362	60.50	39.50	0.59833	0.40167	0.00297	0.49638
KI3648	72.50	27.50	0.71963	0.28037	0.00247	0.34323
KI4143	42.00	58.00	0.39041	0.60959	0.00332	0.85039
KI4143 R2	40.00	60.00	0.37657	0.62343	0.00333	0.88430
Mourne	2.49	97.51	0.01891	0.98109	0.00414	21.89318
NWA2737 R2	73.00	27.00	0.71342	0.28658	0.00234	0.32800
Rockport	1.49	98.51	0.00915	0.99085	0.00412	45.02732
SanCarlos	93.00	7.00	0.91010	0.08990	0.00237	0.26041
LLV ✚	3.00	97.00	0.03026	0.96974	0.00474	15.66424
LFC ✚	2.00	98.00	0.01932	0.98068	0.00413	21.37681

• Samples with high ESD; these samples are not included in the discussion
◆ Samples with unusual Fe distribution
✚ Laihunite Samples

Sample ID	%Mg	%Fe	M2MG	M2FE	M2 ESD	%Uncertainty
NMNH85539	5.50	94.50	0.06303	0.93697	0.00415	6.58417
85540	8.50	91.50	0.10097	0.89903	0.00419	4.14975
90035 •	0.50	99.50	0.01069	0.98931	0.00579	54.16277
90613	6.50	93.50	0.07403	0.92597	0.00382	5.16007
104576 •	1.00	99.00	0.01322	0.98678	0.00533	40.31770
112085	5.00	95.00	0.06036	0.93964	0.00434	7.19019
DH101B	91.00	9.00	0.90126	0.09874	0.00245	0.27184
DH101C ◆	92.50	7.50	0.90640	0.09360	0.00251	0.27692
DH101C R2 ◆	93.00	7.00	0.91256	0.08744	0.00249	0.27286
DH101D ◆	93.50	6.50	0.91869	0.08131	0.00262	0.28519
DH101D R2	93.00	7.00	0.91405	0.08595	0.00285	0.31180
DH101E	93.00	7.00	0.91357	0.08643	0.00240	0.26271
EP3139C	91.54	8.46	0.91260	0.08740	0.00231	0.25312
EP3139C R2	91.54	8.46	0.91618	0.08382	0.00228	0.24886
EP3139D	91.54	8.46	0.91610	0.08390	0.00334	0.36459
EP3139D R2	92.50	7.50	0.91913	0.08087	0.00246	0.26764
H30B1	93.00	7.00	0.91523	0.08477	0.00258	0.28190
H30B1 R2	93.00	7.00	0.92509	0.07491	0.00316	0.34159
H30B4	93.50	6.50	0.93029	0.06971	0.00235	0.25261
KBH941	84.00	16.00	0.84056	0.15944	0.00255	0.30337
KBH941 R2	84.00	16.00	0.84145	0.15855	0.00249	0.29592
KI3054	65.33	34.67	0.65615	0.34385	0.00296	0.45112
KI3054 R2	65.00	35.00	0.65023	0.34977	0.00269	0.41370
KI3362	60.50	39.50	0.61167	0.38833	0.00334	0.54605
KI3648	72.50	27.50	0.72061	0.27939	0.00277	0.38440
KI4143	42.00	58.00	0.43705	0.56295	0.00355	0.81226
KI4143 R2	40.00	60.00	0.41537	0.58463	0.00360	0.86670
Mourne	2.49	97.51	0.02923	0.97077	0.00427	14.60828
NWA2737 R2	73.00	27.00	0.72452	0.27548	0.00257	0.35472
Rockport	1.49	98.51	0.02267	0.97733	0.00425	18.74724
SanCarlos	93.00	7.00	0.91597	0.08403	0.00266	0.29040
LLV ✚	3.00	97.00	0.03661	0.96339	0.00488	13.32969
LFC ✚	2.00	98.00	0.02728	0.97272	0.00422	15.46921

• Samples with high ESD; these samples are not included in the discussion
◆ Samples with unusual Fe distribution
✚ Laihunite Samples

Sample ID	%Mg	%Fe	M1 %ΣFe	ESD	M2 %ΣMg	ESD
NMNH85539	5.50	94.50	50.36	0.15	56.03	2.57
85540	8.50	91.50	50.90	0.17	59.80	1.75
90035 •	0.50	99.50	50.13	0.20	66.69	26.07
90613	6.50	93.50	50.56	0.15	58.24	2.12
104576 •	1.00	99.00	50.20	0.19	70.92	21.11
112085	5.00	95.00	50.58	0.16	61.29	3.11
DH101B	91.00	9.00	50.51	0.84	50.06	0.09
DH101C ◆	92.50	7.50	49.67	0.89	49.97	0.09
DH101C R2 ◆	93.00	7.00	49.67	0.94	49.97	0.09
DH101D ◆	93.50	6.50	47.09	1.00	49.76	0.09
DH101D R2	93.00	7.00	50.46	1.11	50.04	0.10
DH101E	93.00	7.00	50.22	0.94	50.02	0.09
EP3139C	91.54	8.46	52.25	0.92	50.23	0.08
EP3139C R2	91.54	8.46	53.23	0.97	50.32	0.08
EP3139D	91.54	8.46	51.76	1.31	50.17	0.12
EP3139D R2	92.50	7.50	52.50	1.06	50.23	0.09
H30B1	93.00	7.00	50.78	1.04	50.07	0.09
H30B1 R2	93.00	7.00	52.20	1.45	50.19	0.11
H30B4	93.50	6.50	53.30	1.21	50.27	0.08
KBH941	84.00	16.00	52.15	0.57	50.43	0.10
KBH941 R2	84.00	16.00	52.49	0.56	50.50	0.10
KI3054	65.33	34.67	51.46	0.30	50.80	0.15
KI3054 R2	65.00	35.00	50.89	0.26	50.49	0.14
KI3362	60.50	39.50	50.84	0.29	50.55	0.18
KI3648	72.50	27.50	50.09	0.33	50.03	0.13
KI4143	42.00	58.00	51.99	0.23	52.82	0.29
KI4143 R2	40.00	60.00	51.61	0.22	52.45	0.31
Mourne	2.49	97.51	50.26	0.15	60.72	6.28
NWA2737 R2	73.00	27.00	50.99	0.32	50.39	0.12
Rockport	1.49	98.51	50.34	0.15	71.24	9.99
SanCarlos	93.00	7.00	51.69	1.10	50.16	0.10
LLV ✚	3.00	97.00	50.16	0.18	54.75	5.10
LFC ✚	2.00	98.00	50.20	0.15	58.54	6.40

• Samples with high ESD; these samples are not included in the discussion
◆ Samples with unusual Fe distribution
✚ Laihunite Samples

APPENDIX G: NOTES FOR K_D TABLE

Reference	Notes
Artioli et al., 1995: N1RT	Neutron data
Brown and Prewitt, 1973: Lunar Rock 12052	0.010 Ca in M2, mixed cooling history
Brown and Prewitt, 1973: Lunar Rock 12018	0.010 Ca in M2, no stated cooling history
Brown and Prewitt, 1973: Metamorphic OG2B	Slow cooling history
Finger, 1971: 10020	0.008 Ca in M2, Assumed RT, Fe values are Fe+Mn+Cr, rapid cooling history
Finger, 1971: C15-64	0.007 Ca in M2, Assumed RT, Fe values are Fe+Mn+Cr, slow cooling history
Finger and Virgo 1971: Lunar Olivine B1/12018	0.007 Ca in M2, rapid cooling history
Ghose et al., 1976: Anorthosite 67075	Σcations >2.0, assumed RT, uncertainty not stated for M2 values
Heinemann et al., 2006: Bo-2-1	Formula given in paper does not give the KD values reported in the paper
Heinemann et al., 2006: Bo-5-1	Formula given in paper does not give the KD values reported in the paper
Heinemann et al., 2006: Bo-8-1	Formula given in paper does not give the KD values reported in the paper
Heinemann et al., 2006: Bo-10-1	Formula given in paper does not give the KD values reported in the paper
Heinemann et al., 2007: Fa 11.6	Formula given in paper is the same as above, but KD values are correct
Heinemann et al., 2007: Fa 22.3	
Heinemann et al., 2007: Fa 27.8	
Liang and Hawthorne, 1994: Ol SC	
Smyth and Hazen, 1973: Hortonolite	Hortonolite Mg(0.75)Fe(1.10)Mn(0.15)SiO4, slow cooling history (metamorphic)
Wenk and Raymond, 1973	
Wenk and Raymond, 1973	
Wenk and Raymond, 1973	

APPENDIX H: PRE-EDGE PEAK FITTING

Sample ID	%Fe	%Mg	$\%Fe^{3+}$	Peak 1						
				Height	Center	ESD	FWHM	ESD	Area	ESD
104576_a	99.00	1.00	5	0.02	7111.38	0.01	1.01	0.03	0.02	0.000677
104576_b	99.00	1.00	5	0.02	7111.22	0.02	1.15	0.03	0.03	0.000745
104576_c	99.00	1.00	5	0.05	7111.57	0.01	0.91	0.02	0.05	0.00101
85540_a	91.50	8.50	16	0.02	7111.4	0.01	1.09	0.03	0.03	0.0006
85540_b	91.50	8.50	16	0.02	7111.22	0.03	1.01	0.05	0.02	0.00106
85540_c	91.50	8.50	16	0.03	7111.56	0.01	0.83	0.02	0.03	0.000723
DH101b_a	9.00	91.00	3.9	0.01	7111.43	0.03	1.1	0.05	0.02	0.000802
DH101b_b	9.00	91.00	3.9	0.01	7111.26	0.05	1.12	0.08	0.01	0.000744
DH101_c	9.00	91.00	3.9	0.02	7111.65	0.01	0.84	0.02	0.02	0.000499
H30B4_a	6.50	93.50	1.6	0.01	7111.17	0.04	1.01	0.07	0.01	0.000853
H30B4_b	6.50	93.50	1.6	0.01	7111.19	0.04	1.15	0.06	0.02	0.000913
H30B4_c	6.50	93.50	1.6	0.02	7111.4	0.03	1.18	0.05	0.02	0.000978
KI3362_a	39.50	60.50	0	0.02	7111.24	0.02	1.23	0.04	0.03	0.00108
KI3362_b	39.50	60.50	0	0.02	7111.25	0.03	1.08	0.05	0.02	0.000949
KI3362_c	39.50	60.50	0	0.03	7111.4	0.02	1.1	0.03	0.04	0.00103
KI3648_a	27.50	72.50	0	0.03	7111.44	0.01	1.09	0.03	0.03	0.000858
KI3648_b	27.50	72.50	0	0.02	7111.23	0.03	1.08	0.05	0.02	0.000954
KI3648_c	27.50	72.50	0	0.04	7111.57	0.01	1.03	0.02	0.04	0.000685
LFC_a	98.00	2.00	58	0.04	7111.39	0.01	1.08	0.02	0.05	0.00096
LFC_b	98.00	2.00	58	0.03	7111.21	0.02	1.1	0.04	0.03	0.00131
LFC_c	98.00	2.00	58	0.05	7111.5	0.01	0.99	0.02	0.05	0.00127
LV_a	97.00	3.00	67	0.02	7111.36	0.02	1.05	0.04	0.02	0.000882
LV_b	97.00	3.00	67	0.03	7111.19	0.02	1.03	0.03	0.03	0.00107
LV_c	97.00	3.00	67	0.04	7111.44	0.01	1.11	0.002	0.05	0.00116
Mourne_a	97.51	2.49	31.5	0.03	7111.35	0.01	1.07	0.03	0.03	0.000793
Mourne_b	97.51	2.49	31.5	0.03	7111.18	0.03	1.11	0.05	0.03	0.00142
Mourne_c	97.51	2.49	31.5	0.05	7111.58	0.01	0.98	0.02	0.05	0.000948
Mourne_rnd	97.51	2.49	31.5	0.02	7111.24	0.03	1.06	0.05	0.02	0.00111
rockport_011	98.51	1.49	0	0.03	7111.32	0.01	1.18	0.03	0.04	0.00105
rockport_101	98.51	1.49	0	0.05	7111.38	0.02	1.11	0.03	0.06	0.00156
rockport_110	98.51	1.49	0	0.02	7111.26	0.02	1.16	0.04	0.02	0.000689
rockport_111	98.51	1.49	0	0.04	7111.4	0.02	1.03	0.03	0.04	0.00138
rockport_a	98.51	1.49	0	0.03	7111.32	0.02	1.15	0.03	0.04	0.0012
rockport_b	98.51	1.49	0	0.03	7111.16	0.03	1.07	0.05	0.03	0.00158
rockport_c	98.51	1.49	0	0.05	7111.43	0.01	1.13	0.03	0.06	0.00147
SA_KI3648_a	27.50	72.50	0	0.02	7111.44	0.01	1.08	0.03	0.03	0.000757
SA_KI3648_b	27.50	72.50	0	0.02	7111.23	0.03	1.08	0.05	0.02	0.000843

SA_KI3648_c	27.50	72.50	0	0.03	7111.57	0.01	1.03	0.02	0.03	0.000583
SanCarlos_a	7.00	93.00	3	0.01	7111.41	0.02	1.31	0.04	0.02	0.000547
SanCarlos_b	7.00	93.00	3	0.01	7111.21	0.03	1.19	0.07	0.01	0.000608
SanCarlos_c	7.00	93.00	3	0.02	7111.62	0.01	0.97	0.02	0.03	0.000505

Sample ID	**%Fe**	**%Mg**	**%Fe^{3+}**	**Peak 2**						
				Height	Center	ESD	FWHM	ESD	Area	ESD
104576_a	99.00	1.00	5	0.01	7113.11	0.03	0.6	0.07	0.01	0.000721
104576_b	99.00	1.00	5	0.02	7113.07	0.02	0.68	0.04	0.01	0.000652
104576_c	99.00	1.00	5	0.01	7113.2	0.02	0.64	0.05	0.00428	0.000305
85540_a	91.50	8.50	16	0.01	7113.1	0.04	0.51	0.08	0.00368	0.000547
85540_b	91.50	8.50	16	0.01	7113.09	0.01	0.72	0.02	0.01	0.000239
85540_c	91.50	8.50	16	0.01	7113.29	0.02	0.6	0.04	0.00375	0.000226
DH101b_a	9.00	91.00	3.9	0.00481	7113.21	0.02	0.61	0.04	0.00314	0.000187
DH101b_b	9.00	91.00	3.9	0.01	7113.14	0.01	0.63	0.02	0.01	0.000148
DH101_c	9.00	91.00	3.9	0.00383	7113.3	0.02	0.61	0.05	0.0025	0.00017
H30B4_a	6.50	93.50	1.6	0.01	7113.12	0.01	0.74	0.03	0.01	0.000188
H30B4_b	6.50	93.50	1.6	0.00492	7113.16	0.01	0.58	0.04	0.00301	0.000159
H30B4_c	6.50	93.50	1.6	0.00176	7113.36	0.07	0.85	0.19	0.0016	0.000295
KI3362_a	39.50	60.50	0	0.01	7113.12	0.01	0.75	0.02	0.01	0.000232
KI3362_b	39.50	60.50	0	0.01	7113.14	0.01	0.66	0.02	0.01	0.000199
KI3362_c	39.50	60.50	0	0.00233	7113.16	0.04	0.43	0.09	0.00106	0.000181
KI3648_a	27.50	72.50	0	0.01	7113.18	0.05	0.4	0.12	0.00275	0.000746
KI3648_b	27.50	72.50	0	0.00423	7113.15	0.02	0.59	0.05	0.00267	0.000181
KI3648_c	27.50	72.50	0	0.01	7113.26	0.02	-0.63	0.04	0	0.000193
LFC_a	98.00	2.00	58	0.01	7113.14	0.05	0.51	0.1	0.00496	0.000906
LFC_b	98.00	2.00	58	0.01	7113.12	0.01	0.58	0.03	0.00479	0.000237
LFC_c	98.00	2.00	58	0.0044	7113.28	0.03	0.45	0.07	0.00212	0.000278
LV_a	97.00	3.00	67	0.01	7113.15	0.01	0.62	0.03	0.00476	0.000196
LV_b	97.00	3.00	67	0.01	7113.12	0.01	0.5	0.03	0.00323	0.000179
LV_c	97.00	3.00	67	0.00257	7113.32	0.04	0.53	0.11	0.00144	0.000253
Mourne_a	97.51	2.49	31.5	0.01	7113.11	0.03	0.58	0.07	0.01	0.000768
Mourne_b	97.51	2.49	31.5	0.02	7113.06	0.01	0.69	0.02	0.01	0.000281
Mourne_c	97.51	2.49	31.5	0.01	7113.21	0.02	0.6	0.04	0.000429	0.000266
Mourne_rnd	97.51	2.49	31.5	0.02	7113.12	0.01	0.65	0.02	0.01	0.000229
rockport_011	98.51	1.49	0	0.01	7113.15	0.05	0.51	0.1	0.00484	0.000881
rockport_101	98.51	1.49	0	0.01	7113.25	0.03	0.58	0.07	0.00339	0.000337
rockport_110	98.51	1.49	0	0.00374	7113.16	0.02	0.64	0.04	0.00254	0.000137
rockport_111	98.51	1.49	0	0.01	7113.17	0.02	0.56	0.04	0.01	0.000302
rockport_a	98.51	1.49	0	0.0048	7113.22	0.02	0.53	0.05	0.00272	0.000226
rockport_b	98.51	1.49	0	0.00452	7113.13	0.03	0.59	0.07	0.00286	0.000284

rockport_c	98.51	1.49	0	0.01	7113.23	0.02	0.51	0.06	0.00304	0.000294
SA_KI3648_a	27.50	72.50	0	0.01	7113.18	0.05	0.4	0.12	0.00246	0.000664
SA_KI3648_b	27.50	72.50	0	0.00367	7113.15	0.02	0.59	0.05	0.00237	0.00016
SA_KI3648_c	27.50	72.50	0	0.0045	7113.26	0.02	0.64	0.04	0.00304	0.000166
SanCarlos_a	7.00	93.00	3	0.01	7113.16	0.07	0.59	0.15	0.00393	0.000923
SanCarlos_b	7.00	93.00	3	0.01	7113.12	0.02	0.69	0.04	0.01	0.000415
SanCarlos_c	7.00	93.00	3	0.00421	7113.25	0.04	0.62	0.09	0.00277	0.000361